NASA CR-132443

ANALYTIC MODELS OF DUCTED TURBOMACHINERY TONE NOISE SOURCES

Volume I: Analysis

by T. L. Clark, U. W. Ganz, G. A. Graf, and J. S. Westall

May 1974

Prepared under contract NAS1-12257 by

Boeing Commercial Airplane Company
P.O. Box 3707
Seattle, Washington 98124

for

Langley Research Center
NATIONAL AERONAUTICS AND SPACE ADMINISTRATION

54841

File with N74-30244

1 x Uellum

NASA CR-132443

ANALYTIC MODELS OF DUCTED TURBOMACHINERY TONE NOISE SOURCES

Volume I: Analysis

by T. L. Clark, U. W. Ganz, G. A. Graf, and J. S. Westall

D6-43296-1
May 1974

Prepared under contract NAS1-12257 by

Boeing Commercial Airplane Company
P.O. Box 3707
Seattle, Washington 98124

for

Langley Research Center
NATIONAL AERONAUTICS AND SPACE ADMINISTRATION

NASA CR-132443

ANALYTIC MODELS OF DUCTED TURBOMACHINERY TONE NOISE SOURCES

Volume I: Analysis

by T. L. Clark, U. W. Ganz, G. A. Graf, and J. S. Westall

May 1974

Prepared under contract NAS1-12257 by

Boeing Commercial Airplane Company
P.O. Box 3707
Seattle, Washington 98124

for

Langley Research Center
NATIONAL AERONAUTICS AND SPACE ADMINISTRATION

1. Report No.	2. Government Accession No.	3. Recipient's Catalog No.
NASA CR-132443		

4. Title and Subtitle	5. Report Date
ANALYTIC MODELS OF DUCTED TURBOMACHINERY TONE NOISE SOURCES – VOLUME 1: Analysis	May 1974
	6. Performing Organization Code
7. Author(s)	8. Performing Organization Report No.
T.L. Clark, U.W. Ganz, G.A. Graf, and J.S. Westall	D6-43296-1
	10. Work Unit No.
9. Performing Organization Name and Address	
Boeing Commercial Airplane Company P.O. Box 3707 Seattle, Washington 98124	11. Contract or Grant No. NAS1-12257
	13. Type of Report and Period Covered
12. Sponsoring Agency Name and Address	Contractor Report
National Aeronautics and Space Administration Washington, D.C. 20546	14. Sponsoring Agency Code

15. Supplementary Notes

16. Abstract

Volume I of this report describes the analytic models developed for computing the periodic sound pressures of subsonic fans and compressors in an infinite, hardwall annular duct with uniform flow. The basic sound-generating mechanism is the scattering into sound waves of velocity disturbances appearing to the rotor or stator blades as a series of harmonic gusts. The models include component interactions and rotor alone. Volume II of this report describes the computer subprograms developed for numerical computations of sound pressure mode amplitudes from the analysis. Volume III presents some test case results from the computer programs.

17. Key Words (Suggested by Author(s))		18. Distribution Statement
Analytic models	Tone noise	Unclassified – Unlimited
Turbomachinery noise	Fan duct	
Acoustic models		

19. Security Classif. (of this report)	20. Security Classif. (of this page)	21. No. of Pages	22. Price*
Unclassified	Unclassified	156	

*For sale by the National Technical Information Service, Springfield, Virginia 22151

SUMMARY

Analytic models are developed for computing the periodic sound pressures of subsonic fans and compressors in an infinite, hardwall annular duct with uniform flow. The basic sound-generating mechanism is the scattering into sound waves of velocity disturbances appearing to the rotor or stator blades as a series of harmonic gusts. The models include the sources of velocity disturbances arising from the component interactions studied by Kemp and Sears, and non-component-induced inlet distortions at a rotor. The primary result of the models is the computation of the periodic sound pressure mode amplitudes which can be used as inputs to a duct acoustic program for computing the propagation through a finite, multisectioned duct and the radiation to the far field outside the duct. Computer subprograms for the mode amplitude calculations are presented.

CONTENTS

CONTENTS-Concluded

FIGURES

SYMBOLS

a	a constant
a_z, a_ϕ	eddy transverse length scale
A	radial location of the maximum distortion in the cone model
A_n, $A_{n,\kappa 2}$	n^{th} order Glauert coefficients
$A^{\pm}_{mn}$	a mode amplitude, or coefficient of eigenfunction expansion of the pressure spectral density
b_1, b_2	blade spacings of a two-dimensional cascade of blades
C, C_1, C_2, C_{K1}, C_{K2}	airfoil chord lengths
$C_3 \cdots C_{14}$	switches used in the generalized equations for the potential flow field interactions
C_{D1}, C_{D2}	airfoil section drag coefficient
d	axial spacing between midchords of two blade rows
$\frac{dC_L}{d\alpha}$, $\frac{dC_{L1}}{d\alpha}$, $\frac{dC_{L2}}{d\alpha}$, $\frac{dC_{L3}}{d\alpha}$, $\left(\frac{dC_L}{d\alpha}\right)_1$, $\left(\frac{dC_L}{d\alpha}\right)_{K1}$	slope of steady lift versus angle of attack
$\hat{d}_{mn}$	a function defined by equation (B41)
$\hat{D}_{mn}$	a function defined by equation (2.1.22)
D_{mn}	a function defined by equation (2.1.15)
$\vec{e}$	unit vector perpendicular to airfoil chordline
e_z	z-component of $\vec{e}$
e_ϕ	ϕ-component of $\vec{e}$
E_z, E_ϕ, $E_{z\phi}$	bandpass filter factor; see equation (3.3.23)

f	ratio of maximum camber to the half-chord of a thin airfoil
F	strength of single dipole or a surface distribution of dipoles; also, function defined by equation (3.1.15)
$\hat{F}$, $\hat{F}_j$	spectral density of the strength of a single dipole, or a surface distribution of dipoles
F_α	function defined by equation (3.1.20)
F_f	function defined by equation (3.1.21)
$G_{mn\ell}$, $G_{mn\sigma}$	complex term in the equation for the induced velocities resulting from a potential flow field interaction
$g_{\sigma,1}$, $G_{\sigma,1}$, $G_{\kappa,K1}$	airfoil acoustic response function, defined by equation (3.1.39)
h	oblique gust wave number
$\hat{H}$	the nondimensional dipole surface density response function for convected, harmonic gusts
$H_m^{(1)}$	Hankel function of the first kind of order m
$H_o^{(2)}$	Hankel function of the second kind of zeroth order
$H_1^{(2)}$	Hankel function of the second kind of order one
$H_{\sigma,2}$, $H_{\kappa,K2}$	complex term in the equation for the induced velocities resulting from a potential flow field interaction, equation (3.2.31)
I_ℓ	modified Bessel function of the first kind and order ℓ
j	dummy index or blade number index
J	$J_0 + iJ_1$
J_m	Bessel function of order m
J_0	Bessel function of order zero
J_1	Bessel function of order one

k	wave number; also, dummy index
K	one-dimensional Fourier space wave number
K_L	Kemp-Sears lift response function
$K_{mn}^{\pm}$	axial propagation wave number of mn^{th} mode
$K_{\sigma,1}$, $K_{\kappa,K1}$	complex conjugate of Kemp-Sears lift response function
ℓ	dummy index, or harmonic index
L	airfoil section lift force
$\hat{L}_j$	spectral density of airfoil section lift force
L_z, L_ϕ	eddy axial length scale
m	polar angle harmonic index, or spinning mode index
M	duct uniform, axial flow velocity for acoustic calculations
M_E, M_{1E}, M_{2E}, M_{3E}, $M_{E,K}$	mean exit velocity from a blade row, relative to the blades of the row
M_I, M_{II}, M_{2I}, M_{3I}, $M_{M,K1}$	mean inlet velocity to a blade row, relative to the blades of the row
M_M, M_{1M}, M_{2M}, M_{3M}	
$M_{M,1}$, $M_{M,2}$, $M_{M,K}$, $M_{M,K1}$ $M_{M,K2}$	mean velocity through a blade row, relative to the blades of the row
M_T	tip velocity of rotating blades
M_z, M_{1z}, M_{2z}, M_{3z}, $M_{z,K}$	mean axial flow velocity
$\bar{M}_z$	mean axial flow velocity when there is steady distortion
n	dummy index, harmonic index, or radial mode index
N, N_1, N_2, N_3, N_{K2}	number of blades in a blade row

p	linear pressure perturbation
$\hat{p}$	spectral density of linear pressure perturbation
q	exponent in the "power law," equation (3.3.8)
$Q_{\sigma,2}$	complex term in the equation for the induced velocities resulting from a potential flow field interaction, equation (3.2.3)
$\vec{r}$	position vector, field location
$\vec{r}_o$, $\vec{r}_s$	position vector, source location
R	radial location of eddy center
R_m	unnormalized radial eigenfunction
R^*	distance from origin in Prandtl-Glauert scaled coordinates
s_{mn}	axial propagation wave number of mn^{th} mode in Prandtl-Glauert scaled coordinates and frequency
S	Sears function
SPL	sound pressure level, measured in decibels
t	time at field location
t_o, t_s	time at source location
T	function defined by equation (3.1.17)
$T^\dagger$	Filotas lift response function
T_z, T_ϕ, $T_{z,\phi}$	eddy temporal length scale
U	relative velocity of two-dimensional cascade of blades
$\hat{u}$, $\hat{u}_j$	spectral density of perturbation velocity
V	gust convection velocity
V_A	value of the maximum velocity distortion in the cone model

V_1	value of the velocity at the outer radius in the cone model
W, W_j	perturbation velocity, viscous wake defect, unsteady induced velocity
$\bar{W}$	single spatial Fourier transform of W
$\bar{\bar{W}}$	double spatial Fourier transform of W
W_z, W_ϕ	perturbation velocity components at the eddy center
$W_{z\ell}$, $W_{\phi\ell}$	ℓ^{th} Fourier series coefficient of the eddy velocity components
Y, Y', $\bar{Y}'$, Y_1', Y_j'	rectangular coordinate
$Y'_{\ell j}$	rectangular coordinate
Y_m	Neumann function of order m
Y_o	width of viscous wake; also, Neumann function of order o
Z, Z', Z', Z'_1	rectangular coordinate
$Z'_{\ell j}$	rectangular coordinate
$z_{M.C.}$	axial position of midchord plane
*	multiplier
α	mean blade angle of attack
β	relative stagger angle
β_{mn}	square root term defined by equation (2.1.16)
γ, γ_1, γ_2, γ_{K1}, γ_{K2}	stagger angle
$\hat{\gamma}$	Helmholtz equation Green's function
Γ	acoustic propagator
Γ_2 , Γ_{K2}	steady-state circulation of cascade airfoil

δ	Dirac delta function
$\delta_{m-\ell,\sigma N}$	Kronecker delta symbol
Δ_o	factor in viscous wakes formula, equation (3.1.35)
$\bar{\Delta}_z$, $\bar{\Delta}_\phi$	axial eddy strength modulation function
ε	small, positive constant; also, unit step function
ζ	rectangular coordinate normal to the airfoil
η	hub-to-tip ratio, annular duct inner radius
Θ	inverse cosine of nondimensionalized chordwise coordinate
κ	temporal or spacial harmonic index
$\kappa^{\pm}_{mn}$	chordwise compactness parameter; see equation (2.2.18)
λ, λ_1, $\lambda_{\sigma,1}$, $\lambda_{\kappa,K1}$	wave number; also, reduced complex frequency of the chordwise velocity distribution
Λ_ℓ, Λ_σ	Fourier coefficients of typical wake profile
$\mu_{\sigma,1}$	complex frequency of the chordwise velocity distribution
μ_{mn}	annular duct eigenvalue
ν, ν_ℓ, ν_σ, ν_1, $\nu_{\sigma,1}$, $\nu_{\kappa,K1}$	reduced frequency
ξ	chordwise rectangular coordinate
ξ'	chordwise rectangular coordinate nondimensionalized to the half-chord
ρ, ρ_o, ρ_s	polar radial coordinate of cylindrical coordinate system
σ	temporal Fourier series coefficient, dummy index used in summations
τ	time delay resulting from the axial distance between the midchord plane and the eddy center position at the temporal origin; also, t - to

ϕ , ϕ_o , ϕ_s , $\phi_{M.C.}$	polar angle coordinate of cylindrical coordinate system
ϕ_j , ϕ_s' , Φ	
Φ	polar angle coordinate of eddy center
ψ	relative exit flow angle; also, oblique gust angle
ω , ω^* , $\omega_{\sigma,l}$	angular frequency
Ω	angular velocity of rotor

Subscripts:

E	blade row exit flow
I	blade row inlet flow
j	j^{th} blade
K	either K1 or K2
K1	sound-producing blade row
K2	velocity-inducing blade row
ℓ	spatial harmonic index
m	spinning mode index
M	blade row mean flow
M. C.	midchord point location
n	radial mode index
S	source
z	axial direction, axial eddy velocity component
κ	either σ or ℓ
σ	temporal Fourier series index
ϕ	angular direction, angular eddy velocity component
o	source

1	inlet stator parameter, upstream component in viscous wakes interaction, or unsteady lift-producing component in potential flow field interaction
2	rotor parameter, downstream component in viscous wakes interaction, or velocity-inducing component in potential flow field interaction
3	outlet stator parameter

Superscripts:

$\pm$	downstream (+) and upstream (-) propagation
$\dagger$	complex conjugate
*	complex conjugate; also, generalized Prandtl-Glauert transform variable
'	blade-attached rectangular coordinate non-dimensionalized to the half-chord
$\vec{\ }$	vector
^	temporal Fourier integral transform
-	spacial Fourier series transform
$\bar{\ }$	blade-attached rectangular coordinate system in viscous wakes interaction, polar angle in the rotating system, or averaged value of a variable
=	double spatial Fourier series transform

1.0 INTRODUCTION

1.1 Background

Gutin (ref. 1) in 1936 published the first analytic model for the tone noise generated by rotating machinery. His idea was to replace a rotating propeller by a disc of applied acoustic dipoles, the strengths of which were determined by the steady air forces acting on the propeller blades and the frequencies of which were determined by the propeller shaft frequency and the number of blades. Not until 1963, when Van de Vooren and Zandbergen (ref. 2) published their work, did the problem receive an essentially different formulation: The rotating and translating blades were replaced by dipoles and monopoles, the strengths of which were to be determined by solving a linear boundary value problem. They did not, however, solve this problem, but returned, instead, to the momentum considerations of Gutin for the strengths of these moving sources.

The advent of the turbofan engine gave a new impetus to the construction of analytic models for the generation of tone noise by rotating machinery. In 1961 Slutsky, et al. (ref. 3) developed analytic models for the generation of tone noise by a turbofan stage assuming for the sources of sound the steady, rotating vorticity of the rotor blades and the unsteady vorticity of the rotor and stator blades induced by the two-dimensional cascade aerodynamic interactions studied by Kemp and Sears (refs. 4 and 5). These noise models were for a ducted fan stage and included, in principle, the transmission and reflection at the termination of the duct. Tyler and Sofrin (ref. 6) reported upon similar, althrough less detailed, work, e.g., no explicit source modeling, in 1962, and a year later Hetherington (ref. 7) reported upon a source modeling scheme essentially the same as that used by Slutsky (whose work did not receive general notice until much later). Griffith (1964, ref. 8) added randomness to the phasing considerations in the blade row interaction tone noise generation processes and Hulse, et al. (ref. 9) added similar, although less detailed, considerations to the Gutin-type of free-rotor tone noise mechanism. At this time Lighthill's (ref. 10) theory of aerodynamic noise, and Curle's (ref. 11) extended version, began to be applied to the problem of the analytical modeling of the

tone noise generation by fans and compressors, particularly by Lowson (refs. 12 and 13. Ffowcs Williams and Hawkins (ref. 14) advanced an argument based on the Lighthill theory for a tone noise generating mechanism for a fan or compressor rotor that was neither a surface dipole or monopole, but a fluid volume quadrupole. They did not, however, develop the idea into a working analytic model. Wright (ref.15) and Morse and Ingard (ref. 16) developed working models for tone noise generation by free rotors in steady nonuniform flow using time-dependent Gutin-type dipoles, and Lowson (ref. 17) added to these models the element of non-steadiness in the nonuniform flow at the rotor (see Griffiths and Hulse). Pfenninger (ref. 18) gave physical insight to the problem of tone noise generation by turbofans in non-steady, non-uniform inflow conditions. By employing an interesting combination of Griffith's and Pfenninger's ideas, Hanson (ref. 19) has recently advanced a model (without explicit source modeling) for computing the complete spectrum of sound radiated by a free rotor with turbulent inflow, and a similar blade row interaction model (refs. 19 and 20, with explicit source modeling). Detailed source modeling for the tone noise generation by a ducted rotor in uniform flow is being investigated by Lordi (ref. 21) while Drischler (ref. 22) has computed pressures in the duct of a ducted propeller using a Gutin-type dipole model for the blades. Schaut (ref. 23), in using the Morse and Ingard radiation model for a free rotor, modeled the blade pressures after the design profiles.

1.2 Present Work

It was the purpose of the present work to develop an analytical procedure and a set of computer subprograms for computing the sound pressure at the harmonics of the blade passing frequency which is radiated from an axial flow compressor or fan stage in an infinite, hardwalled annular duct. The problem is presented in the form of a boundary value problem to which approximate solutions are adapted from the published literature on the aerodynamics of thin airfoils. The radiated pressure in the duct is most conveniently expressed in terms of an eigenfunction

expansion, with the coefficients of the expansion determined by the pressure on the fan rotor and stator blades. By the familiar process of linear analysis, these coefficients then can be used as inputs to problems involving a large variety of ducts. Zorumski (ref. 24) has recently proposed a very extensive and systematic scheme based on mode matching techniques, which utilizes these infinite-duct coefficients as the elements of an input, or known, vector in an inhomogeneous matrix equation wherein the unknown vector is the set of coefficients for the pressure expansion in the eigenfunctions appropriate to the section of duct contiguous with the inlet or exit of a finite, multisectioned duct, which, when known, allows the computation of the far-field pressure outside the duct (see, e.g., Slutsky [ref. 3], Lansing [ref. 25], and Clark [ref. 26]). The inverse of the matrix multiplying the unknown vector represents the multiple transformations which the pressure expansion coefficients undergo between the duct section containing the compressor or fan, and the section contiguous with either the inlet or the exit. It was, in part, to supply computer subprograms for computing input vectors to this matrix equation that the present work was performed. Examples of this matrix equation in the present context can be found in Zorumski's report and Lansing and Zorumski (ref. 27).

The models considered include the blade row interactions of Kemp and Sears and the rotor alone in steady and quasi-steady nonuniform inflow. The computer subprograms have been coded in standard FORTRAN for a CDC 6600 scientific computer. They have been designed to compute the nondimensionalized, infinite duct coefficients, or mode amplitudes, for the eigenfunction expansion of the radiated pressure for each of the models. Since these are subprograms and their outputs are intermediate results in the computation of the radiated pressure, a user must supply a main program for computing pressures from the expansion coefficients.

2.0 ACOUSTIC THEORY

This analysis is based upon the linearized theory of compressible fluids, thus restricting the applicability of the results to lightly loaded blades and to subsonic subcritical relative flow velocities. Some of the tone noise characteristics of modern transonic fans, e.g., the "buzz saw" phenomenon, are, therefore, excluded from consideration. It is assumed that under these conditions the most efficient discrete frequency sound-generating mechanism is the scattering into outgoing pressure waves of flow perturbations which appear to the turbomachinery blades as unsteady velocity disturbances. Since a perturbation-free flow is difficult to achieve under the best of conditions, this mechanism, it seems, will persist into the flow regimes in which, presently, dynamic calculations cannot be made. Under linear conditions, the strengths of the outgoing pressure waves are proportional to the strengths of the velocity disturbances at the fan rotor and/or stator faces. The analysis consists of determining the transfer function for general velocity disturbances and then identifying and describing the velocity disturbances which occur in the operation of ducted turbomachines. Although little work has been done in the determination of the transfer function, even less has been done in analyzing and describing these velocity disturbances.

To obtain the transfer function requires doing two things: solving the convective wave equation with a dipole singularity as an inhomogeneous term, and then solving for the induced dipole distribution that is required to cancel out the incident velocity perturbations that are normal to the rotor and/or stator blades, which are taken to be thin airfoils. These are discussed in this section, leaving to the next section the details of the tone noise models that result when the incident velocities are specified.

2.1 The Acoustic Propagator

The geometry of the problem is depicted in figure 1. The mathematical conventions and the nondimensionalized form of the linearized fluid

Annulus formed by concentric cylinders.

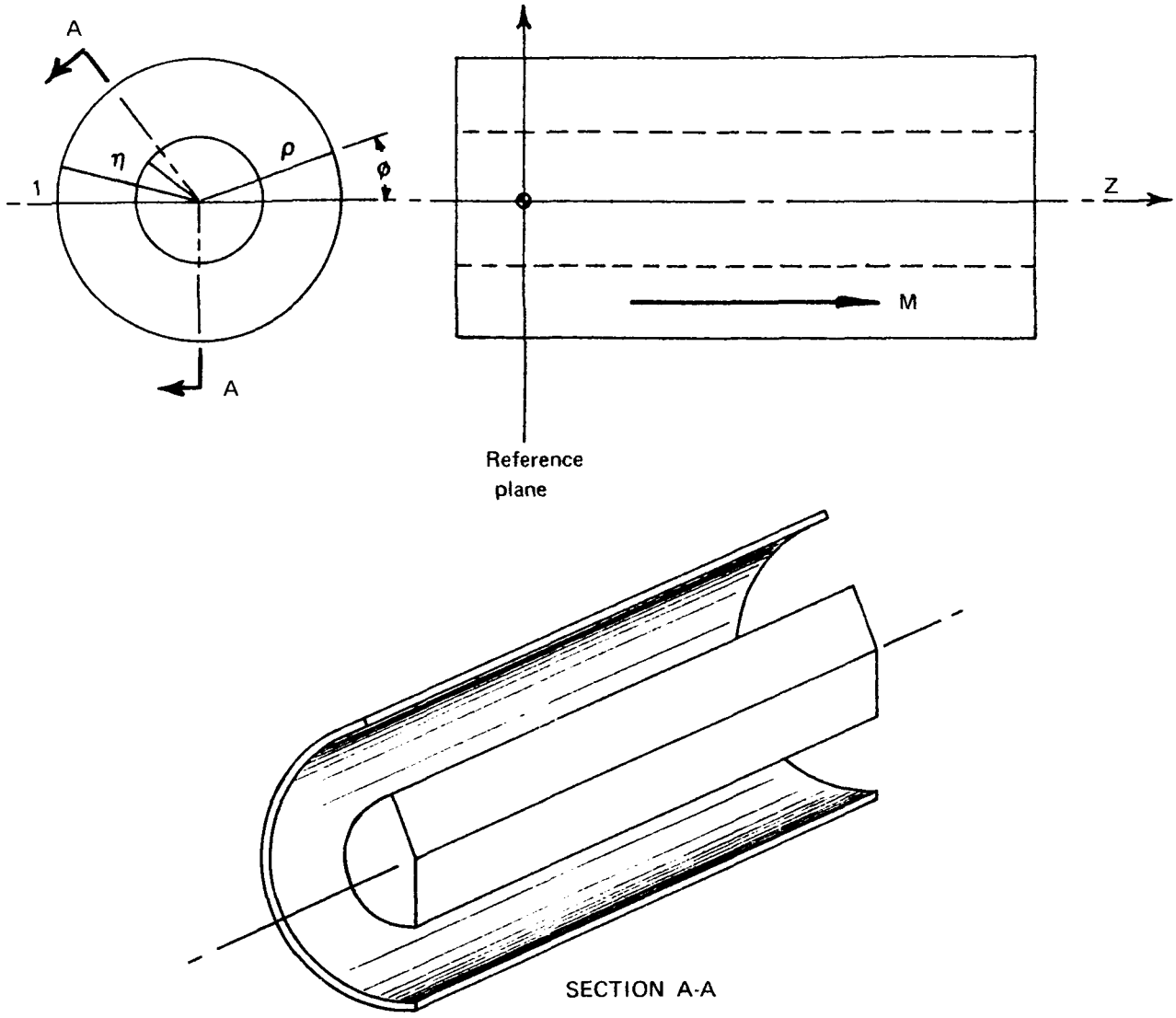

FIGURE 1. – DUCT GEOMETRY

equations are presented in appendix A. The governing equation for the linear pressure variations in a fluid with uniform mean flow velocity, M, parallel to the positive z-axis of the coordinate system, that results from the presence of a dipole of strength -F(t), orientation

$$\vec{e} = \left\{ o, e_\phi, ez \right\} \quad \text{and position} \quad \vec{r}_s = \left\{ \rho_s, \phi_s, z_s \right\} \quad \text{is}$$

$$-\Box_c P(\vec{r},t) = F(t)\vec{e}\cdot\vec{\nabla}_s \, \delta(\vec{r} - \vec{r}_s) \tag{2.1.1}$$

where $\Box_c$ is the convective D'Alembertian,

$$\Box_c \equiv \left(\frac{\partial}{\partial t} + M\frac{\partial}{\partial z}\right)^2 - \nabla^2 \tag{2.1.2}$$

$$= \left(\frac{\partial}{\partial t} + M\frac{\partial}{\partial z}\right)^2 - \frac{1}{\rho}\frac{\partial}{\partial \rho}\rho\frac{\partial}{\partial \rho} - \frac{1}{\rho^2}\frac{\partial^2}{\partial \phi^2} - \frac{\partial^2}{\partial z^2}$$

and $\vec{\nabla}_s$ is the gradient with respect to the s-subscripted coordinates.

If a solution to the simpler equation

$$-\Box_c \Gamma(\vec{r},\vec{r}_o,t-t_o) = \delta(\vec{r}-\vec{r}_o)\delta(t-t_o) \tag{2.1.3}$$

is found, then the solution to equation (2.1.1) is

$$p(\vec{r},t) = \int_{-\infty}^{\infty} F(t_o)\vec{e}\cdot\vec{\nabla}_o \Gamma(\vec{r},\vec{r}_o, t-t_o)\Big/_{\vec{r}_o=\vec{r}_s} dt_o \tag{2.1.4}$$

In this report Γ will be referred to as the acoustic "propagator," a descriptive word often used in similar contexts in elementary particle physics, e.g., Feynman (ref. 28). It satisfies causality but, in this

case, not reciprocity, so that it is not a Green's function in the commonly accepted sense, e.g., Morse and Feshbach, chapter 7 (ref. 29). For equation (2.1.4) to hold, Γ must satisfy the same boundary conditions as does p. These conditions are that the normal gradient of p at the inner and outer duct walls should vanish,

$$\frac{\partial p}{\partial \rho} = 0 \text{ at } \rho=1, \ \rho=\eta, \tag{2.1.5}$$

and that only outgoing waves should exist. The problem is simplified by defining the temporal Fourier transform of Γ by

$$\overset{\Lambda}{\Gamma}(\vec{r},\vec{r}_o,\omega) = \int_{-\infty}^{\infty} \Gamma(\vec{r},\vec{r}_o,\tau)e^{i\omega\tau}d\tau \tag{2.1.6}$$

and the "generalized Prandtl-Glauert" transformation by

$$\overset{\Lambda}{\Gamma}(\vec{r},\vec{r}_o,\omega) = \frac{e^{-i\frac{M\omega(z-z_o)}{1-M^2}}}{\sqrt{1-M^2}} \hat{\gamma}(\vec{r}^*,\vec{r}_o^*,\omega^*) \tag{2.1.7}$$

where $\omega^* = \dfrac{\omega}{\sqrt{1-M^2}}$ (2.1.8)

and $\vec{r}^* = \{\rho,\phi,z^*\}$

with $z^* = \dfrac{z}{\sqrt{1-M^2}}$ (2.1.9)

Then the equation $\hat{\gamma}$ must satisfy is

$$\nabla^2\hat{\gamma} + \omega^{*2}\hat{\gamma} = \delta(\vec{r}^{*} - \vec{r}_o^{*}) \tag{2.1.10}$$

with the boundary conditions that

$$\frac{\partial\hat{\gamma}}{\partial\rho} = 0 \quad \text{at } \rho=1,\ \rho=\eta, \tag{2.1.11}$$

and for $|z-z_s| \to \infty$, a = constant,

$$\hat{\gamma} \sim e^{-a|z-z_o|\mathrm{Im}(\omega^*)} \tag{2.1.12}$$

This last condition is the statement that if the fluid is considered to have a small absorptivity, equivalent to letting ω^* have a small imaginary part, then the pressure decays exponentially away along the axis. However, when the absorptivity is neglected, $\mathrm{Im}(\omega^*) = 0$, then at least a part of the pressure does not decay for $|z-z_s| \to \infty$ (neglecting, of course, all other absorption mechanisms). It is convenient to solve for $\hat{\gamma}$ as the sum of a particular integral to the inhomogeneous equation neglecting the presence of the duct walls, with the general solution to the homogeneous equation, and then adjust the undetermined parameters in the general solution to satisfy the hardwall duct boundary conditions.

This is done in appendix B, from which equation (B42) is found:

$$\hat{\gamma} = \frac{1}{2\pi}\sum_{m=-\infty}^{\infty} e^{im(\phi-\phi_o)} \sum_{n=0}^{\infty} R_m(\mu_{mn}\rho) R_m(\mu_{mn}\rho_o)\, \hat{d}_{mn}\ (z^* - z_o^*, \omega^*) \tag{2.1.13}$$

with the definitions as given in appendix B. This result could be referred to appropriately as the Prandtl-Glauert space Green's function. The acoustic propagator is, then, from equation (2.1.7):

$$\hat{\Gamma} = \frac{1}{2\pi}\sum_{m=-\infty}^{\infty} e^{im(\phi-\phi_o)} \sum_{n=0}^{\infty} \mathcal{R}_m(\mu_{mn}\rho)\mathcal{R}_m(\mu_{mn}\rho_o) * \hat{D}_{mn}(z-z_o,\omega) \tag{2.1.14}$$

with

$$\hat{D}_{mn} = \frac{e^{-i\frac{M\omega}{1-M^2}(z-z_o)}}{\sqrt{1-M^2}} \hat{d}_{mn}(z^*-z^*_o,\omega^*)$$

$$= e^{-i\frac{M\omega}{1-M^2}(z-z_o)} \frac{e^{i\frac{\beta_{mn}}{1-M^2}|z-z_o|}}{2i\beta_{mn}} \tag{2.1.15}$$

where

$$\beta_{mn} = \sqrt{\omega^2-(1-M^2)\mu^2_{mn}} \tag{2.1.16}$$

and β_{mn} has the same properties as a function of ω that s_{mn} has a function of ω^* (see appendix B), but with different branch points.

An alternative way of expressing $\hat{D}_{mn}$ is

$$\hat{D}_{mn} = \hat{D}^+_{mn} + \hat{D}^-_{mn} \tag{2.1.17}$$

with

$$\hat{D}^{\pm}_{mn} = \varepsilon(\pm(z-z_o))\ \frac{e^{iK^{\pm}_{mn}(z-z_o)}}{2i\beta_{mn}} \tag{2.1.18}$$

$$\varepsilon(X) = \begin{cases} 1, X>o \\ o, X<o \end{cases} \tag{2.1.19}$$

and

$$K^{\pm}_{mn} = \frac{-\omega M \pm \beta_{mn}}{1-M^2} \tag{2.1.20}$$

This makes explicit the distinction between downstream (+) and upstream (-) propagation.

Finally, the time-dependent propagator is given by

$$\Gamma(\vec{r},\vec{r}_o,\tau) = \frac{1}{2\pi}\sum_{m=-\infty}^{\infty} e^{im(\phi-\phi_o)} \sum_{n=-\infty}^{\infty} R_m(\mu_{mn}\rho) R_m(\mu_{mn}\rho_o) D_{mn}(z-z_o,\tau) \tag{2.1.21}$$

with

$$D_{mn} = \frac{1}{2\pi}\int_{-\infty}^{\infty} \hat{D}_{mn}(z-z_o,\omega) e^{-i\omega\tau} d\omega$$

$$= D^{+}_{mn} + D^{-}_{mn} \tag{2.1.22}$$

and

$$D^{\pm}_{mn} = \varepsilon\left(\tau \pm \frac{z-z_o}{1\pm M}\right) J_o\left(\mu_{mn}\sqrt{\tau^2-(z-z_o-M\tau)^2}\right) \tag{2.1.23}$$

This result follows from the discussion in Morse and Feshbach, chapter 2, (ref. 29), on the Klein-Gordon equation and the elastically braced string. This reference also is useful for understanding how the channeling by the duct walls results in the fluid being a dispersive medium for acoustic propagation. Otherwise, this result for D_{mn} can be found by converting the Fourier inversion to a Laplace inversion for causal functions, and looking up the result in a table of Laplace transforms (e.g., equation [29.3.92], p. 1027 of Abramowitz and Stegun, ref. 30).

2.2 Radiation from Dipoles in Ducts

The solution to equation (2.1.1) for a stationary dipole ($\vec{r}_s$ independent of time) is, from equations (2.1.4) and (2.1.14),

$$p(\vec{r},\tau) = \frac{1}{2\pi}\int_{-\infty}^{\infty} \hat{p}(\vec{r},\omega)e^{-i\omega t}d\omega$$

where

$$\hat{p}(\vec{r},\omega) = \hat{F}(\omega)\vec{e}\cdot\vec{\nabla}_s\hat{\Gamma}(\vec{r},\vec{r}_s,\omega)$$

$$= \frac{1}{2\pi}\sum_{m=-\infty}^{\infty}\sum_{n=o}^{\infty}\left[\varepsilon(z-z_s)A^{+}_{mn}(\omega)e^{iK^{+}_{mn}z}\right. \tag{2.2.1}$$

$$\left. + \varepsilon(z_s-z)A^{-}_{mn}(\omega)e^{iK^{-}_{mn}z}\right]\mathcal{R}_m(\mu_{mn}\rho)e^{im\phi}$$

with

$$A^{\pm}_{mn}(\omega) = -\hat{F}(\omega)\left[\frac{\frac{m}{\rho_s}e_\phi + K^{\pm}_{mn}e_z}{2\beta_{mn}}\right]\mathcal{R}_m(\mu_{mn}\rho_s)e^{-i(m\phi_s + K^{\pm}_{mn}z_s)} \tag{2.2.2}$$

These are the downstream or upstream mode amplitudes for a stationary dipole source. Since F(t) is a real function, it follows from the definition of β_{mn} (see the discussion of s_{mn} in appendix B) that $A^{\pm}_{mn}(\omega)$ has the symmetry property

$$A_{-\bar{m}n}^{\pm}(-\omega) = (A_{\bar{m}n}^{\pm}(\omega))^{\dagger} \cdot (-1)^{m} \tag{2.2.3}$$

allowing negative frequency mode amplitudes to be known in terms of positive frequency mode amplitudes. This symmetry guarantees that p(r,t) is real, and

$$p(\vec{r},t) = \frac{1}{2\pi} \int_{0}^{\infty} 2 \text{ REAL} \left[\hat{p}(\vec{r},\omega) e^{-i\omega t} \right] d\omega \tag{2.2.4}$$

When the same dipole is rotating at the constant rotational frequency Ω while maintaining its orientation with respect to the local cylindrical coordinate triad, its position vector, $\vec{r}_s$, becomes time-dependent,

$$\vec{r}_s = \left\{ \rho_s, \phi_s(t), z_s \right\}$$

with

$$\phi_s(t) = \Omega t + \bar{\phi} - 2\pi, \ell = -\infty, \cdots o, \cdots, +\infty \tag{2.2.5}$$

where ℓ is the revolution counter and $\bar{\phi}$ is the angle coordinate of the dipole for $\ell = 0$ and $t = 0$. Then,

$$F(t) \longrightarrow F(\phi(t),t) = F(t) \sum_{\ell=-\infty}^{\infty} \delta(\phi - \Omega t + \bar{\phi} + 2\pi\ell) \tag{2.2.6}$$

and the pressure field of this rotating dipole is given by

$$p(r,t) = \int_{-\infty}^{\infty}\int_{o}^{2\pi} F\left(\phi_o(t_o),t_o\right) \vec{e}\cdot\vec{\nabla}_o \Gamma(\vec{r},\vec{r}_o,t-t_o)\Big|_{\substack{\rho_o=\rho_s \\ z_o=z_s}} d\phi_o dt_o$$

$$= \frac{1}{2\pi}\sum_{m=-\infty}^{\infty}\sum_{n=o}^{\infty} \mathcal{R}_m(\mu_{mn}\rho)\mathcal{R}_m(\mu_{mn}\rho_o)\, e^{im\phi}$$

$$*\sum_{\ell=-\infty}^{\infty}\int_{-\infty}^{\infty}\int_{o}^{2\pi} \delta\,(\phi_o-\Omega t_o-\phi+2\pi\ell)F(t_o)$$

$$* \left[-e_\phi \frac{im}{\rho_s} D_{mn}(z-z_s,t) + \frac{\partial D_{mn}(z-z_s,t)}{\partial z_s} e_z\right] e^{im\phi_o}\, d\phi_o dt_o \qquad (2.2.7)$$

The evaluation of this expression is performed in appendix C. The result is, for the pressure spectral density downstream and upstream, (±), respectively,

$$\hat{p}^{\pm}(\vec{r},\omega) = \frac{1}{2\pi}\sum_{m=-\infty}^{\infty}\sum_{n=o}^{\infty} A^{\pm}_{mn}(\omega)\mathcal{R}_m(\mu_{mn}\rho)e^{i(m\phi + K^{\pm}_{mn}z)} \qquad (2.2.8)$$

with

$$A^{\pm}_{mn}(\omega) = -\hat{F}(\omega - m\Omega)\left[\frac{\frac{m}{\rho_s}e_\phi + K^{\pm}_{mn}e_z}{2\beta_{mn}}\right]\mathcal{R}_m(\mu_{mn}\rho_s)e^{i(m\bar{\phi} + K^{\pm}_{mn}z_s)} \tag{2.2.9}$$

The same symmetry property prevails, as it must, but there are two differences from the mode amplitudes for a stationary dipole: $\bar{\phi}$ is the angle coordinate for the dipole location in the reference frame rotating with the dipole, and the dipole spectral density is shifted differently for each spinning mode (m is the spinning mode index).

The pressure field of a stationary surface distribution of dipoles is the sum of the individual dipoles associated with each infinitesimal area of the surface. Letting

$$\hat{F}(\omega) \rightarrow \hat{F}(\rho_s, \xi(\phi_s, z_s), \omega) \tag{2.2.10}$$

be the dipole surface density spectral density, where it is assumed that the surface extends from the inner to the outer duct wall and for each radius the lateral extent of the surface projection onto a duct cross section is sufficiently small so that a straight line can replace the arc (see fig. 2). The surface can then be taken to be made up of different straight line segments having projections on ϕ and z, but not on ρ which are strung together from inner to outer duct radius, i.e., a fan blade whose surface is, at each span segment, approximated by its chord line. If $\vec{e} = \{o, e_\phi, e_z\}$ is the unit vector normal to the surface for a given radius, then the local rectangular coordinates are ξ, ζ, where (see fig. 2)

$$\xi = -\rho_s\phi'_s e_z + z'_s e_\phi$$

$$\zeta = \rho_s\phi'_s e_\phi + z'_s e_z \tag{2.2.11}$$

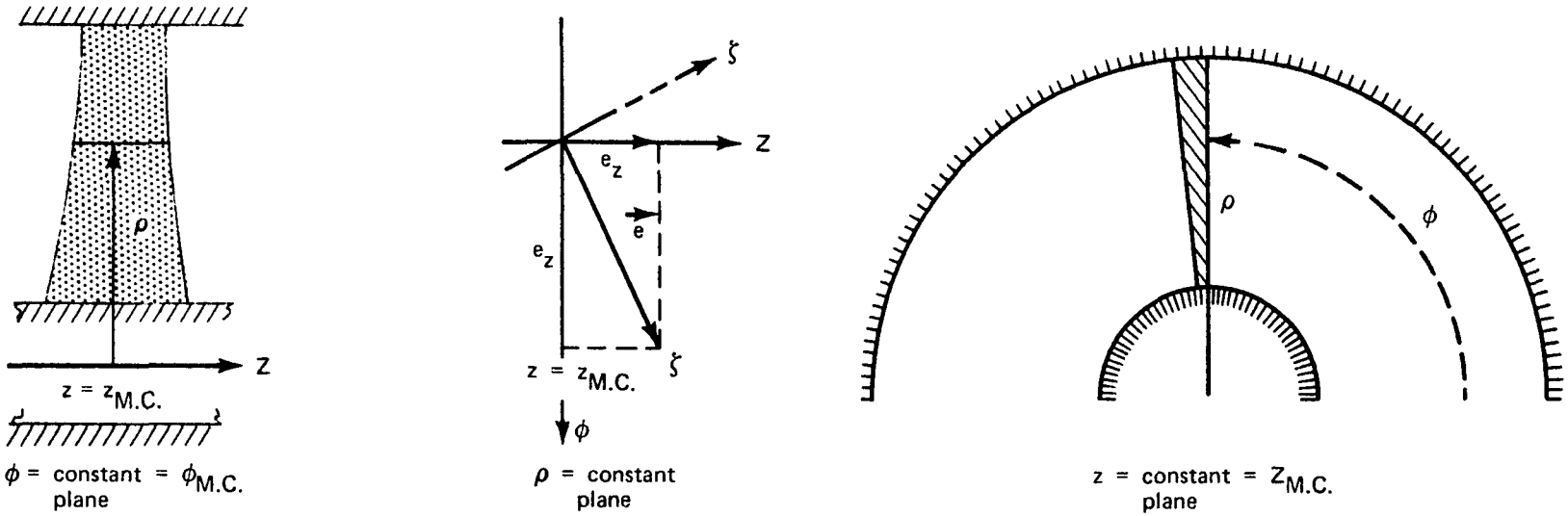

FIGURE 2. – DIPOLE SURFACE GEOMETRY

and

$$z'_s = \zeta e_z + \xi e_\phi$$

$$\rho_s \phi'_s = \zeta e_\phi - \xi e_z \qquad (2.2.12)$$

with

$$\phi_s = \phi_{M.C.} + \phi'_s$$

$$z_s = z_{M.C.} + z'_s \qquad (2.2.13)$$

where $\phi_{M.C.}$, $z_{M.C.}$ are the midchord coordinates at the radial station, ρ_s. The phase factor in the expression for $A^{\pm}_{mn}$ in equation (2.2.2) becomes

$$e^{-i\,(m\phi_s + K^{\pm}_{mn} z_s)} = e^{-i\,(m\phi_{M.C.} + K^{\pm}_{mn} z_{M.C.})}\; e^{-i\,(K^{\pm}_{mn} e_\phi - \frac{m}{\rho_s} e_z)\xi} \qquad (2.2.14)$$

when evaluated at $\zeta = 0$, i.e., on the chord line. Hence, the mode amplitude to be used in the expansion for the pressure radiated by this distribution of dipoles is

$$A^{\pm}_{mn}(\omega) = -\frac{e^{-i(m\phi_{M.C.} + K^{\pm}_{mn} z_{M.C.})}}{2\beta_{mn}} \int_\eta^1 \left[e_\phi \frac{m}{\rho_s} + e_z K^{\pm}_{mn} \right] \mathcal{R}_m (\mu_{mn}\rho_s)$$

$$* \int_{-c/2}^{c/2} \hat{F}(\rho_s, \xi, \omega) e^{-i\,(K^{\pm}_{mn} e_\phi - \frac{m}{\rho_s} e_z)\,\xi}\, d\xi d\rho_s \qquad (2.2.15)$$

with c the lateral extent of the surface at the radius, ρ_s, i.e., the chord of the equivalent blade segment. When there are N such surfaces equispaced about the annulus with the same $z_{M.C.}$ but with

$$\phi_{M.C.} \to \phi_j = \frac{2\pi j}{N} \qquad (2.2.16)$$

and

$$\hat{F} \rightarrow \hat{F}_j,$$

then

$$A^{\pm}_{mn}(\omega) = \sum_{j=o}^{N-1} A^{\pm}_{mnj}(\omega)$$

$$= -\frac{e^{-iK^{\pm}_{mn} z_{M.C.}}}{2\beta_{mn}} \int_{\eta}^{1} \left[e_{\phi} \frac{m}{\rho_s} + e_z K^{\pm}_{mn} \right] \mathcal{R}_m (\mu_{mn} \rho_s) \qquad (2.2.17)$$

$$* \frac{c}{2} \int_{-1}^{1} \left\{ \sum_{j=o}^{N-1} e^{-im\frac{2\pi j}{N}} \hat{F}_j (\rho_s, \xi', \omega) \right\} e^{-i\kappa^{\pm}_{mn} \xi'} d\xi', d\rho_s$$

with $\xi' = \xi/c/2$ and

$$\kappa^{\pm}_{mn} = \left[K^{\pm}_{mn} e_{\phi} - \frac{m}{\rho_s} e_z \right] \frac{c}{2} \qquad (2.2.18)$$

Similarly, for a rotating set of surfaces

$$A^{\pm}_{mn}(\omega) = -\frac{e^{-i\kappa^{\pm}_{mn} z_{M.C.}}}{2\beta_{mn}} \int_{\eta}^{1} \left[\frac{m}{\rho_s} e_{\phi} + K^{\pm}_{mn} e_z \right] \mathcal{R}_m (\mu_{mn} \rho_s)$$

$$* \frac{c}{2} \int_{-1}^{1} \left\{ \sum_{j=o}^{N-1} e^{-im\frac{2\pi j}{N}} \hat{F}_j \left(\rho_s, \xi', \omega - m\Omega\right) \right\}$$

$$* e^{-i\kappa_{mn}^{\pm} \xi'} d\xi' d\rho_s \qquad (2.2.19)$$

2.3 The Dipole Surface-Density Function

The dipole surface-density functions are the pressure difference functions of thin airfoil theory and must be determined from the condition that the normal velocities at the airfoil surfaces vanish. When the blades comprising a fan or compressor blade row are unstaggered, flat plates, a precise formulation in terms of a set of integral equations can be made (see appendix D). A similar formulation for a blade row which performs a net turning of the mean flow is as yet unavailable (see Atassi and Goldstein, ref. 31, for a linear formulation for the unsteady lift with finite camber and angle of attack of a single two-dimensional airfoil). It was not, however, the intention of this work to develop this formulation and seek solutions within it. The intention was to recognize the basic requirements for such a formulation and seek means of approximately satisfying these requirements. The basic requirement is that the incident velocity perturbations normal to the blade surfaces should be cancelled by the induced velocities of the ducted blade row. The approximations to the satisfaction of this requirement are determined by the available aerodynamic calculations and the form of the result of these calculations. It is desired that the result be in the form of known mathematical functions or numerical routines the evaluation of which is not much more cumbersome than the evaluation of known functions. A further requirement is that the approximations should be consistently employed. The approximation used in this work is that the incident normal velocities are cancelled by the velocities induced in an incompressible fluid neglecting three-dimensional effects, the presence of the other blades in the row, and the duct walls (see appendix D). In particular, the calculations of Sears (ref. 32), Kemp (ref. 33), Horlock (ref. 34), Naumann and Yeh (ref. 35), and Filotas (ref. 36) are used. The mean

flow conditions are assumed to be those through the staggered row (see fig. 3). The general form for the dipole surface-density function is, then,

$$\hat{F}_j\ (\rho_s, \xi', \omega) = \frac{dC_L}{d\alpha} M_M \hat{u}_j (\rho_s, z_s, \omega)\ \frac{1}{\pi} \hat{H} (\rho_s, \xi', \omega) \tag{2.3.1}$$

where:

M_M = mean nondimensionalized velocity through the row,

$\hat{u}_j$ = spectral density of the normal velocity perturbation incident on the j^{th} blade

$\frac{1}{\pi} \hat{H}$ = nondimensional dipole surface-density response function for convected, harmonic gusts

Of the models to be considered, only the potential field blade row interaction model does not make use of the assumption that the incident velocities can be taken to be "frozen-convected gusts." Under this assumption, $\hat{u}_j\ (\rho_s, z_s, \omega)$ is taken to be independent of ξ', i.e., its variation over the chord of the airfoil is negligibly small and $z_s \simeq z_{M.C.}$, or some other appropriate value such as the axial coordinate of the point on the airfoil one-quarter chord from the leading edge (see Sears, ref. 32). The item $dC_L/d\alpha$ is the slope of the steady lift versus angle of attack curve, which for a flat, two-dimensional airfoil is 2π. The use of $dC_L/d\alpha$ instead of 2π arose from the quasi-steady lift considerations: if low-frequency sound pressure is proportional to the section unsteady lift, and

$$\frac{1}{\pi} \int_{-1}^{1} \hat{H} (\rho_s, \xi', \omega)\ d\xi' \underset{\omega \approx 0}{\rightarrow} 1,$$

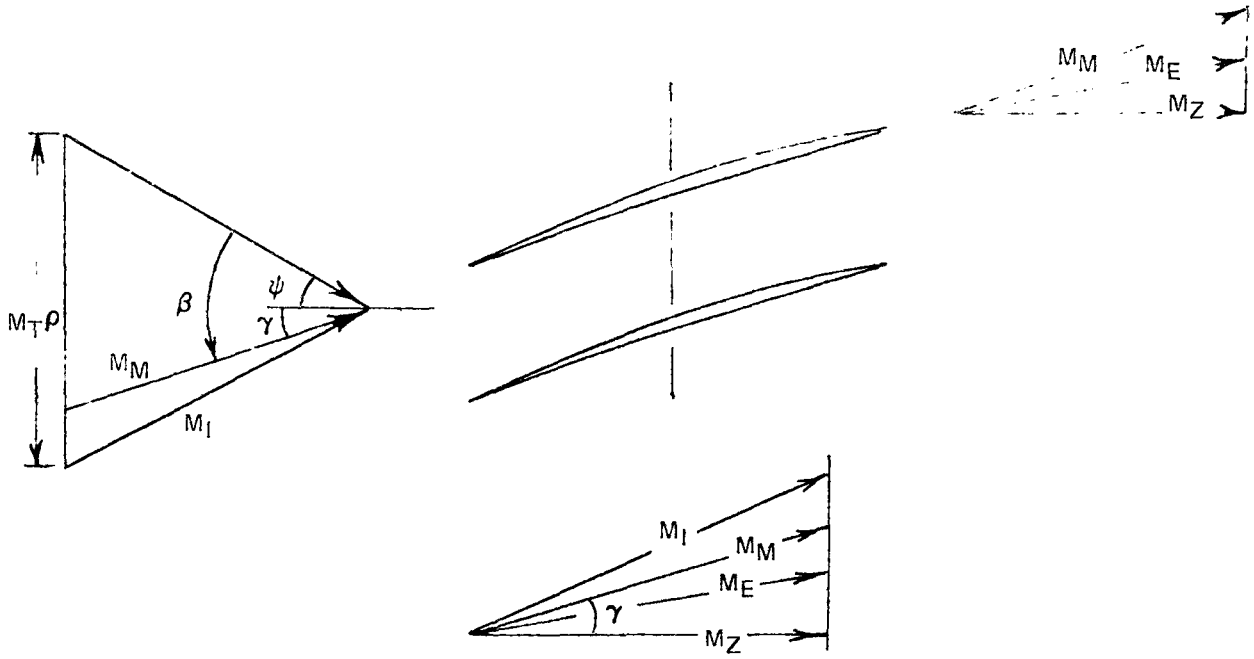

FIGURE 3. – MEAN FLOW THROUGH STAGGERED ROW

then

$$\delta L \simeq \frac{1}{2} c M_M^2 \frac{dC_L}{d\alpha} \delta\alpha$$

with

$$\delta\alpha \approx \frac{\hat{u}}{M_M}$$

where:

δL = section lift variation

$\delta\alpha$ = angle of attack variation .

3.0 MODELS FOR TONE NOISE GENERATION

The four models discussed in this section are referred to as the viscous wake interaction model, the potential field interaction model, the rotor in steady distortion model, and the rotor in nonsteady distortion model (or the "single eddy" model). A model consists of defining the $\hat{u}_j$ in equation (2.3.1) along with appropriate $\hat{H}$. Lifting-line models result when the $\kappa_{mn}^{\pm}$ in the chordwise integration is taken to be zero. The potential field interaction model is a lifting-line model, while the other models include the lifting-line assumption as an option. Assuming a lifting line is equivalent to assuming the blade is a chordwise compact acoustic source. It is felt, in turn, that a first order model for a chordwise noncompact airfoil is achieved by not setting $\kappa_{mn}^{\pm}$ equal to zero. Higher order estimates will include compressibility in the dipole surface-density function, which means including the effects of the other blades in the row and the duct walls as well as the propagation of pressure waves from one part of the airfoil to another.

The specific results of each model will be an analytical procedure for computing the mode amplitudes of the pressure radiated by a single component of a fan stage, i.e., equation (2.2.17) or equation (2.2.19), with a specification of the chordwise integral

$$\frac{c}{2}\int_{-1}^{1}\left\{\sum_{j=o}^{N-1} e^{-im\frac{2\pi j}{N}}\hat{F}_j\,(\rho_s,\xi',\omega)\right\} e^{-i\kappa_{mn}^{\pm}\xi'}\,d\xi' \qquad (3.0.1)$$

or, in the lifting-line models,

$$\sum_{j=o}^{N-1} e^{-im\frac{2\pi j}{N}}\hat{L}_j\,(\rho_s,\omega) \qquad (3.0.2)$$

where

$$\hat{L}_j(\rho_s,\omega) = \frac{c}{2}\int_{-1}^{1} \hat{F}_j(\rho_s,\xi',\omega)\, d\xi' \qquad (3.0.3)$$

3.1 The Viscous Wake Interaction Model

In an ideal axial flow fan or compressor stage, the inlet flow and exit flow are axial. To achieve this requires at least two components--a rotor and a stator. Viscous wake interactions occur when a rotor cuts through the viscous wakes from the blades of an upstream stator and when the viscous wakes from an upstream rotor sweep by the blades of a stator. These possibilities are given a two-dimensional cascade representation in figures 4 and 5. Consider first the inlet stator-rotor configuration (fig. 4). Since the wake defect will be known in the primed coordinate system attached to the inlet stator blades, it is necessary to determine the transformation from this coordinate system to the system attached to the rotor blades (the "bar-primed" coordinates of fig. 4). This transformation is (subscript 1 is for upstream row and subscript 2 is for downstream row)

$$\begin{aligned} Z' &= \bar{Z}' \cos\beta + \bar{Y}' \sin\beta + d\cos\psi + Ut\sin\psi \\ Y' &= \bar{Z}' \sin\beta + \bar{Y}' \cos\beta - d\sin\psi + Ut\cos\psi \end{aligned} \qquad (3.1.1)$$

Then the coordinates for the ℓ^{th} wake in the j^{th} rotor blade coordinate system are

$$\begin{aligned} Z'_{\ell j} &= \bar{Z}'_j \cos\beta + \bar{Y}'_j \sin\beta + d\cos\psi + Ut\sin\psi + (j\,b_2 - \ell b_1)\sin\psi \\ \bar{Y}'_{\ell j} &= -\bar{Z}'_j \sin\beta + \bar{Y}'_j \cos\beta - d\sin\psi + Ut\cos\psi + (jb_2 - \ell b_1)\cos\psi \end{aligned} \qquad (3.1.2)$$

where all the symbols correspond to those used in figure 4 and:

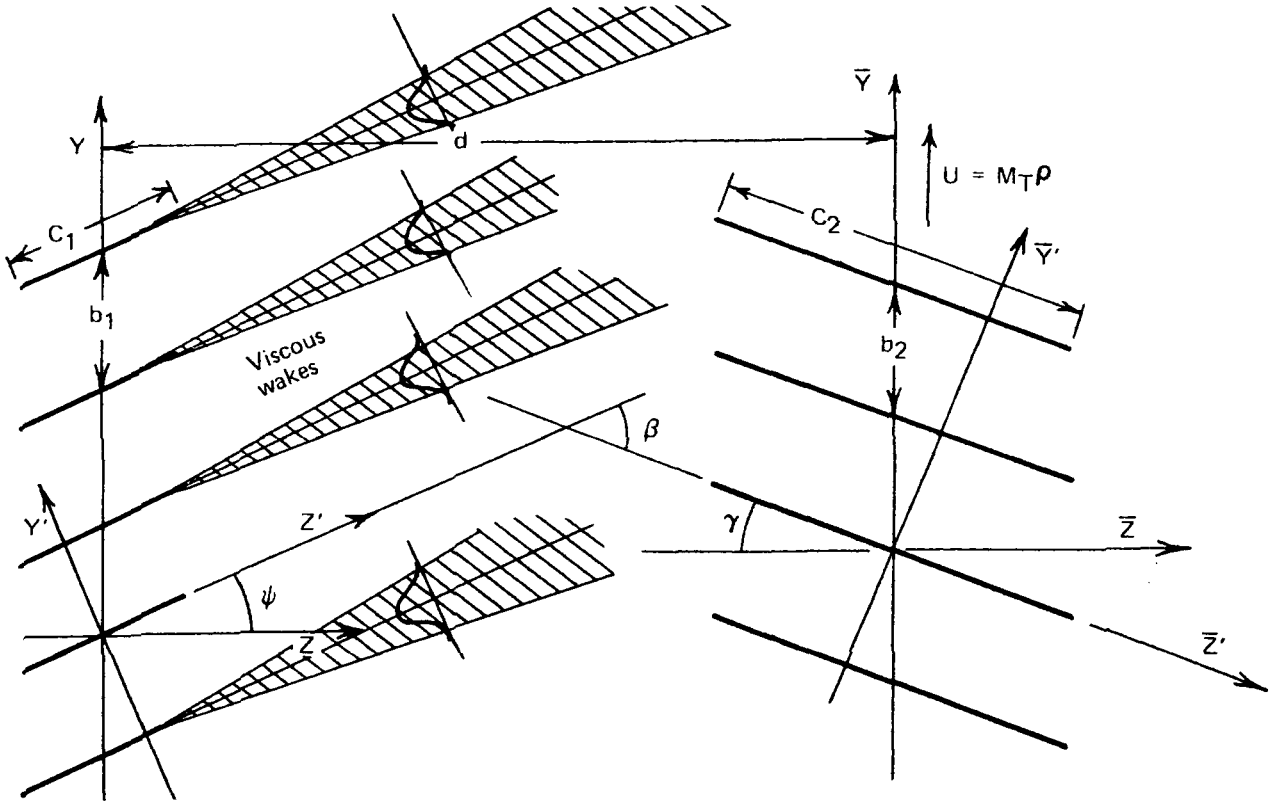

FIGURE 4. CASCADE REPRESENTATION OF INLET STATOR ROTOR COMBINATION

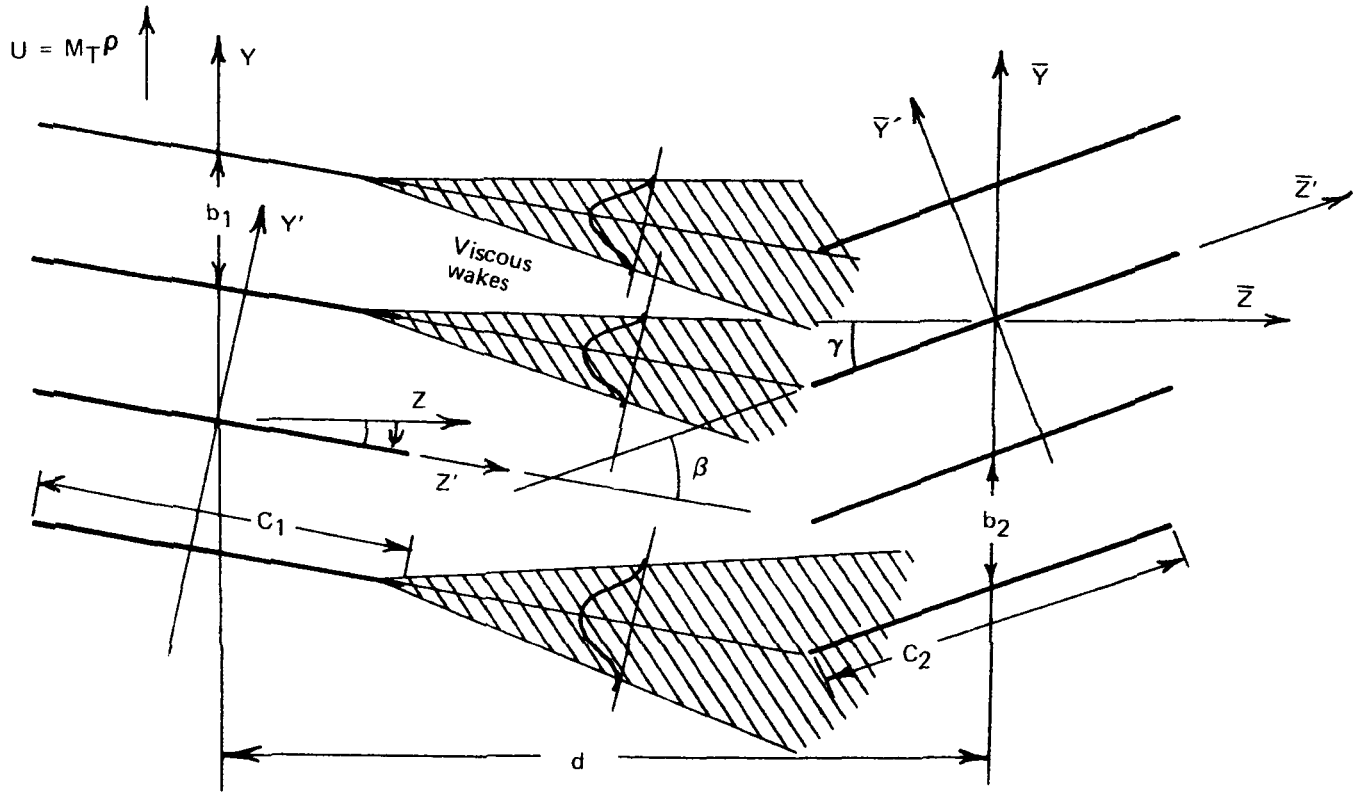

FIGURE 5. – CASCADE REPRESENTATION OF ROTOR OUTLET STATOR COMBINATION

U =

rotor blade nondimensionalized speed equal to $M_T\rho$

M_T =

rotor blade tip nondimensionalized speed

β = relative stagger angle, $\gamma + \psi$

γ = rotor blade row stagger angle,

ψ = exit angle of the stator row.

If N_1 is the number of blades in the upstream row, the stator row, and N_2 is the number of blades in the downstream row, the rotor row, then

$$b_1 = 2\pi\rho/N_1$$

and

$$b_2 = 2\pi\rho/N_2 \tag{3.1.3}$$

Representing the wake defect velocity behind the ℓ^{th} stator blade in the j^{th} rotor blade coordinates by $W_{\ell j}$ and assuming it can be developed in a double spatial Fourier integral, then

$$W_{\ell j} = \iint_{-\infty}^{\infty} \frac{d\lambda}{2\pi} \frac{dK}{2\pi} \bar{\bar{W}}(K,\lambda) e^{i\,(KY'_{\ell j} + \lambda Z'_{\ell j})} \tag{3.1.4}$$

and the velocity due to all the stator blades is

$$W_j = \sum_{\ell=-\infty}^{\infty} W_{\ell j}$$

$$= \iint_{-\infty}^{\infty} \frac{d\lambda}{2\pi} \frac{dK}{2\pi}\ \bar{\bar{W}}(K,\lambda) \sum_{\ell=-\infty}^{\infty} e^{i(KY'_{\ell j} + \lambda Z'_{\ell j})} \tag{3.1.5}$$

(3.1.5) cont.

$$= \int_{-\infty}^{\infty}\int_{-\infty}^{\infty} \frac{d\lambda}{2\pi}\frac{dK}{2\pi} \overline{\overline{W}}(K,\lambda) e^{iK\left[-\bar{Z}'_j \,SIN\beta + \bar{Y}'_j COS\beta - dSIN\psi + UtCOS\psi\right]}$$

$$* e^{i\lambda\left[\bar{Z}'_j COS\beta + \bar{Y}'_j SIN\beta + dCOS\psi + UtSIN\psi\right]}$$

$$* e^{i\left[KCOS\psi + \lambda SIN\psi\right] jb_2}$$

$$* \sum_{\ell=-\infty}^{\infty} e^{-i\ell b_1\left[KCOS\psi + \lambda SIN\psi\right]}$$

From the Poisson sum rule

$$\frac{1}{2\pi}\sum_{\ell=-\infty}^{\infty} e^{-i\ell b_1\left[KCOS\psi + \lambda SIN\psi\right]} = \frac{1}{b_1 COS\psi}\sum_{n=-\infty}^{\infty}\delta\left[K-\left(\frac{2\pi n}{b_1 COS\psi} - \lambda TAN\psi\right)\right] \tag{3.1.6}$$

so that the velocity at the surface of the j^{th} rotor blade is

$$W_j\left(\bar{Y}'_j = 0\right) = \frac{1}{b_1 COS\psi}\sum_{n=-\infty}^{\infty} e^{2\pi i n j \frac{b_2}{b_1}} e^{-2\pi i n \frac{dTAN\psi}{b_1}} \tag{3.1.7}$$

(3.1.7) cont.

$$*e^{-2\pi i \frac{n}{b_1 COS\psi}(\overline{Z}'_j SIN\beta - UtCOS\psi)}$$

$$*\int_{-\infty}^{\infty}\frac{d\lambda}{2\pi}\,\overline{\overline{W}}\left(\frac{2\pi n}{b_1 COS\psi} - \lambda TAN\psi, \lambda\right)e^{i\lambda\frac{d+\overline{Z}'_j COS\gamma}{COS\psi}}$$

If the stator wakes do not decay too rapidly along Z', then $\overline{\overline{W}}(K,\lambda)$ will be concentrated in a narrow bandwidth about $\lambda = 0$. Then, if ψ is not close to $\pi/2$ the tan ψ term in the K-dependence of $\overline{\overline{W}}$ can be dropped, giving for the λ integral,

$$\int_{-\infty}^{\infty}\frac{d\lambda}{2\pi}\,\overline{\overline{W}}\left(\frac{2\pi n}{b_1 COS\psi} - \lambda TAN\psi, \lambda\right)e^{i\lambda\frac{d+\overline{Z}'_j COS\gamma}{COS\psi}}$$

$$\approx\int_{-\infty}^{\infty}\frac{d\lambda}{2\pi}\,\overline{\overline{W}}\left(\frac{2\pi n}{b_1 COS\psi}, \lambda\right)e^{i\lambda Z'}$$

$$= \overline{W}\left(\frac{2\pi n}{b_1 COS\psi}, Z'\right) \qquad (3.1.8)$$

where Z' is the same for all blades and is the distance from the stator midchord to the axial plane cutting through the rotor blade quarter chord (see the discussion after equation [2.3.1]) as measured along the mean streamlines from the stator row (see fig.4).

Then, when b_1 and b_2 from equation (3.1.3) are used,

$$W_j\left(\bar{Y}'_j = o\right) = \frac{1}{2\pi}\frac{N_1}{\rho COS\psi}\sum_{n=-\infty}^{\infty}\bar{W}\left(\frac{nN_1}{\rho COS\psi}, Z'\right)$$

$$*e^{inN_1\frac{2\pi j}{N_2}}\ e^{-inN_1\frac{dSIN\psi}{\rho COS\psi}} \qquad (3.1.9)$$

$$*e^{-inN_1\frac{SIN\beta}{\rho COS\psi}(\bar{Z}'_j - Vt)}$$

with $$V = \frac{UCOS\beta}{SIN\psi} \qquad (3.1.10)$$

This velocity perturbation on the j^{th} rotor blade is thus a sum of frozen-convected harmonic gusts, with $\hat{u}_j$ given by

$$\hat{u}_j\left(\rho_s, z', \omega\right) = SIN\beta\int_{-\infty}^{\infty} W_j\left(\bar{Y}'_j = o, \bar{Z}'_j = o\right)\ e^{i\omega t}dt$$

(3.1.11)

$$= \sum_{n=-\infty}^{\infty}\frac{N_1}{\rho_s}\frac{SIN\beta}{COS\psi}\bar{W}\left(\frac{nN_1}{\rho COS\psi}, Z'\right)e^{inN_1\frac{2\pi j}{N_2}}$$

$$e^{-inN_1\frac{dTAN\psi}{\rho}}\ \delta(\omega + nN_1M_T)$$

This form for W_j justifies the use of the pressure difference function induced by frozen-convected harmonic gusts given in reference 35 (see equation [26]of this reference) for the nondimensional dipole surface-density response function (with $\xi' = -\cos\theta$)

$$\hat{H}(\rho_s,\xi',\omega) = S(\nu)\ \mathrm{COT}\frac{\theta}{2} - \mathrm{COT}\beta\left[\alpha\mathrm{COT}\frac{\theta}{2}\, e^{i\nu\cos\theta}\right. \tag{3.1.12}$$

$$\left. + f\left\{F(\nu)\mathrm{COT}\frac{\theta}{2} + 2\,\mathrm{SIN}\theta\, e^{i\nu\cos\theta} + \frac{4}{\nu}\sum_{k=1}^{\infty} i^{k-1}J_k(\nu)\ \mathrm{SIN}k\theta\right\}\right]$$

with the reduced frequency defined by

$$\nu = \frac{\omega}{V}\frac{c_2}{2} \tag{3.1.13}$$

and $S(\nu)$ is the Sears function

$$S(\nu) = -\frac{1}{\frac{\pi\nu}{2}\left(-H_o^{(2)}(\nu) + iH_1^{(2)}(\nu)\right)} \tag{3.1.14}$$

and $F(\nu)$ is defined by

$$F(\nu) = T(\nu)\left[J^*(\nu) - \frac{J_1(\nu)}{\nu}\right] - J(\nu) + \frac{J_1(\nu)}{\nu} \tag{3.1.15}$$

with

$$J(\nu) = J_o(\nu) + iJ_1(\nu) \tag{3.1.16}$$

and

$$T(\nu) = \frac{H_0^{(2)}(\nu) + i\, H_1^{(2)}(\nu)}{-H_0^{(2)}(\nu) + i\, H_1^{(2)}(\nu)} \tag{3.1.17}$$

and $H_0^{(2)}$, $H_1^{(2)}$ are the Hankel functions of the second kind. The chordwise integration gives the acoustic response function of the airfoil span section

$$\frac{1}{\pi}\int_{-1}^{1} \hat{H}(\rho_s, \xi', \omega)\; e^{-i\kappa_{mn}^{\pm}\xi'}\, d\xi' = S(\nu)\; J\left(\kappa_{mn}^{\pm}\right)$$

$$-\cot\beta\left[\alpha\; J(\nu + \kappa_{mn}^{\pm}) + f\left\{F(\nu)\; J\left(\kappa_{mn}^{\pm}\right) + \frac{2\, J_1(\nu + \kappa_{mn}^{\pm})}{\nu + \kappa_{mn}^{\pm}}\right.\right.$$

$$\left.\left.\frac{2}{\nu}\sum_{k=1}^{\infty}(-1)^k J_k(\nu)\;\left\{J_{k+1}\left(\kappa_{mn}^{\pm}\right) + J_{k-1}\left(\kappa_{mn}^{\pm}\right)\right\}\right\}\right] \tag{3.1.18}$$

The section lift response is from (equation [27] of ref.35):

$$\frac{1}{\pi}\int_{-1}^{1} \hat{H}\;(\rho_s, \xi', \omega)\; d\xi' = S(\nu) - \mathrm{COT}\;\beta\;\left[\alpha F_\alpha(\nu) + f\; F_f(\nu)\right] \tag{3.1.19}$$

with

$$F_\alpha(\nu) = J(\nu) \tag{3.1.20}$$

and

$$F_f(\nu) = F(\nu) + 4\frac{J_1(\nu)}{\nu} \tag{3.1.21}$$

In these formulas, α is the small angle of attack (in radians) and f is the ratio of maximum camber of a slightly cambered airfoil over the half-chord length (see fig. 6).

Combining these results with equation (2.3.1), the chordwise integration in equation (2.2.19) becomes (with $\Omega = M_T$)

$$\frac{c_2}{2}\int_{-1}^{1}\sum_{j=o}^{N-1} e^{-im\frac{2\pi j}{N_2}}\hat{F}_j(\rho_s,\xi',\omega - mM_T)\,e^{-i\kappa^{\pm}_{mn}\xi'}\,d\xi'$$

$$= \sum_{n=-\infty}^{\infty}\frac{c_2}{2}\frac{dC_{L2}}{d\alpha}M_{2M}\frac{N_1}{\rho_s}\frac{SIN\beta}{COS\psi}\bar{W}\left(\frac{nN_1}{\rho_s COS\psi},\ Z'\right)$$

$$*e^{-inN_1\frac{dTAN\psi}{\rho_s}}\frac{1}{\pi}\int_{-1}^{1}\hat{H}(\rho_s,\xi',\omega - mM_T)\,e^{-i\kappa^{\pm}_{mn}\xi'}\,d\xi'$$

$$*\sum_{j=o}^{N_2-1} e^{2\pi j\frac{nN_1-m}{N_2}}\ \delta(\omega - mM_T + nN_1M_T) \tag{3.1.22}$$

(See appendix E for a discussion of the d-dependent phase).

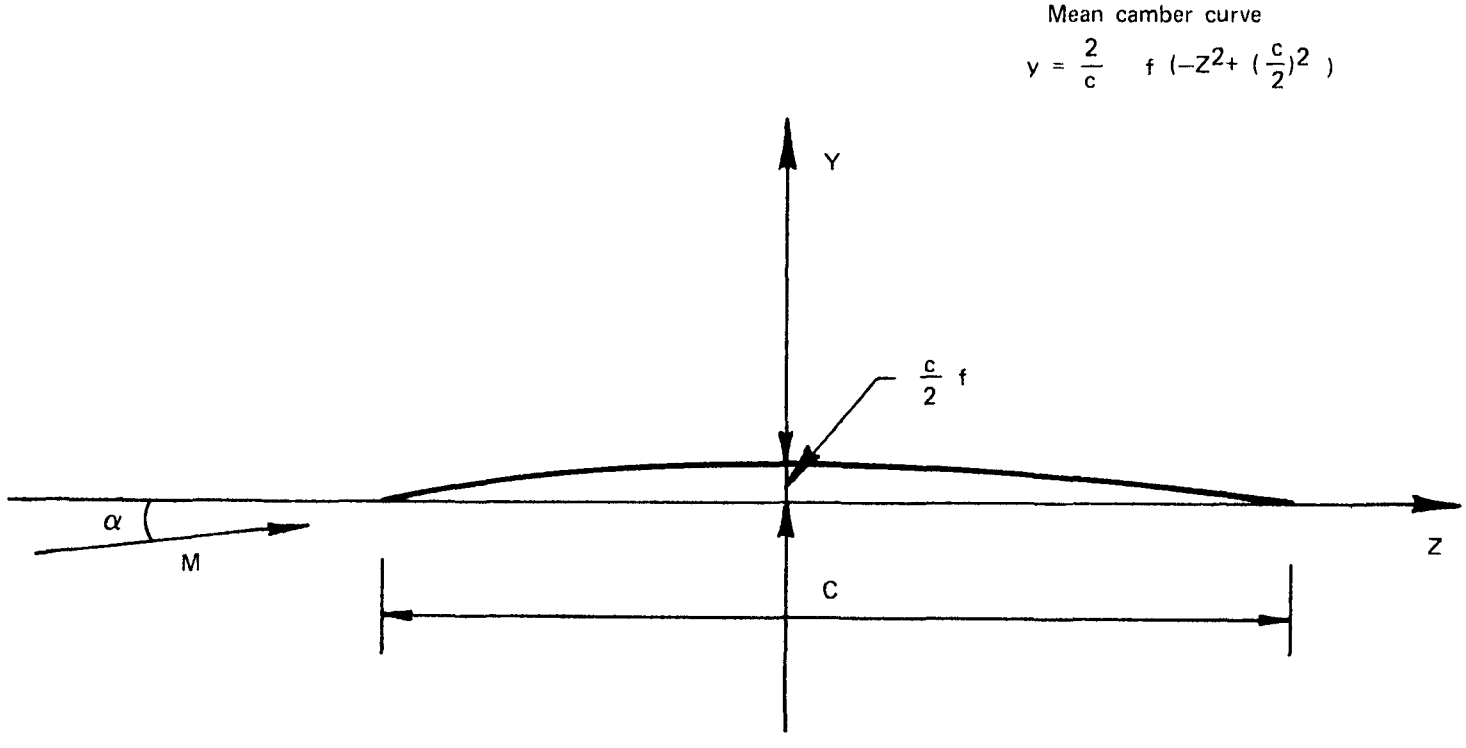

FIGURE 6. – THIN AIRFOIL WITH ANGLE OF ATTACK AND CAMBER

The sum on j can now be done:

$$\sum_{j=o}^{N_2-1} e^{2\pi j \frac{nN_1-m}{N_2}} = \begin{cases} N_2, \text{ FOR } nN_1 - m = -\sigma N_2, \sigma = o, \pm 1, \cdots \\ o, \text{ otherwise} \end{cases} \tag{3.1.23}$$

and gives new form for the right-hand side of equation (3.1.22), where $n \to \ell$ to avoid confusion with the mode amplitude n index,

$$\text{R.H.S.} = \frac{N_1 N_2}{\rho_s} \frac{c_2}{2} \frac{dC_{L2}}{d\alpha} M_{2M} \frac{\text{SIN}\beta}{\text{COS}\psi} \sum_{\ell=-\infty}^{\infty} \bar{W}\left(\frac{\ell N_1}{\rho_s \text{COS}\psi}, Z'\right) \tag{3.1.24}$$

$$* e^{-i\ell N_1 \frac{d\text{TAN}\psi}{\rho_s}} \delta(\omega - \sigma N_2 M_T) \left[S(\nu_\ell) J(\kappa^{\pm}_{mn}) \right.$$

$$- \cot\beta \left\{ \alpha J(\nu_\ell + \kappa^{\pm}_{mn}) + f \left\{ F(\nu_\ell) J(\kappa^{\pm}_{mn}) + \frac{2J_1(\nu_\ell + \kappa^{\pm}_{mn})}{\nu_\ell + \kappa^{\pm}_{mn}} \right.\right.$$

$$\left.\left.\left. - \frac{2}{\nu_\ell} \sum_{j=1}^{\infty} (-1)^j J_j(\nu_\ell) \{ J_{j+1}(\kappa^{\pm}_{mn}) + J_{j-1}(\kappa^{\pm}_{mn}) \} \right\} \right\} \right] \delta_{\ell N_1, m-\sigma N_2}$$

with

$$\nu_\ell = \ell N_1 \frac{M_T}{M_{2M}} \frac{c_2}{2} \tag{3.1.25}$$

where V is approximated by M_{2M}, and β by the sum, $\gamma + \psi$ (see fig. 3).

There remains to be defined the wake defect in terms of the primed coordinates of a typical stator blade, $W(Y', Z')$, in order to get

$$\overline{W}\ (K,Z') = \int_{-\infty}^{\infty} W(Y',Z')\ e^{-iKY'}\, dY' \tag{3.1.26}$$

The choice is made to use the empirical formulas of Silverstein, et al - (ref. 37):

$$W(Y',Z') = W_o(Z')\ \cos^2\left(\pi\ \frac{Y'}{Y_o}\right) \tag{3.1.27}$$

where

$$W_o(Z') = M_{1E}\ \frac{1.21\ \sqrt{C_{D1}}}{\frac{Z'}{c_1} - 0.2} \tag{3.1.28}$$

and $$Y_o(Z') = 1.36\sqrt{C_{D1}}\ c_1\sqrt{\frac{Z'}{c_1} - 0.35} \tag{3.1.29}$$

where:

C_{D1} = drag coefficient of the stator blade at ρ_s,

M_{1E} = exit velocity from the stator row at ρ_s,

c = stator blade chord at ρ_s.

These formulas give for

$$\bar{W}(K,Z') = \frac{W_o Y_o}{2} \frac{\text{SIN}\pi \frac{KY_o}{2\pi}}{\pi \frac{KY_o}{2\pi}} \frac{1}{1-\left(\frac{KY_o}{2\pi}\right)^2} \tag{3.1.30}$$

with

$$W_o Y_o = M_{1E}\ 1.65\ C_{D1}\ c_1 \sqrt{\frac{1}{\frac{Z'}{c_1} - 0.2} - \frac{0.15}{\left(\frac{Z'}{c_1} - 0.2\right)^2}} \tag{3.1.31}$$

and

$$\frac{K\ Y_o}{2\pi} = \ell \frac{Y_o}{2\pi\rho_s \text{COS}\psi/N_1} \tag{3.1.32}$$

from $K = \ell\ N_1/\rho_s \cos\psi$

This completes the specification of the mode amplitude calculation for the viscous wake interaction model with a rotor downstream of an inlet stator. The final formula is

$$A^{\pm}_{mn}(\omega) = -\frac{e^{-iK^{\pm}_{mn} z}\ M.C.}{\beta_{mn}} \frac{N_1 N_2}{8} \int_{\eta}^{1} \left[\frac{m}{\rho_s} e_\phi + K^{\pm}_{mn} e_z\right] \mathcal{R}_m(\mu_{mn}\rho_s)$$

$$* c_1 c_2 \frac{dC_{L2}}{d\alpha} M_{2M} M_{1E} \frac{\text{SIN}\beta}{\rho_s \text{COS}\ \psi} \Delta_o(Z')$$

$$* \Lambda_\ell\ e^{-i\ell N_1 \frac{d\text{TAN}\psi}{\rho_s}} G_{mn\ell}\ d\rho_s\ \delta\ (\omega - \sigma N_2 M_T) \tag{3.1.33}$$

with

$$\ell N_1 = m - \sigma N_2$$

$$e_\phi = \cos\gamma \tag{3.1.34}$$

$$e_z = \sin\gamma$$

$$\Delta_o = 1.65\ C_{D1} \sqrt{\frac{1}{\frac{Z'}{c_1} - 0.2} - \frac{0.15}{\left(\frac{Z'}{c_1} - 0.2\right)^2}} \tag{3.1.35}$$

$$\Lambda_\ell = \frac{\sin \pi \ell \frac{Y_o}{\delta}}{\pi \ell \frac{Y_o}{\delta}} \cdot \frac{1}{1 - \left(\ell \frac{Y_o}{\delta}\right)^2} \tag{3.1.36}$$

$$\delta = \frac{2\pi\rho_s \cos\psi}{N_1} \tag{3.1.37}$$

$$\sin\beta = \frac{M_{2z}}{M_{2M}\, M_{1E}} \left(\sqrt{M_{2M}^2 - M_{2z}^2} + \sqrt{M_{1E}^2 - M_{2z}^2}\right) \tag{3.1.38}$$

(see fig. 3) and,

$$G_{mn\ell} = S(\nu_\ell)\, J(\kappa^{\pm}_{mn}) - \cot\beta \left[\alpha\, J(\nu_\ell + \kappa^{\pm}_{mn}) + f\left\{F(\nu_\ell)\, J(\kappa^{\pm}_{mn}) + \frac{2\, J_1(\nu_\ell + \kappa^{\pm}_{mn})}{\nu_\ell + \kappa^{\pm}_{mn}} - \frac{2}{\nu_\ell} \sum_{j=1}^{\infty} (-1)^j\, J_j(\nu_\ell) \left\{J_{j+1}(\kappa^{\pm}_{mn}) + J_{j-1}(\kappa^{\pm}_{mn})\right\}\right\}\right] \tag{3.1.39}$$

The computer subprogram AAAAA (see section 3.1.1, volume II) computes the factor multiplying the frequency spike,

$$\delta(\omega - \sigma N_2 M_T), \quad \text{for } \omega \text{ in the propagating region.}$$

With subscript 1 referring to the *upstream rotor* and subscript 2 to the *downstream stator*, the same development for the viscous wake interaction model with a rotor and an outlet stator can be made, and gives for the mode amplitude

$$A^{\pm}_{mn}(\omega) = -\frac{e^{-iK^{\pm}_{mn} z_{M.C.}}}{\beta_{mn}} \frac{N_1 N_2}{8} \int_{\eta}^{1} \left[\frac{m}{\rho_s} e_{\phi} + \kappa^{\pm}_{mn} e_z\right] \qquad (3.1.40)$$

$$* \mathcal{R}_m(\mu_{mn}\rho_s) \; c_1 c_2 \frac{d C_{L2}}{d\alpha} M_{2M} M_{1E} \frac{\text{SIN}\beta}{\rho_s \text{COS}\psi}$$

$$* \sum_{\sigma} \Delta_0(Z') \Lambda_{\sigma} e^{-i\sigma N_1 \frac{d \text{TAN}\psi}{\rho_s}} G_{mn\sigma} d\rho_s \delta(\omega - \sigma N_1 M_T)$$

where:

$$e_{\phi} = -\text{COS}\,\gamma$$

$$e_z = \text{SIN}\,\gamma$$

and with the restriction that

$$m = \sigma N_1 + \ell N_2 \qquad (3.1.41)$$

Δ_o is given by equation (3.1.35), Λ_σ by equations (3.1.36) and (3.1.37), with $\ell \to \sigma$, and $G_{mn\sigma}$ is given by equation (3.1.38) with

$$\nu_\ell \to -\nu_\sigma = -\sigma N_1 \frac{M_T}{M_{2M}} \frac{c_2}{2} \tag{3.1.42}$$

The computer subprogram AAAAA computes the factor multiplying the frequency spike for ω in the propagating region.

3.2 The Potential Field Interaction Model

In the close vicinity of a blade row, the potential flow field is not uniform. This is due to the noncontinuous distribution of the aerodynamic forces that are exerted by the blades onto the medium. If an airfoil moves through this nonuniform flow field, it will experience unsteady lift forces. In this section, we are concerned with the interaction of a blade row with the potential flow field of another blade row. The analysis is based on the formulas developed by Kemp and Sears (ref. 4).

The following assumptions were made to compute the induced velocities at an airfoil resulting from the potential flow field of all the blades of an adjacent blade row.

- The flow through a rotor-stator combination is represented by nonviscous, incompressible flow through a two-dimensional cascade.

- The airfoils of both blade rows, the velocity inducing and the lift producing, are represented by vortex sheets.

- The steady vorticity representing a blade is located on a straight line, that is parallel to the mean flow velocity through the cascade and that has the length of the local blade chord.

- Only the unsteady lift forces resulting from the relative motion of an airfoil through the potential flow field of the steady vorticity of a blade row are considered. All unsteady lift forces resulting from secondary interactions are neglected.

- Only the transverse component of the induced velocity is considered in the computation of the unsteady lift.

Four different interactions are possible between the potential flow fields of a rotor-stator combination:

1) Rotor downstream of stator, unsteady lift induced at stator
2) Rotor downstream of stator, unsteady lift induced at rotor
3) Stator downstream of rotor, unsteady lift induced at rotor
4) Stator downstream of rotor, unsteady lift induced at stator

The analysis will be summarized for the first case, then the equations will be generalized so that they can be used for all four interactions. In reference 4 the following equation was derived for the induced, unsteady velocities at a stator blade located upstream of a moving rotor blade row:

$$W(z_1', t) = \frac{\Gamma_2}{\pi C_1} \sum_{\sigma=1}^{\infty} g_{\sigma,1} e^{\sigma N_2 \frac{z_1'}{\rho}} e^{-i\gamma_1} e^{i\sigma N_2 M_t t} \tag{3.2.1}$$

$$= \frac{\Gamma_2}{\pi C_1} \sum_{\sigma=1}^{\infty} g_{\sigma,1} e^{-i\mu_{G,1} \frac{z_1'}{M_{M,1}}} e^{i\omega_{G,1} t}$$

with

$$g_{\sigma,1} = \frac{C_1 N_2}{2\rho} \; e^{-i\gamma_1} \, Q_{\sigma,2} e^{-\sigma \frac{C_2 N_2}{2\rho} \left[\frac{2d}{C_2} \left(1 + i \tan\left(\gamma_2\right) - i \frac{\rho M_t}{M_{M,1} \cos\gamma_1} \right) - i \frac{\rho M_t}{M_{M,2}} \right]} \tag{3.2.2}$$

$$Q_{\sigma,2} = J_o \left[\frac{\sigma C_2}{2\rho} \; N_2 e^{i\left(\frac{\pi}{2} - \gamma_2\right)} \right] + \sum_{n=1}^{\infty} (-i)^n \frac{A_{n+1}^2 - A_{n-1}^2}{A_o^2 + A_1^2} \; J_n \left[\frac{\sigma C_2}{2\rho} N_2 e^{i\left(\frac{\pi}{2} - \gamma_2\right)} \right] \tag{3.2.3}$$

$$\Gamma 2 = \pi \; C_2 \; M_{M,2} \left(A_o^2 + A_1^2 \right) \tag{3.2.4}$$

$$\omega_{\sigma,1} = \sigma \; N_2 \; M_t \tag{3.2.5}$$

$$\mu_{\sigma,1} = \sigma \; N_2 \; \frac{M_{M,1}}{\rho} \; e^{i\left(\frac{\pi}{2} - \gamma_1\right)} \tag{3.2.6}$$

where:

$\omega_{\sigma,1}$	=	temporal frequency
$\mu_{\sigma,1}$	=	complex frequency of the chordwise velocity distribution
γ	=	stagger angle
c	=	chord length
d	=	midchord plane separation
M_M	=	mean relative flow velocity
A_n	=	Glauert coefficients of n^{th} order

Index 1 = stator parameter

Index 2 = rotor parameter

The Glauert coefficients are the coefficients used in the series representation of the steady vorticity of an airfoil introduced by Glauert (ref. 38).

The geometrical relationships upon which these equations are based are shown in figure 7. The unsteady, induced velocities described by equation (3.2.1) are characterized by two properties:

1) They decay exponentially with increasing distance from the source.

2) They are not medium bound and can, therefore, move at speeds different from the medium velocity.

For these reasons, they cannot be treated as frozen convected gusts.

Equation (3.2.1) defines the induced velocities only along the chord of the zeroth stator blade. A small modification of the term $g_{\sigma,1}$ will make it possible to compute W(z,t) at any point of the stator flow field.

$$g_{\sigma,1}(\gamma_1) = \frac{C_1 N_2}{2\rho} e^{-i\gamma_1} H_{\sigma,2} e^{-\sigma \frac{N_2}{\rho}\left[d\left(1 + i \tan\gamma_2 - i \frac{\rho M_t}{M_{M,1}\cos\gamma_1} - i \frac{\gamma_1'}{d} e^{-i\gamma_1}\right) - i \frac{C_2}{2} \frac{M_t \rho}{M_{M,2}}\right]}$$

(3.2.7)

The term $g_{\sigma,1}$ can be modified using the following approximation

$$-\tan\gamma_1 = \tan\gamma_2 - \frac{\rho M_t}{M_{M,1}\cos\gamma_1}$$

(3.2.8)

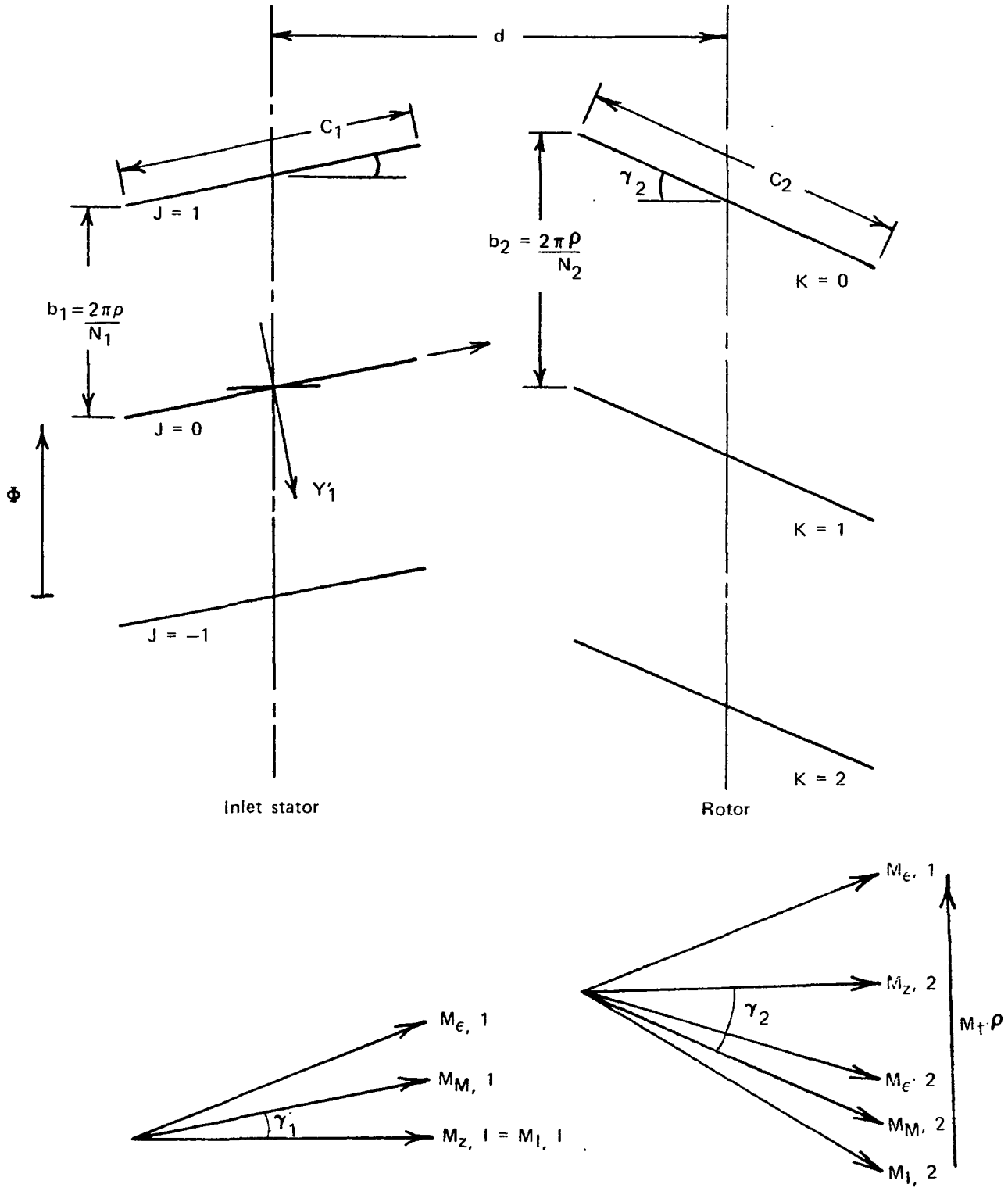

FIGURE 7. – CASCADE REPRESENTATION FOR THE POTENTIAL FIELD INTERACTION

$$g_{\sigma,1} = \frac{C_1}{2\rho} N_2 \, e^{-\sigma N_2 \frac{d}{\rho}} \, H_{\sigma,2} \, e^{-i\left[\gamma_1 - \sigma N_2\left(\frac{d}{\rho}\tan\gamma_1 + \frac{C_2}{2}\frac{M_t}{M_{M,2}}\right)\right]} \tag{3.2.9}$$

For the computation of the unsteady section lift we need to know the induced velocities at the midchord point. For the zeroth stator it is

$$W_1\left(Z_1' = o, t\right) = \frac{\Gamma_2}{\pi C_1} \sum_{\sigma=1}^{\infty} g_{\sigma,1} \, e^{i\sigma N_2 M_t t} \tag{3.2.10}$$

The midchord plane is defined by the relationship

$$Z_1' = -Y_1' \, \mathrm{TAN}\, \gamma_1 \tag{3.2.11}$$

and the induced velocities at its location are defined as follows:

$$W_1\left(Z_1', Y_1', t\right) = \frac{\Gamma_2}{\pi C_1} \sum_{\sigma=1}^{\infty} g_{\sigma,1} \, e^{i\sigma N_2 \frac{Y_1'}{\rho}} e^{-i\gamma_1} \, e^{-i\sigma N_2 \frac{Z_1'}{\rho}} e^{i\left(\frac{\pi}{2} - \gamma_1\right)} \, e^{i\omega_{\sigma,1} t}$$

$$= \frac{\Gamma_2}{\pi C_1} \sum_{\sigma=1}^{\infty} g_{\sigma,1} \, e^{i\sigma N_2 \frac{1}{\rho}\left[Y_1' e^{-i\gamma_1} - Z_1' e^{i\left(\frac{\pi}{2} - \gamma_1\right)}\right]} \, e^{i\omega_{\sigma,1} \cdot t}$$

$$= \frac{\Gamma_2}{\pi C_1} \sum_{\sigma=1}^{\infty} g_{\sigma,1} \, e^{i\sigma N_2 \frac{Y_1'}{\rho \cos\gamma_1}} \cdot e^{i\omega_{\sigma,1} \cdot t}$$

With the following definition of the blade separation distance, the induced velocity at the midchord of the j^{th} blade can be computed

$$\frac{Y_j'}{\cos \gamma_1} = - \frac{2\pi\rho}{N_1} j$$

(3.2.13)

$$W_j(t) = \frac{\Gamma_2}{\pi C_1} \sum_{\sigma=1}^{\infty} g_{\sigma,1} e^{-i\sigma N_2 \frac{2\pi}{N_1} j} e^{i\omega_{\sigma,1} t}$$

(3.2.14)

In reference 4 it is shown that for the transverse gust velocities described by equation (3.2.1), the lift response function K_L assumes the following form:

$$K_L(\nu_1, \lambda_1) = \left[J_o(\lambda_1) - i J_1(\lambda_1) \right] \frac{H_1^{(2)}(\nu_1)}{H_1^{(2)}(\nu_1) + i H_o^{(2)}(\nu_1)} + \frac{i\nu_1}{\lambda_1} J_1(\lambda_1)$$

(3.2.15)

$$\nu_1 = \frac{\omega C_1}{2 M_{M,1}} = \frac{M_t N_2 C_1}{2 M_{M,1}} \sigma$$

(3.2.16)

$$\lambda_1 = \frac{\mu C_1}{2 M_{M,1}} = N_2 \frac{C_1}{2\rho} \sigma e^{i\left(\frac{\pi}{2} - \gamma_1\right)}$$

(3.2.17)

where:

ν_1 = reduced frequency

λ_1 = reduced complex frequency of chordwise velocity distribution

J_0, J_1 = Bessel functions of the first kind

$H_o^{(2)}, H_1^{(2)}$ = Hankel functions of the second kind

Knowing the lift response function and the transverse gust velocity at the midchord point, the unsteady section lift can now be computed:

$$\ell_j = \frac{\Gamma_2 M_{M,1}}{2\pi} \left(\frac{dC_L}{d\alpha}\right)_1 \sum_{\sigma=1}^{\infty} g_{\sigma,1} \cdot K_L \left(\nu_{\sigma,1}, \lambda_{\sigma,1}\right) e^{-i\sigma N_2 \frac{2\pi j}{N_1}} e^{i\omega_{\sigma,1} t} \qquad (3.2.18)$$

The Kemp-Sears lift response function is referred to as K_L. If the imaginary part of λ_1 is equal to zero, and if the real part is equal to ν_1, then K_L becomes the Sears function. If the imaginary part of λ_1 is not equal to zero, it increases proportionally to σ and K_L, then diverges for large values σ because of the character of the Bessel functions. But, even then will the unsteady section lift assume finite values. This is due to the exponential decrease of the term $g_{\sigma,1}$ with increasing values of σ. It can be shown that the section lift remains finite for large values of σ, if the following restriction is satisfied:

$$\frac{1}{2}\left(C_1 \cos \gamma_1 + C_2 \cos \gamma_2\right) < d \qquad (3.2.19)$$

which indicates that the two interacting blade rows do not overlap, thus allowing relative motion.

If the amount of turning is small in each of two interacting blade rows — that is, if the relative inflow and exit flow angles of a blade row can be set equal to the stagger angle — then λ_1 can be approximated by the following equation:

$$\lambda = \nu \left(\frac{1. + i \cot \gamma_1}{1. + \tan \gamma_2 \cot \gamma_1} \right) \tag{3.2.20}$$

In this case, λ_1 is, therefore, only a function of ν_1 for a given combination of stagger angles. In figure 8, Kemp-Sears lift response functions are shown for three different combinations of stagger angles.

Due to the convention (see appendix A) used for the Fourier transformations, the complex conjugate of the section lift computed in equation (3.2.18) will be used in this analysis and the summation over σ is modified to extend from $-\infty$ to $+\infty$. The new formula for the unsteady section lift is therefore

$$L_j(\rho,t) = \frac{\Gamma_2 M_{M1}}{4\pi} \left(\frac{dC_L}{d\alpha} \right)_1 \sum_{\sigma=-\infty}^{\infty} G_{\sigma,1} K_{\sigma,1} e^{i\sigma N_2 \frac{2\pi j}{N_1}} e^{-i\omega_{\sigma,1} t} \tag{3.2.21}$$

with

$$K_{\sigma,1} = \begin{cases} \left[K_L \left(\nu_{\sigma,1}, \lambda_{\sigma,1} \right) \right]^* & \text{FOR } \nu_{\sigma,1} \geq o \\ \left[K_L \left(-\nu_{\sigma,1}, -\lambda^*_{\sigma,1} \right) \right] & \text{FOR } \nu_{\sigma,1} < o \end{cases} \tag{3.2.22}$$

$$G_{\sigma,1} = \begin{cases} \left(g_{\sigma,1} \right)^* & \text{FOR } \sigma > o \\ o & \text{FOR } \sigma = o \\ \left(g_{-\sigma,1} \right) & \text{FOR } \sigma < o \end{cases} \tag{3.2.23}$$

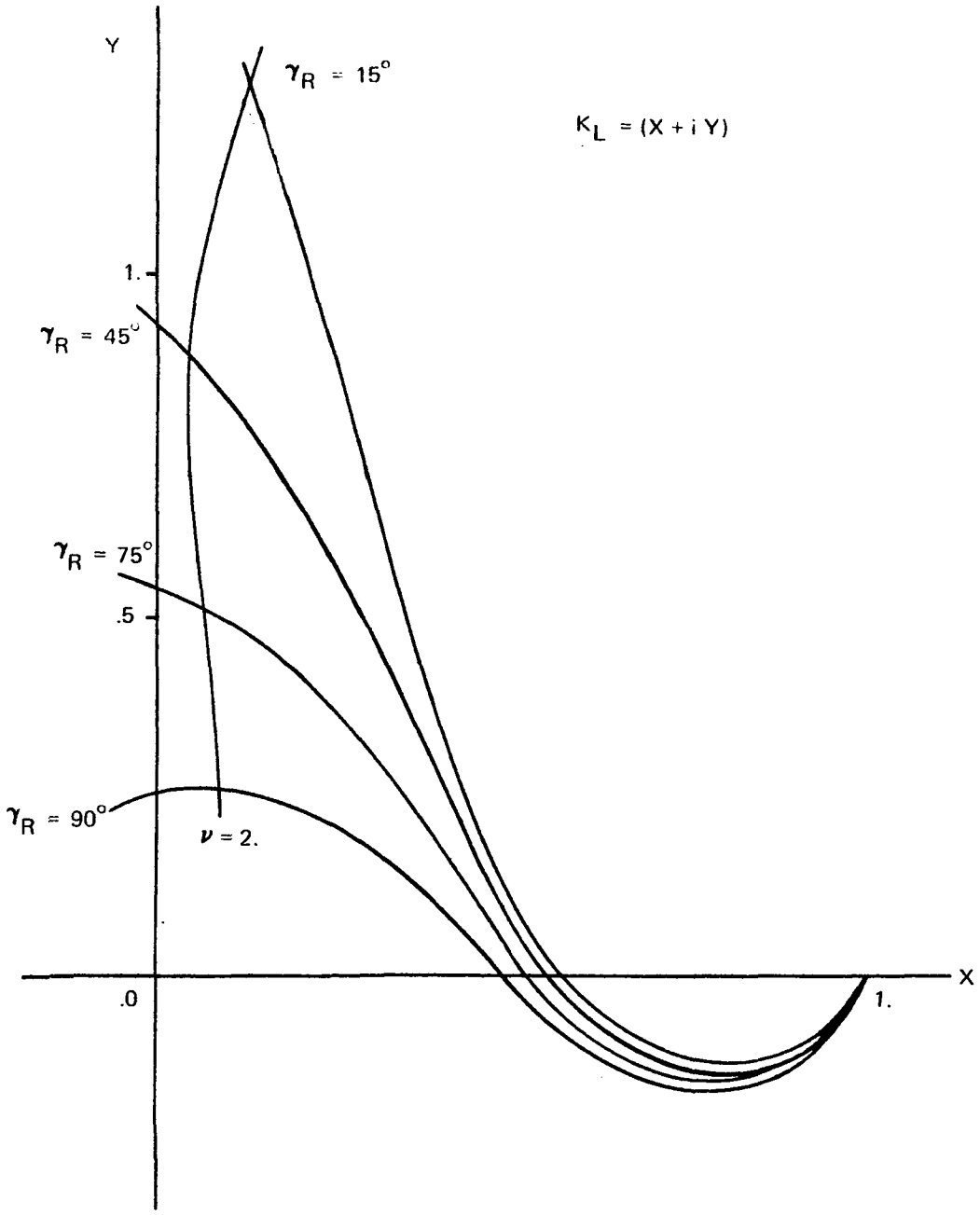

Inlet stator-rotor interaction
unsteady lift response of rotor.

γ_R = Rotor stagger angle

γ_{IS} = Inlet stator stagger angle · 45°

γ_{IS} = Inlet stator stagger angle — 45°

γ_R = 90° gives Sears function

υ = Reduced frequency

FIGURE 8. — KEMP-SEARS LIFT RESPONSE FUNCTION

Since this is a lifting-line model, equations (3.0.2) and (2.2.17) will be used to compute the mode amplitudes. Therefore, the temporal Fourier transform of $L_j(\rho,t)$ has to be determined.

$$\hat{L}_j(\rho,\omega) = \frac{\Gamma_2 M_{M,1}}{4\pi}\left(\frac{dC_L}{d\alpha}\right)_1 G_{\sigma,1}\, K_{\sigma,1}\, e^{i\sigma N_2 \frac{2\pi j}{N_1}} \int_{-\infty}^{\infty} e^{-i\left(\omega_{\sigma,1}-\omega\right)t}\, dt$$

$$= \frac{\Gamma_2 M_{M,1}}{2}\left(\frac{dC_L}{d\alpha}\right)_1 G_{\sigma,1}\, K_{\sigma,1}\, e^{i\sigma N_2 \frac{2\pi j}{N_1}}\, \delta\left(\omega_{\sigma,1}-\omega\right) \tag{3.2.24}$$

$$\sum_{j=o}^{N_1-1} e^{-im\frac{2\pi j}{N_1}} \cdot \hat{L}_j(\rho,\omega) = \frac{\Gamma_2 M_{M,1}}{2}\left(\frac{dC_L}{d\alpha}\right)_1 G_{\sigma,1}\, K_{\sigma,1}\, \delta\left(\omega_{\sigma,1}-\omega\right) \cdot$$

$$\cdot \sum_{j=o}^{N_1-1} \cdot e^{i\sigma N_2 \frac{2\pi j}{N_1}}\, e^{-im\frac{2\pi j}{N_1}} \tag{3.2.25}$$

$$\sum_{j=o}^{N_1-1} e^{-i\left(m-\sigma N_2\right)\frac{2\pi j}{N_1}} = \begin{cases} N_1 \text{ IF } \left(m-\sigma N_2\right) = \ell N_1 \quad \ell = o, \pm 1, \pm 2, \cdots \\ o \text{ OTHERWISE} \end{cases} \tag{3.2.26}$$

$$\sum_{j=o}^{N_1-1} e^{-im\frac{2\pi j}{N_1}} \hat{L}_j(\rho,\omega) = N_1\, \Gamma_2 M_{M,1}\, \frac{1}{2}\left(\frac{dC_L}{d\alpha}\right)_1 G_{\sigma,1}\, K_{\sigma,1}\, \delta\left(\omega_{\sigma,1}-\omega\right) \tag{3.2.27}$$

The duct mode amplitudes can now be computed using equation (2.2.17).

$$A^{\pm}_{mn}(\omega) = -\frac{e^{-iK^{\pm}_{mn} Z_{M.C.}}}{2\beta_{mn}} \int_{\eta}^{1} \left[\frac{m e_{\phi}}{\rho} + K^{\pm}_{mn} e_z\right] \mathcal{R}_m\left(\mu_{mn}\rho\right) \sum_{j=o}^{N_1-1} e^{-im\frac{2\pi j}{N_1}}\, \hat{L}_j(\rho,\omega)\, d\rho$$

$$A^{\pm}_{mn}(\omega) = -\frac{e^{-iK^{\pm}_{mn}Z_{M.C.}}}{4\beta_{mn}} N_1 \int_{\eta}^{1} M_{M,1}\, \Gamma_2 \left(\frac{dC_L}{d\alpha}\right)_1 G_{\sigma,1}\, K_{\sigma,1} \left[\frac{me_{\phi}}{\rho} + K^{\pm}_{mn} e_z\right]$$

$$\cdot \mathcal{R}_m\left(\mu_{mn}\rho\right) \delta\left(\omega_{\sigma,1} - \omega\right) d\rho \qquad (3.2.29)$$

with

$$G_{\sigma,1} = \frac{C_1}{2\rho} N_2 e^{-\sigma N_2 \frac{d}{\rho}} H_{\sigma,2}\, e^{-i\left[-\gamma_1 + \sigma N_2\left(\frac{d}{\rho}\tan\gamma_1 + \frac{C_2}{2}\frac{M_t}{M_{M,2}}\right)\right]}$$

(3.2.30)

$$H_{\sigma,2} = J_o\left(\sigma \frac{C_2}{2\rho} N_2 e^{i\left(\frac{\pi}{2} - \gamma_2\right)}\right) + \sum_{n=1}^{\infty} (i)^n \frac{A_{n+1,2} - A_{n-1,2}}{A_{o,2} + A_{1,2}} J_n\left(\sigma \frac{C_2}{2\rho} N_2 e^{i\left(\frac{\pi}{2} - \gamma_2\right)}\right)$$

$$K_{\sigma,1} = \left[K_L\left(\nu_{\sigma,1}, \lambda_{\sigma,1}\right)\right]^* \qquad (3.2.31)$$

$$\nu_{\sigma,1} = \frac{M_t N_2 C_1}{2M_{M,1}} \sigma \qquad (3.2.32)$$

$$\lambda_{\sigma,1} = N_2 \frac{C_1}{2\rho} \sigma\, e^{i\left(\frac{\pi}{2} - \gamma_1\right)} \qquad (3.2.33)$$

The equations for the other three potential flow field interactions possible in a rotor-stator combination are summarized in appendix F.

The computer subprogram AABAA (see section 3.1.2, volume II) computes the factor multiplying the frequency spike in equation (3.2.29) with ω in the propagating region.

3.3 Rotor-Alone Models

A ducted fan will seldom, if ever, consist of a rotor alone, but the velocity disturbances at the rotor can be separated, in principle, into the component interactions and non-component-induced inflow distortions. The latter are the disturbances considered in these models. An exit stator will straighten out the flow so that upstream and downstream of the stage the flow will be axial. The inflow disturbances can be categorized as being either steady or nonsteady distortions. Steady distortion can occur under different conditions including for the fan stage of aircraft engines all conditions in which the air enters the duct inlet at a relative angle of attack, and the distortions which result from the inlet and duct contours. Under static engine test conditions such distortions can result from ingesting the persistent nonuniformities in the air characteristic of the facility. Nonsteady distortions can be further classified according to their duration at the rotor. The classification parameter might be, for instance, the duration of the distortion times the blade passing frequency of the rotor. Steady distortions then lie at one end of this parametric scale, while small-scale turbulence lies at the other end. To have well-defined tone noise resulting from the distortion, the parameter must be, from purely intuitive reasoning, greater than unity. One possibility for the occurrence of distortions in this range is atmospheric turbulence, whose eddies can be stretched as they accelerate into the duct (for low-speed flight or ground static testing); see Pfenninger (ref. 18) and Hanson (ref. 19). It is a particular representation of this possibility that is developed into the model discussed in section 3.3.2.

Figure 9 illustrates the rotor blade section velocity triangles. As in the component interaction models, the velocity disturbances must be determined in the coordinates attached to the blades. This is done in

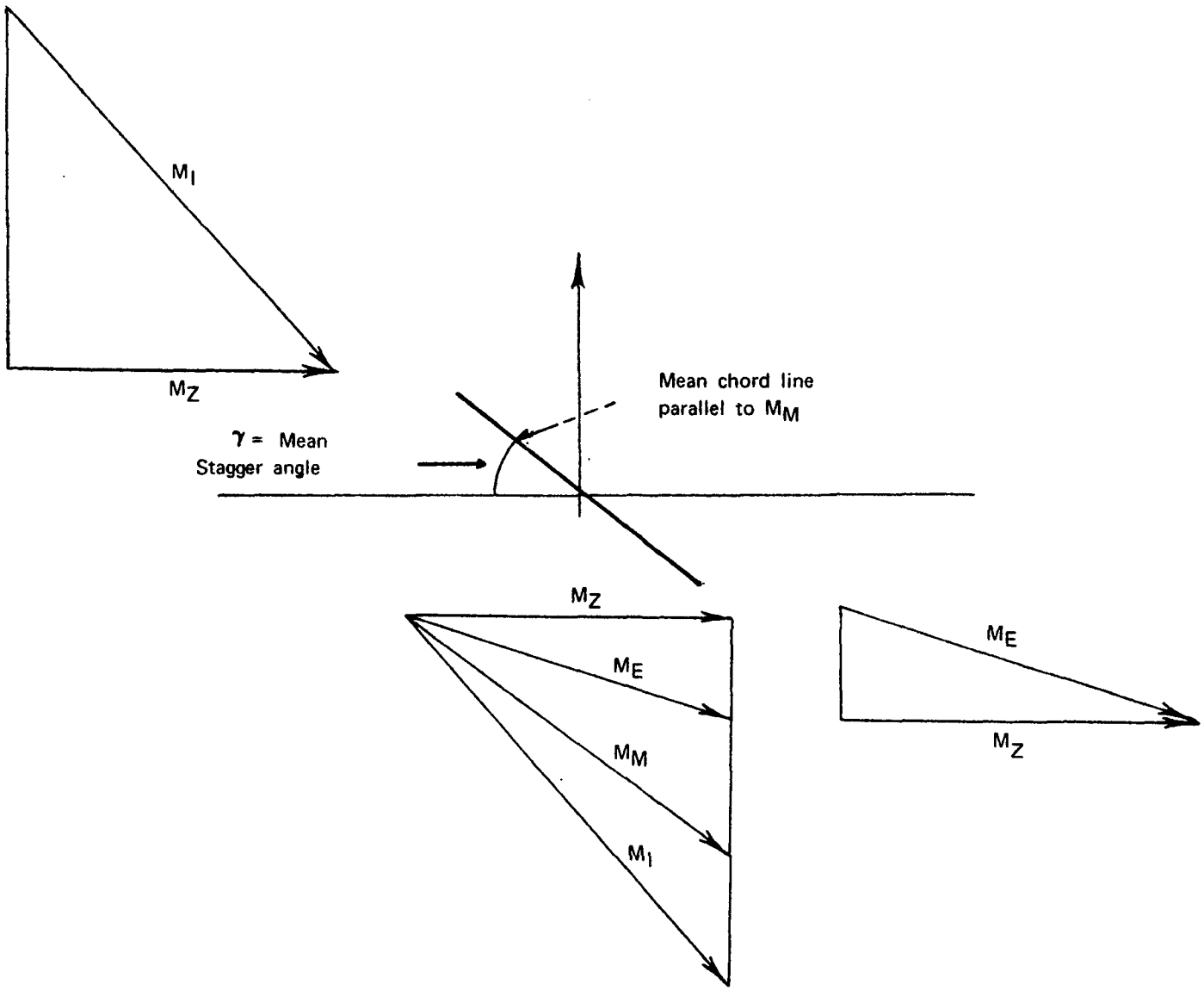

FIGURE 9. – ROTOR BLADE VELOCITY TRIANGLES

appendix G for an unspecified distortion, use of which is then made in sections 3.31 and 3.32 for the particular models.

3.3.1 Steady Distortion. — When the distortion is expressed as the ratio of the deviation from the mean to the mean velocity,

$$W = \frac{\bar{M}_z - M_z}{\bar{M}_z} \tag{3.3.1}$$

then, from equation (G19), with

$$W_n \rightarrow \bar{M}_z W_n \quad ,$$

$$\hat{u}_j = \bar{M}_z \, \mathrm{SIN}\, \gamma \sum_{\ell=-\infty}^{\infty} W_\ell \, e^{i\ell\phi_j} \, \delta\left(\omega + \ell M_T\right) \tag{3.3.2}$$

Substituting this result into equation (2.3.1) gives, from equations (3.0.1) and (2.2.19),

$$A^{\pm}_{mn}(\omega) = - \frac{e^{-iK^{\pm}_{mn} z}}{\beta_{mn}} \, M.C. \, \frac{1}{4} \int_{\eta}^{1} \left[\frac{m}{\rho_s} e_\phi + K^{\pm}_{mn} e_z \right]$$

$$\cdot \mathcal{R}\left(\mu_{mn} \rho_s\right) c \frac{dC_L}{d\alpha} M_M \bar{M}_z \, \mathrm{SIN}\, \gamma \sum_{\ell=-\infty}^{\infty} W_\ell G_{mn\ell} \, d\rho_s$$

$$\cdot \sum_{j=o} e^{2\pi i \frac{\ell-m}{N} j} \, \delta\left(\omega-(m-\ell)M_T\right) \tag{3.3.3}$$

The sum on j can be performed to give

$$\sum_{j=o}^{N-1} e^{2\pi i \frac{\ell-m}{N} j} = \begin{cases} N \text{ if } \ell-m = -\sigma N, \sigma = o, \pm 1, \pm 2, \cdots \\ o \text{ otherwise} \end{cases} \tag{3.3.4}$$

The expression for the mode amplitude then becomes

$$A^{\pm}_{mn}(\omega) = -\frac{e^{-iK^{\pm}_{mn} z_{M.C.}}}{\beta_{mn}} \frac{N}{4} \int_{\eta}^{1} \left[\frac{m}{\rho_s} e_{\phi} + K^{\pm}_{mn} e_z \right] \mathcal{R}_m(\mu_{mn} \rho_s)$$

$$\cdot c \frac{dC_L}{d\alpha} M_M \bar{M}_z \text{ SIN } \gamma \sum_{\ell=-\infty}^{\infty} \sum_{\sigma=-\infty}^{\infty} W_{\ell} G_{mn\ell} \delta_{\ell, m-\sigma N} \delta(\omega - \sigma N M_T) d\rho_s \tag{3.3.5}$$

with

$$\ell = m - \sigma N \tag{3.3.6}$$

and

$$\nu_{\ell} = \frac{\ell M_T}{M_M} \frac{c}{2} \tag{3.3.7}$$

and $G_{mn\ell}$ is given by equation (3.1.39) for this ν_{ℓ}, M_M is used to approximate V, i.e., γ is taken as the mean stagger angle. All references to subscripts 1 and 2 have been dropped since there is only the one component under consideration, the rotor. The computer subprogram BCDAA

computes the factor multiplying a frequency spike for ω in the propagating region.

This model is analytically similar in all respects but one to the inlet stator-rotor mode of the viscous wake interaction model. The exception is in the origin and specification of the velocity disturbances. In the viscous wake model, studies had been made, data had been correlated, and some theoretical ideas had been employed (Prandtl's mixing length theory) to determine the empirical formulas for the wake defects of airfoils (Silverstein, et al., ref. 37). Although much data has been gathered on the steady distortion of fan duct inlets, no work known to the authors has been published in which this data has been studied with the view of deriving a general empirical formula for computing the velocity distortion. In lieu of a sound theoretically or experimentally supported procedure, acousticians have begun to develop rather crude empirical models of their own in order to perform calculations. Wright (ref. 15), Lowson (ref. 17), Lowson and Ollerhead (ref. 39), and Barry and Moore (ref. 40) have investigated a "power law" for "blade loading harmonics." That is, in the present language, they represented the velocity distortion at a rotor disc in a Fourier series on the polar angle about the axis, at some average radius, and assumed that the coefficients monotonically decreased as ℓ^{-q}, with ℓ the Fourier series index and q some positive number [loading harmonics are actually velocity harmonics times lift responses; see Hanson, chapter 6 of (ref. 19) for a discussion of this "law"]. This model is included in the computational possibilities of the computer subprogram BCDAA. It requires knowing besides the power, q, the first harmonic coefficient of the cosine series, the determination of which can possibly be determined from on axis microphone measurements (see Barry and Moore), i.e.,

$$W_\ell = \frac{a_1}{2}\,\ell^{-q} \tag{3.3.8}$$

The other options in this subprogram include inputting the Fourier cosine and sine series coefficients as determined by the user (a simple

integration scheme is supplied outside the subprogram for computing these coefficients from distortion data), and a simple analytical model, the "cone model." This model was part of a study intended to clarify the power law discussed above and is given in terms of the formula

$$W(\rho,\phi) = \frac{1-\frac{V_1}{V_A}}{1-A^2}\left(A\,\rho\,\cos\phi - \sqrt{(A\,\rho\,\cos\phi-1)^2-(1-A^2)(1-\rho^2)}\right) \tag{3.3.9}$$

where:

V_A/V_1 = ratio of maximum to minimum distortion

A = span position of the maximum

When the coefficients of the cosine and sine series are input, then

$$W_\ell = \frac{a_\ell - i\,b_\ell}{2} \tag{3.3.10}$$

and

$$W_{-\ell} = W_\ell^\dagger \tag{3.3.11}$$

with a_ℓ, b_ℓ the cosine and sine coefficients, respectively.

3.3.2 Nonsteady Distortion. — Reference is made to Pfenninger (ref. 18) for a discussion of the origin and occurrence of stretched eddies in fan ducts. Hulse, et al. (ref. 9) put forth the idea of isolated "patches" of distortion convecting through a rotor to explain some of their results, and Hanson (ref. 19) has gathered some data relevant to the occurrence of stretched eddies in fan ducts. This model puts into an analytical form some of these ideas. In appendix G an expression for

the velocity perturbation on a rotor blade due to the convection through the rotor of a stretched eddy is developed; see equation (G23).

Substituting for $\hat{u}_j$ from this equation into equation (2.3.1), there results for the dipole surface density function the expression

$$\hat{F}_j\left(\rho_s,\xi',\omega\right) = \frac{dC_L}{d\alpha}\ M_M \frac{1}{\pi}\hat{H}\left(\rho_s,\xi',\omega\right) \sum_{\ell=-\infty}^{\infty} e^{i\ell\phi_j}$$

$$\cdot \left\{ \text{SIN}\ \gamma\ W_{z\ell}\ \frac{\bar{\Delta}_z\left(\frac{\omega + \ell M_T}{M_z}\right)}{2\pi M_z} + \text{COS}\ \gamma\ W_{\phi\ell}\ \frac{\bar{\Delta}_\phi\left(\frac{\omega + \ell M_T}{M_z}\right)}{2\pi M_z} \right\} \qquad (3.3.12)$$

where $W_{z\ell}$ is the ℓ^{th} coefficient in the complex Fourier series representation of the axial component of the eddy cross section at the radius ρ_s. The cross-sectional profile of an eddy is time independent, the assumption being that shape changes with z or $z - M_z t$ are less significant than magnitude changes. The term $W_{\phi\ell}$ is the ℓ^{th} coefficient in the series for the circumferential component of the eddy cross section at the radius ρ_s. Assuming the stretched eddy has cylindrical symmetry about its own axis, then a reasonable choice for a cross-sectional profile is the Gaussian (see fig. 10),

$$W_z\left(\rho_s,\phi_s\right) = W_z\, e^{-\frac{1}{2a_z^2}\left[\rho_s^2 + R^2 - 2\rho R\,\text{COS}\left(\phi_s - \phi\right)\right]} \qquad (3.3.13)$$

and similarly for $W_\phi(\rho_s,\phi_s)$ with W_ϕ and a_ϕ, where W_z, W_ϕ and a_z, a_ϕ are the maxima of the distortions and the "transverse length scales" of the distortions, respectively. The location of the cross-sectional center

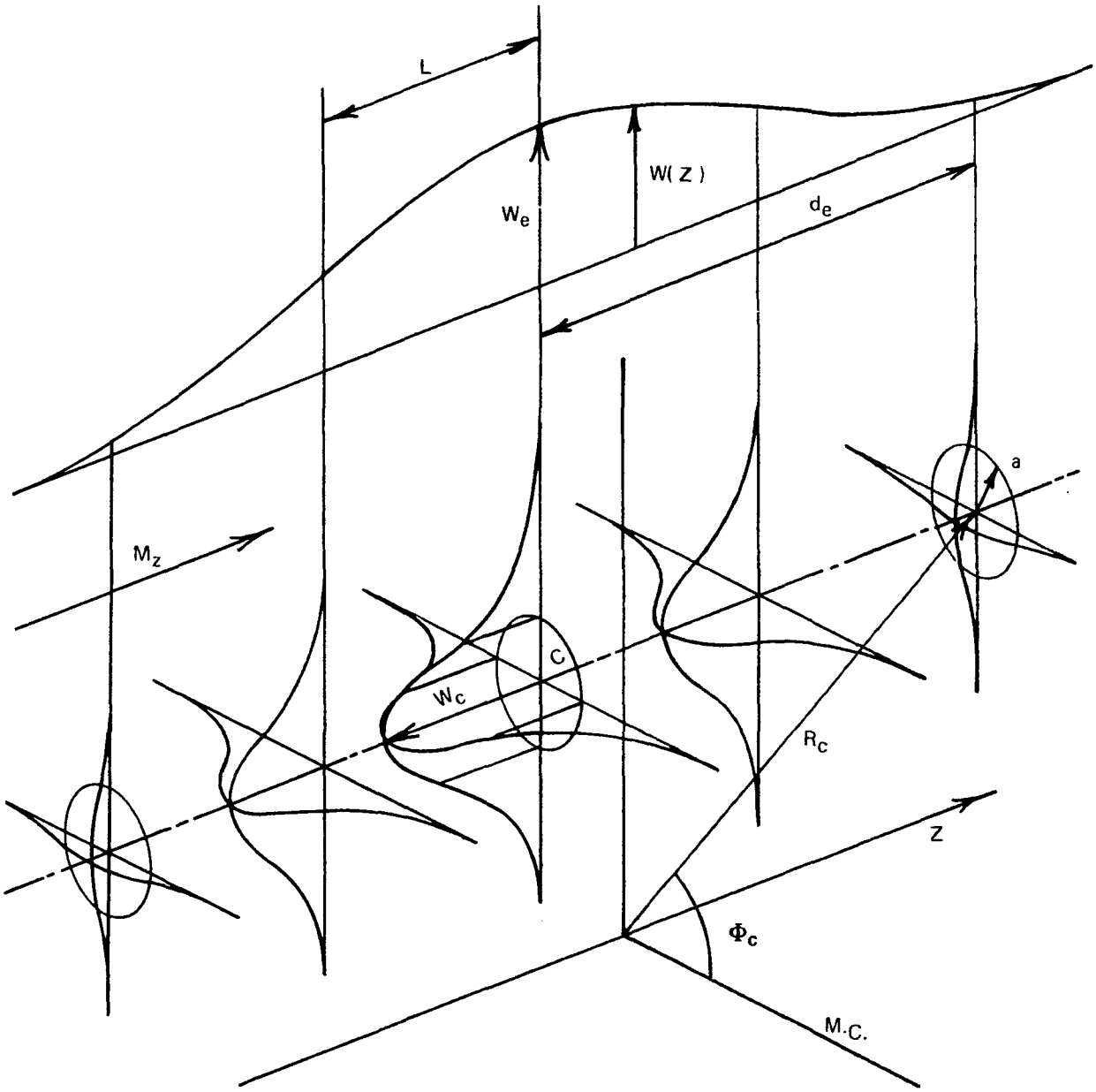

$(R, \Phi, Z_{M.C.} - d_c)$	=	location of eddy center C at t = 0
$d_c = M_Z$.	=	axial position of C referenced to the rotor midchord plane
L, a	=	eddy length scales
W (Z)	=	axial eddy velocity distribution

FIGURE 10. – EDDY VELOCITY SPATIAL DISTRIBUTION AT TEMPORAL ORIGIN (t = 0)

of the eddy is given by $\left\{R, \Phi\right\}$. This gives for $W_{z\ell}(\rho_s)$

$$W_{z\ell}\left(\rho_s\right) = 2\pi W_z e^{-\frac{\left(\rho_s - R\right)^2}{2a_z^2}} e^{-\frac{\rho_s R}{a_z^2}} I_\ell\left(\frac{\rho_s R}{a_z^2}\right) e^{-i\ell\Phi} \qquad (3.3.14)$$

with I_ℓ the modified Bessel function of the first kind of order ℓ. Similarly,

$$W_{\phi\ell}\left(\rho_s\right) = 2\pi W_\phi e^{-\frac{\left(\rho_s - R\right)^2}{2a_z^2}} e^{-\frac{\rho_s R}{a_\phi^2}} I_\ell\left(\frac{\rho_s R}{a_z^2}\right) e^{-i\ell\Phi} \qquad (3.3.15)$$

Expressions for $\bar{\Delta}_z$ and $\bar{\Delta}_\phi$ are developed in appendix G, equation (G22), from which

$$\frac{1}{2\pi M_z}\,\bar{\Delta}_z\left(\frac{\omega + \ell M_T}{M_z}\right) = \frac{T_z}{\sqrt{2\pi}} e^{-i\left(\omega + \ell M_T\right)\tau} e^{i\left(\omega + \ell M_T\right)\frac{z_{M.C.}}{M_z}}$$

$$\cdot\, e^{-\frac{1}{2}T_z^2\left(\omega + \ell M_T\right)^2} \qquad (3.3.16)$$

and

$$\frac{1}{2\pi M_z}\,\bar{\Delta}_\phi\left(\frac{\omega + \ell M_T}{M_z}\right) = \frac{T_\phi}{\sqrt{2\pi}} e^{-i\left(\omega + \ell M_T\right)\tau} e^{i\left(\omega + \ell M_T\right)\frac{z_{M.C.}}{M_z}}$$

$$\cdot\, e^{-\frac{1}{2}T_z^2\left(\omega + \ell M_T\right)^2} \qquad (3.3.17)$$

where:

$T_z = L_z / M_z$

$T_\phi = L_\phi / M_z$

L_z, L_ϕ = axial length scales of the eddy

τ = time at which the axial center of the eddy coincides with the midchord plane of the rotor

Upon substituting these results into equation (3.0.1), the sum on j gives

$$\sum_{j=o}^{N-1} e^{2\pi i \frac{\ell-m}{N} j} = \begin{cases} N \text{ if } \ell-m = -\sigma N,\ \sigma = o, \pm 1,\ \pm 2, \cdots \\ o \text{ otherwise} \end{cases} \tag{3.3.18}$$

Hence, from equation (3.0.1),

$$\frac{c}{2} \int_1^1 \sum_{j=o}^{N-1} e^{-im \frac{2\pi j}{N}} \hat{F}_j \left(\rho_s, \xi', \omega - m\dot{M}_T\right) e^{-i\kappa^{\pm}_{mn} \xi'} d\xi' =$$

$$\cdot \frac{N}{2} c \frac{dC_L}{d\alpha} M_M \sum_{\sigma=-\infty}^{\infty} \left\{ W_{Z\ell} \text{ SIN } \gamma \frac{\bar{\Delta} z}{2\pi M_z} + W_{\phi\ell} \text{ COS } \gamma \frac{\bar{\Delta}_\phi}{2\pi M_z} \right\}$$

$$\cdot \frac{1}{\pi} \int_1^1 \hat{H} \left(\rho_s, \xi', \omega - m M_T\right) e^{i\kappa^{\pm}_{mn} \xi'} d\xi' \tag{3.3.19}$$

with $\ell = m-\sigma N$. Substituting this result into equation (2.2.19) for the mode amplitude gives

$$A^{\pm}_{mn}(\omega) = -\frac{N}{4}\sum_{\sigma=-\infty}^{\infty}\frac{e^{-iK^{\pm}_{mn}z}}{\beta_{mn}}\,M.C.\int_{\eta}^{1}\left[\frac{m}{\rho_s}e_{\phi}+K^{\pm}_{mn}e_z\right]\mathcal{R}_m\left(\mu_{mn}\rho_s\right)$$

$$\cdot\, c\frac{dC_L}{d\alpha}M_M\left\{W_{z\ell}\,SIN\,\gamma\,\frac{\bar{\Delta}_z\left(\frac{\omega-\sigma NM_T}{M_z}\right)}{2\pi M_z}\right. \tag{3.3.20}$$

$$\left.+\,W_{\phi\ell}\,COS\,\gamma\,\frac{\bar{\Delta}_{\phi}\left(\frac{\omega-\sigma NM_T}{M_z}\right)}{2\pi M_z}\right\}\delta_{m-\ell,\sigma N}$$

$$\cdot\,\frac{1}{\pi}\int_{-1}^{1}\hat{H}\left(\rho_s,\xi',\omega-mM_T\right)e^{-i\kappa^{\pm}_{mn}\xi'}\,d\xi'\;\;d\rho_s$$

This spectrum for the mode amplitude is two series of Gaussians centered on the harmonics of blade passing frequency, with two-thirds of the power of each bump within plus or minus $2\pi/T_z$ and $2\pi/T_{\phi}$. For purposes of computing a single mode amplitude for each harmonic, the Gaussian "bumps" are replaced by weighted delta functions (see fig. 11).:

$$\frac{\bar{\Delta}_z\left(\frac{\omega-\sigma NM_T}{M_z}\right)}{2\pi\,M_z}\longrightarrow E_z\,\delta\left(\omega-\sigma NM_T\right) \tag{3.3.21}$$

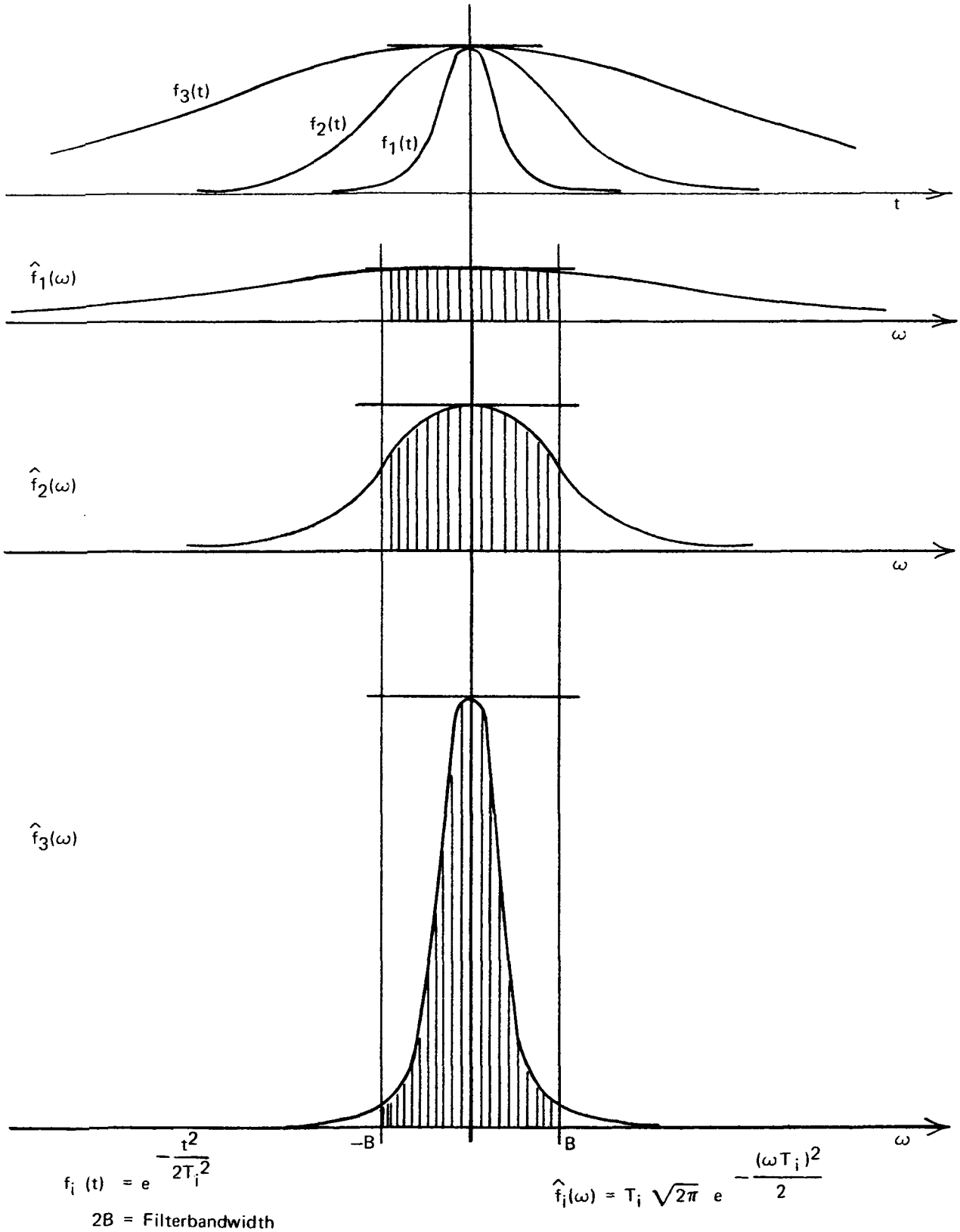

FIGURE 11. – BANDPASS FILTER FOR TONES

and

$$\frac{\bar{\Delta}_{\phi}\left(\frac{\omega-\sigma NM_T}{M_z}\right)}{2\pi\ M_z} \rightarrow E_{\phi}\ \delta\left(\omega-\sigma NM_T\right) \tag{3.3.22}$$

with

$$E_{z,\phi} = \int_{-B}^{B} \frac{\bar{\Delta}_{z,\phi}\left(\frac{\omega'}{M_z}\right)}{2\pi\ M_z}\ d\omega' \tag{3.3.23}$$

$$= \frac{1}{\sqrt{2\pi}}\ T_{z,\phi} \int_{-B}^{B} e^{-\frac{1}{2}\omega'^2 T_{z,\phi}^2} \cos\left(\omega'\frac{\xi_o}{M_z}\right) d\omega'$$

where 2B is the bandwidth of the filter used to define the tone and the subscripts z and ϕ refer to the z and ϕ components, respectively. The frequency-dependent parts of $A^{\pm}_{mn}(\omega)$ are then evaluated at harmonics of blade passing frequency, giving

$$A^{\pm}_{mn}(\omega) = -\frac{N}{4}\frac{e^{iK^{\pm}_{mn}z_{M.C.}}}{\beta_{mn}} \int_{\eta}^{1} \left[\frac{m}{\rho_s} e_{\phi} + K^{\pm}_{mn} e_z\right]$$

$$\cdot \mathcal{R}_m\left(\mu_{mn}\rho_s\right) c \frac{dC_L}{d\alpha} M_M \Big\{ W_{z\ell} \sin\gamma\ Ez$$

(3.2.24)

$$+W_{\phi\ell} \cos\gamma\ E_{\phi}\Big\} \frac{1}{\pi} \int_{-1}^{1} \hat{H}\left(\rho_s, \xi', \omega-mM_T\right) e^{-i\kappa^{\pm}_{mn}\xi'} d\xi' \sum_{\sigma=-\infty}^{\infty} \delta\left(\omega-\sigma NM_T\right) d\rho_s$$

with

$$\ell = m - \sigma N$$

Two methods are used to evaluate the chordwise integration of equation (3.3.24). One is to employ the pressure difference function of Naumann and Yeh (ref. 35) as was done in the steady distortion model of section 3.3.1, giving

$$A^{\pm}_{mn}(\omega) = -\frac{N}{4}\,\frac{e^{-iK^{\pm}_{mn}z_{M.C.}}}{\beta_{mn}} \int_{\eta}^{1} \left[\frac{m}{\rho_s} e_{\phi} + K^{\pm}_{mn} e_z\right] \mathcal{R}_m\left(\mu_{mn}\rho_s\right)$$

$$\cdot\, c\frac{dC_L}{d\alpha} M_M \left\{W_{z\ell} \sin\gamma\, E_z + W_{\phi\ell} \cos\gamma\, E_{\phi}\right\} G_{mn\ell} \cdot$$

$$\sum_{\sigma=-\infty}^{\infty} \delta\left(\omega - \sigma N M_T\right) d\rho_s \qquad (3.3.25)$$

with $G_{mn\ell}$ given by equation (3.1.39). The other method is to assume a lifting-line model with the lift response function developed by Filotas (ref. 36) for oblique gusts, the assumption being that the radial variations of a compact eddy present to the blade oblique gusts made up of harmonic gusts in the chordwise and radial directions. Following in spirit the calculation "Distortion of Standing Wave by Strip" in chapter 11 of Morse and Feshbach (ref. 29), for calculating the section lift response of a three-dimensional gust, the blade is assumed to be a two-dimensional airfoil. The radial variation of the incident gust is decomposed into harmonics that travel up and down the span. These harmonics combined with the chordwise harmonic gusts produce oblique gusts at a given span position as required in the formulation of Filotas (see fig. 12).

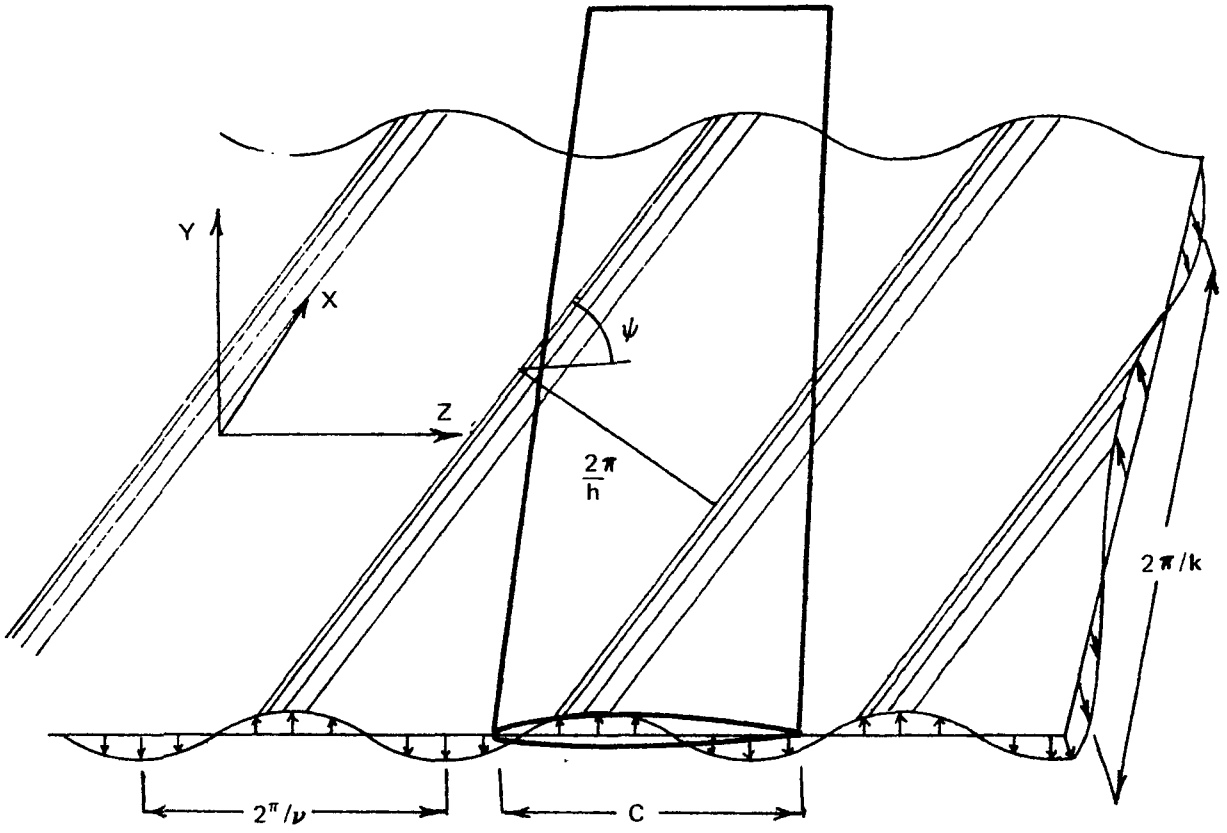

FIGURE 12. – SCHEMATIC OF OBLIQUE HARMONIC GUST

For this purpose the most significant radial variation in $W_{z\ell}$ and $W_{\phi\ell}$ is isolated, then the rectangular coordinate x is substituted for ρ_s in this factor to derive the plane wave expansion. Since the most significant radial variation resides in the Gaussian factor of equations (3.3.15) and (3.3.16), the exporential and the modified Bessel function tend to be inversely related; then

$$\bar{W}_{z\ell}(k) = \int_{-\infty}^{\infty} W_{z\ell}\left(\rho_s, x\right) e^{-ikx} dx$$

$$\approx 2\pi\, W_z e^{-\frac{P_s R}{a_z^2}} I_\ell\left(\frac{\rho_s R}{a_z^2}\right) e^{-i\ell\Phi} \int_{-\infty}^{\infty} e^{-\frac{(x-R)^2}{2a_z^2}} e^{-ikx} dx$$

$$= 2\pi\, W_z e^{-\frac{\rho_s R}{a_z^2}} I_\ell\left(\frac{\rho_s R}{a_z^2}\right) e^{-i\ell\Phi} \sqrt{2\pi}\, a_z e^{-ikR} e^{-\frac{1}{2} a_z^2 k^2} \tag{3.3.26}$$

Similarly,

$$\bar{W}_{\phi\ell}(k) \approx 2\pi\, W_\phi e^{-\frac{\rho_s R}{a_\phi^2}} I_\ell\left(\frac{\rho_s R}{a_\phi^2}\right) e^{-i\ell\Phi} \sqrt{2\pi}\, a_\phi e^{-ikR} e^{-\frac{1}{2} a_\phi^2 k^2} \tag{3.3.27}$$

These results produce oblique gusts of the form

$$e^{-ih\left[\left(\bar{z}' - Vt\right) \mathrm{SIN}\, \psi - x\, \mathrm{COS}\, \psi\right]} \tag{3.3.28}$$

with

$$h = \sqrt{k^2 + \left(\frac{2\nu_\ell}{c}\right)^2}$$

where, from appendix G,

$$\nu_\ell = \frac{c}{2}\frac{\ell}{\rho_s} \text{ SIN } \gamma \tag{3.3.29}$$

and

$$\psi = \text{TAN}^{-1}\left(\frac{2\nu_\ell}{kc}\right) \tag{3.3.30}$$

Since the gust wave form used by Filotas is with $\psi \to -\psi$ and since (see appendix H)

$$T(h,-\psi) = T^{\dagger}(h,\ \psi), \tag{3.3.31}$$

it is the complex conjugate of the oblique gust response function that is required here. Computing the section lift resulting from each k and adding them up then gives

$$W_{z\ell}\frac{1}{\pi}\int_{-1}^{1}\hat{H}\left(\rho_s,\xi',\omega - mM_T\right)d\xi' \longrightarrow$$

$$W_z e^{-\frac{\rho_s R}{a_z^2}} I_\ell\left(\frac{\rho_s R}{a_z^2}\right) e^{-i\ell\Phi}\sqrt{2\pi}\, a_z \int_{-\infty}^{\infty} e^{ik\left(\rho_s - R\right)}$$

$$\cdot\ e^{-\frac{1}{2}a_z^2 k^2}\ T^{\dagger}(h,\psi)\ dk = \tag{3.3.32}$$

$$2\pi\, W_z e^{-\frac{\rho_s R}{a_z^2}} I_\ell\left(\frac{\rho_s R}{a_z^2}\right) e^{-i\ell\Phi} \frac{2a_z}{\sqrt{2\pi}} \text{REAL} \int_0^\infty e^{ik\left(\rho_s - R\right)} e^{-\frac{1}{2} a_z^2 k^2} T^\dagger(h,\psi)\, dk$$

Similarly, for $W_{\phi\ell} \frac{1}{\pi} \int_{-1}^{1} \hat{H}\left(\rho_s, \xi', \omega - nM_T\right) d\xi'$

with W_ϕ and a_ϕ in place of W_z, a_z.

Substituting these results into equation (3.3.24) then gives the mode amplitude by this method. Subprogram BBCAA computes the mode amplitudes for ω in the propagating region using one of two methods, i.e., the factor multiplying the frequency spike in equation (3.3.25) or that in equation (3.3.24) with the substitutions from equation (3.3.32) and the ω equivalent equation.

3.4 Numerical Considerations

Each of the models produce an expression for a mode amplitude which can be written quite generally in the form

$$A^{\pm}_{mn\sigma} = -\frac{e^{-iK^{\pm}_{mn} z_{M.C.}}}{2\beta_{mn}} \int_\eta^1 \left[\frac{m}{\rho_s} e_\phi + K^{\pm}_{mn} e_z\right] \mathcal{R}_m\left(\mu_{mn}\rho_s\right) f_{mn}\left(\rho_s\right) d\rho_s \qquad (3.4.1)$$

where σ is the harmonic index specifying the frequency under consideration. To compute all of the upstream- or downstream-propagating mode amplitudes for this harmonic, the set of m's and n's for these modes must be determined from the cut-on criterion,

$$\omega^* = \frac{\sigma N_R M_T}{\sqrt{1-M^2}} = E_B > \mu_{mn} \quad , \tag{3.4.2}$$

where:

N_R = number of rotor blades

E_B = a bound for the eigenvalues to be computed .

Having determined the indexes for the propagating modes, the corresponding set of μ_{mn}'s are computed. These preliminaries determine the set of integrals that have to be computed. The integrand of each of the integrals is then subjected to the following factorization: the factors that are independent of the radial, or span, variable ρ_s, i.e., the constant factors, are identified and placed outside the integral sign. Then the integration interval is subdivided into a number of equal subintervals, the number of subdivisions being determined by the number of oscillations of the most oscillatory factor. The remaining ρ_s-dependent integrand is then factored into a part that varies significantly, possibly changing sign, within the subinterval, and a part that varies slowly, allowing its average value to represent it within the subinterval. The calculation can then be written symbolically in the form

$$A^{\pm}_{mn\sigma} = (\text{CONSTANT}) \cdot \sum_{j=1}^{N} (\text{AVE OF SLOWLY VARYING FACTOR}) \cdot \int_{a_j}^{a_{j+1}} (\text{OSCILLATORY FACTOR})\, d\rho_s \tag{3.4.3}$$

with a_j the left endpoint of the $_j$th subinterval. The integration on each subinterval is then performed using an 8-point Gaussian rule.

4.0 USERS GUIDE TO COMPUTER SUBPROGRAMS

These subprograms compute all the mode amplitudes for a given harmonic of blade passing frequency for either upstream- or downstream-propagating modes. Subroutine AAAAA does this for the viscous wake interaction model, subroutine AABAA for the potential field interaction model, subroutine BCDAA for the rotor in steady distortion model, and subroutine BBCAA for the rotor in nonsteady distortion model (see fig. 13).

4.1 Calling Sequence

All four primary subroutines have the same calling sequence and are called as follows:

```
      DIMENSION MUSE(MDIM),MAXN(MDIM),
     *   ARMUMN(NDIM,MDIM),ARMISC(40), AR(MAXDIM,MAXJ,3)

      COMPLEX ALPHAMN(NDIM,MDIM)
         .
         .
         .
      CALL { AAAAA } (ARMISC,MAXDIM,MAXJ,AR,MDIM,NDIM,
           { AABAA }
           { BCDAA }
           { BBCAA }
     *                ARMUMN,NOFM,MUSE,ALPHAMN,IERROR)
```

4.2 Input, Input — Output, Output

INPUT

ARMISC — an array of dimension 40 used for input and fully described in the section below.

AAAAA – Viscous wake interaction

AABAA – Potential field interaction

BCDAA – Rotor in steady distortion

BBCAA – Rotor in non-steady distortion

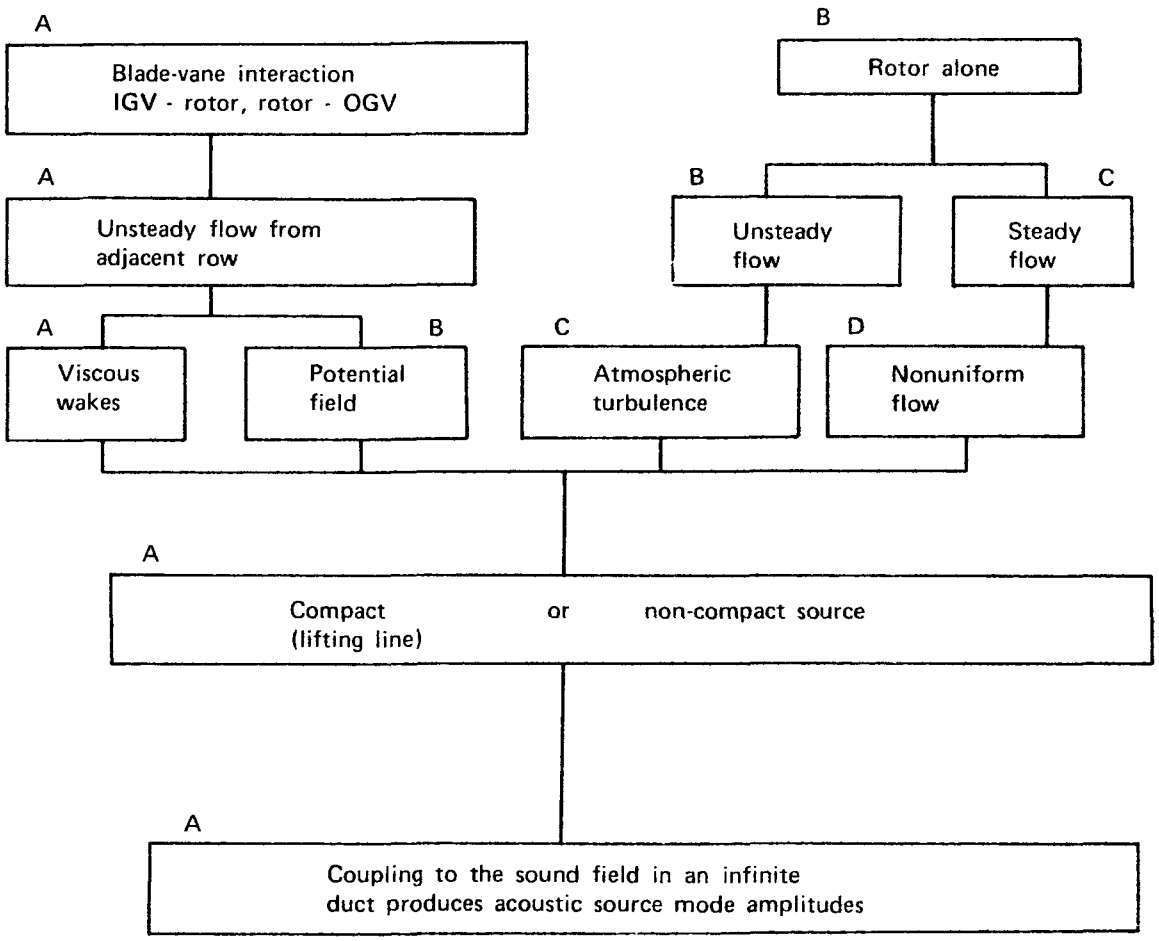

FIGURE 13. – PRIMARY SUBROUTINES

MAXDIM — The first variable dimension of the array AR, which corresponds to the radial positions and must be dimensioned at least 2 more than the largest number of radial positions to be input for any component (inlet stator, rotor, or outlet stator).

MAXJ — The second variable dimension of the array AR, corresponding to the number of aerodynamic and geometric variables input and, per package, must be at least

Package	Value
1 (AAAAA)	11
2 (AABAA)	$9 + \max\{\text{ARMISC(I)}: \text{I=18,19,20}\}$ where: $\max \text{ARMISC(I)} \geq 3$, I=18,19,20
3 (BCDAA)	11 if ARMISC(22) = 0,1 12 if ARMISC(22) = 2 11+ARMISC(23) if ARMISC(22) = 3
4 (BBCAA)	9 if ARMISC(25) = 4 11 if ARMISC(25) = 3

AR — A three-dimensional array of geometric and aerodynamic variables, described in the section 4.4.

MDIM — The variable dimension corresponding to the maximum number of spinning mode indexes. MDIM should be at least $2E_B + 1$ but need be no more than 201 to ensure that all spinning mode indexes can be calculated ($E_B = \omega^*$; see equation [2.1.8]).

NDIM — The variable dimension corresponding to the number of radial mode indexes, limited to at most 40.

INPUT/OUTPUT

ARMUMN — The real array-dimensioned NDIM x MDIM-that contains the eigenvalues calculated in the primary subroutine. Upon subsequent calls to the primary subroutine the eigenvalues from the previous case are reused if the parameters used in calculating the eigenvalues remain unchanged.

NOFM — The number of spinning mode indexes computed by the program; can be reused as discussed in ARMUMN.

MUSE — An integer array-dimensioned MDIM-that contains the NOFM spinning mode indexes and can be reused as discussed under ARMUMN.

MAXN — An integer array-dimensioned MDIM-containing the maximum radial mode indexes corresponding to the spinning mode indexes in array MUSE. Array MAXN can be reused as discussed in ARMUMN.

OUTPUT

ALPHAMN — The complex array-dimensioned NDIM x MDIM-containing the calculated mode amplitudes. For any index IOFM (IOFM = 1..., NOFM), M = MUSE (IOFM) is an available spinning mode index. For this M, the available radial mode indexes are N = 1, 2,..., MAXN (IOFM). Then the corresponding mode amplitude is ALPHAMN (N, IOFM) and the corresponding eigenvalue is ARMUMN (N, IOFM).

ERROR RETURN

IERROR 0 = all calculations have been complete successfully

2 = an incomplete set of eigenvalues is calculated, and the corresponding mode amplitudes are calculated

4 = there are no eigenvalues, hence, there are no mode amplitudes

4.3 Input Array ARMISC

In this and following sections, the code given below is used to refer to the subroutine packages:

Package	Code
AAAAA	1
AABAA	2
BCDAA	3
BBCAA	4

In the following definitions, all variables referred to as nondimensional are nondimensionalized as prescribed in appendix A.

ARMISC

ARMISC array index	Packages used in	Definition
1	1, 2	Nondimensional average distance between the midchord planes of the inlet-stator and the rotor; see figure 4.

ARMISC array index	Packages used in	Definition
2	1,2	Nondimensional average distance between the midchord planes of the rotor and the outlet-stator vanes; see figure 5.
3	1,2,3,4	The hub-to-tip ratio of the duct
4	1,2,3,4	-1 for upstream sound propagation 1 for downstream sound propagation
5	1,2	1 indicates inlet stator-rotor interaction 2 indicates rotor-outlet stator interaction
6	1,2,3,4	Trace printout option, where 0 = no trace printout 1 = trace printout of major factors in the primary subroutine 2 = detailed printout of the eigenvalue calculation in subroutine ZEROS; see section 3.2.2 of volume II
7	1,2,3,4	M_T, the rotor blade tip Mach number
8	1,2	N_{ISV}, the number of inlet-stator vanes
9	1,2	N_{OSV}, the number of outlet-stator vanes

ARMISC array index	Packages used in	Definition
10	1,2,3,4	N_{RB}, the number of rotor blades
11	---	Not used
12	1	ϕ_{OS}, in radians; phase angle for adjustment of skewness of the incident wakes on the outlet stator; see **appendix E.**
13	1	ϕ_{R}, in radians; phase angle for adjustment of skewness of the incident wakes on the rotor; see **appendix E.**
14	1,2,3,4	The harmonic index
15	1,2	Z_{IS}, the axial position of the inlet stator
16	1,2	Z_{OS}, the axial position of the outlet stator
17	1,2,3,4	Z_{R}, the axial position of the rotor
18	2	-1 means the upstream blade row is the sound generator in a potential flow field interaction 1 means the downstream blade row is the sound generator in a potential flow field interaction

ARMISC array index	Packages used in	Definition
19	2	The number of inlet stator vane Glauert coefficients, which is 0 if ARMISC(5) = 2 or ARMISC (18) = -1 n where $3 \leq n \leq 15$ if ARMISC(5) = 1 and ARMISC(18) = 1 (see sec. 3.2)
20	2	The number of rotor blade Glauert coefficients, which is 0 if ARMISC(5) + ARMISC(18) = 1 or 2 n where $3 \leq n \leq 15$ if ARMISC(5) + ARMISC(18) = 0 or 3 (see sec. 3.2)
21	2	The number of outlet stator Glauert coefficients, which is 0 if ARMISC(5) = 1 or ARMISC(18) = 1 n where $3 \leq n \leq 15$ if ARMISC(5) = 2 and ARMISC(18) = -1 (see sec. 3.2)
22	3	0 = no distortion 1 = distortion is represented by the cone model

ARMISC array index	Packages used in	Definition
		2 = distortion is represented by the power model 3 = distortion coefficients are input
23	3	V_A/V_1 if ARMISC(22) = 1 q if ARMISC(22) = 2 Total number of distortion coefficients if ARMISC(22) = 3
24	3	A if ARMISC(22) = 1 Skip factor used with distortion coefficients if ARMISC(23) = 3
25	1,2,3,4	Defines the lift function to be used: 2 = LIFTFN2, the generalized Sears lift response function; see equation (24) of appendix I; used in package 2 only. 3 = LIFTFN3 or NONCPT; LIFTFN3 is the combination of lift response functions as developed in reference 6; NONCPT is the lift response function for noncompact source theory, see equation (22) of appendix I; used in packages 1, 3, and 4. 4 = LIFTFN4, Filotas lift response function; see equation (25) of appendix I; used in package 4.

ARMISC array index	Package used in	Definition
26	---	Not used
27	---	Not used
28	4	R, radial position of the eddy center
29	4	ϕ, angular position of the eddy center in radians
30	4	W_z, axial eddy velocity component at the eddy center, nondimensionalized with the average axial flow velocity; see figure 10.
31	4	W_ϕ, angular eddy velocity component at the eddy center, nondimensionalized with the average axial flow velocity; see figure 10.
32	4	a_Z, eddy length scale in the direction normal to the average flow velocity for the axial eddy velocity component; see figure 10.
33	4	a_ϕ, eddy length scale in the direction normal to the average flow velocity for the angular eddy velocity component; see figure 10.

ARMISC array index	Packages used in	Definition
34	4	L_Z, eddy length scale in the direction of the average flow velocity for the axial eddy velocity component; see figure 10.
35	4	L_ϕ, eddy length scale in the direction of the average flow velocity for the angular eddy velocity component; see figure 10.
36	4	B, upper bound of the frequency band considered in the generation of tone duct mode amplitudes by nonsteady distortion; see figure 11.
37	4	τ, time when eddy center is located in rotor plane
38	1,3,4	0 compact source (LIFTFN3 is used) $\neq 0$ noncompact source (NONCPT is used)
	Note: ARMISC(38) can be used if and only if ARMISC(25) = 3.	
39	---	Not used
40	---	Not used

4.4 Input Array AR

AR is an array of dimension MAXDIM x MAXJ x 3 which contains geometric and aerodynamic data as either average values across the span or as values

given at spanwise positions. The values of the array AR, AR(I,J,K), are defined according to the use of each index I, J, and K.

AR array index	Package used in	Definition
K = 1	1,2	Refers to inlet stator data and is used when ARMISC(5) = 1.
K = 2	1,2,3,4	Refers to rotor data, i.e., AR(I,J,2) contains the rotor data.
K = 3	1,2	Refers to outlet stator data and is used when ARMISC(5) = 2.
I = 1	1,2,3,4	AR(1,J,K) = { 0 if average value of quantity corresponding to J and K indexes is to be used; n(K) if spanwise data corresponding to J and K indexes is to be used where n(K) = number of spanwise positions for index K
I = 2	1,2,3,4	AR(2,J,K) refers to the average value of the quantity corresponding to J and K indexes.

AR array index	Package used in	Definition
I = 3,4...	1,2,3,4	AR(I,J,K), I = 3,4 ... refers to spanwise data corresponding to J and K indexes. AR(3,J,K) refers to first nondimensional duct radial position, AR(4,J,K) refers to second nondimensional duct radial position, and so on, in monotonic increasing order.
J = 1	1,2,3,4	ρ, nondimensional duct radial position
J = 2	1,2,3,4	C, nondimensional chord
J = 3	---	Not used
J = 4	1	C_D, drag coefficient
J = 5	---	Not used
J = 6	1,2,3,4	$dC_L/d\alpha$, derivative of steady-state lift coefficient, C_L, with respect to incident angle, α
J = 7	1,2,3,4	M_I, relative inflow Mach number of a blade row; see figure 3.
J = 8	1,2,3,4	M_E, relative exit flow Mach number of a blade row; see figure 3.
J = 9	1,2,3,4	M_Z, axial flow Mach number; see figure 3. Note: the average value, AR(2,9,K), must always be given.

For the remaining definitions of J, the subroutine packages are discussed separately.

For package 1 (AAAAA):

AR array index	Definition
J = 10	f, the ratio of maximum blade camber to the half-chord
J = 11	α, the blade angle of attack

For package 2 (AABAA)

Let NGC = max $\{$ARMISC(18+K): K = 1,2,3$\}$
= number of Glauert coefficients (see sec. 3.2)

AR array index	Definition
J = 10	A^0, Glauert coefficient of order 0
J = 11	A^1, Glauert coefficient of order 1
.	
.	
.	
J = 9 + NGC	A^{NGC-1}, Glauert coefficient of order NGC-1

For package 3 (BCDAA):

If ARMISC(22) = 0, 1:

AR array index	Definition
J = 10	f, the ratio of maximum blade camber to the half-chord
J = 11	α, the blade angle of attack

If ARMISC(22) = 2:

AR array index	Definition
J = 10	f, the ratio of maximum blade camber to the half-chord
J = 11	α, the blade angle of attack
J = 12	a_1, which is used in the power model; see equation (3.3.8)

If ARMISC(22) = 3:

Let NDC = ARMISC(23) = total number of distortion coefficients and let SF = ARMISC(24) = skip factor.

AR array index	Definition
J = 10	f, the ratio of maximum blade camber to the half-chord
J = 11	α, the blade angle of attack
J = 12	a_{SF}, distortion coefficient
J = 13	b_{SF}, distortion coefficient
J = 14	a_{2*SF}, distortion coefficient
J = 15	b_{2*SF}, distortion coefficient
.	.
.	.
.	.
J = 10 + NDC	$a_{\frac{NDC}{2}*SF}$, distortion coefficient
J = 11 + NDC	$b_{\frac{NDC}{2}*SF}$, distortion coefficient

For package 4 (BBCAA):

If ARMISC(25) = 4, no further J's are required and array AR is complete; if ARMISC(25) = 3:

AR array index	Definition
J = 10	f, the ratio of maximum blade camber to the half-chord
J = 11	α, the blade angle of attack

4.5 Restrictions and Limitations

The use and restrictions on the input arrays ARMISC and AR and the special input/output NOFM, MUSE, MAXN, and ARMUMN are given in the previous section.

The maximum spinning mode index is limited (see subroutine EGNVAL2, sec. 3.2.1 of vol. II) in absolute value to 100 and the maximum radial mode index is at most 34.

4.6 Diagnostics

Diagnostic messages related to the computation of eigenvalues are provided according to the printout control parameter ARMISC(6) and the error return parameter IERROR.

When ARMISC(6) $\neq$ 0 and IERROR = 2, the following is printed:

```
A REDUCED SET OF EIGENVALUES IS AVAILABLE
COMPUTATIONS WILL PROCEED.
```

and when ARMISC(6) $\neq$ 0 and IERROR = 4, the following is printed:

```
THERE ARE NO PROPAGATING RADIAL MODES
NO COMPUTATIONS CAN BE MADE.
```

4.7 Storage

Each subroutine package with the subprograms listed in section 4.9 requires the following approximate storage (octal):

	Package	Storage
1	(AAAAA)	12,000
2	(AABAA)	15,000
3	(BCDAA)	12,100
4	(BBCAA)	20,100

4.8 Timing

The timing in general is dominated by the calculation of the eigenvalues. For the sample cases run, the average time per case is:

Subroutine Package	Time in decimal seconds
1	55
2	62
3	117
4	145

4.9 Internal Subprogram Relationships

The following listing gives the subprograms required for each package except the standard CDC - issued system routines such as SORT, SIN, etc. An "X" indicates that the subprogram is used and a blank indicates nonuse. The subprograms used are described either in this documentation (vol. II), or NASA Langley Research Center library subprograms (refs. 41, 42, 43), which are marked by an asterisk.

Subprogram	AAAAA	AABAA	BCDAA	BBCAA
EGNVAL2	X	X	X	X
ZEROS	X	X	X	X
EQATION	X	X	X	X
UNEGNFN	X	X	X	X
EGNNORM	X	X	X	X
FACTINT	X			
FACTIN2		X		
FACTIN3			X	
FACTIN4				X
LIFTFN2		X		
LIFTFN3	X		X	X
LIFTFN4				X
DISINT			X	
FUNIN4				X
NONCPT	X		X	X
APROX1	X	X	X	X
APROX2	X	X	X	X
JARRATT	X	X	X	X
GAUSS			X	X
GAUSS2	X	X	X	X
BSSLS	X	X	X	X
BESNX	X		X	X
BESJLA				X
BESIE				X
BESIK				X

Subprogram	AAAAA	AABAA	BCDAA	BBCAA
ROCABES		X		X
SICI				X
GRTHFCN				X
BF4F*	X	X	X	X
MTLUP*	X	X	X	X
ALGAMF*		X		X

5.0 RESULTS AND CONCLUSIONS

Analytic models for computing the sound pressure at harmonics of the blade passing frequency generated by a single stage of a fan or compressor operating in an infinite, hardwall annular duct have been developed and programmed to give numerical results on a CDC 6600 computer. The outputs of the programs are the hardwall, plug flow mode amplitudes for those harmonics above cutoff—the propagating-mode amplitudes. Using the mode function of section 2.2, the pressures at field points in the duct on either side of the fan stage can be computed by first adding up the product of the mode amplitudes times mode functions to get $\hat{p}$ and then using equation (2.2.4) to get the pressure. Since the pressure is nondimensional, the appropriate reference pressure will have to be used to get the correct SPL level. A simple procedure is to compute the SPL from the computed pressure and add 197 dB, the SPL level of standard atmospheric pressure. However, the more important use to which the results of the programs can be put is as inputs to a duct acoustic program such as the one envisioned by Zorumski (ref. 24).

No attempt has been made to seek out data to compare with the results of this analysis. This should be done, but the data should be well gathered. That is, the experiments should be performed under sufficiently controlled conditions so that a determination can be made on which part of the models—the incident velocity disturbances or the acoustic response of the blade rows—gives the variance.

The interaction models produce the rotor-stator blade number ratio results of Tyler and Sofrin, and Lowson, and they allow studies to be made of the relative importance for sound generation of the potential fields versus the viscous wakes and the fall-off of sound level with blade row spacing. Among other possibilities, the rotor-alone models could be used to gain a better understanding of the differences between static test data and flight data by considering the different inflow conditions of the two situations.

It is felt that to improve these models, one would seek better definition of the velocity disturbances and a less restrictive approximation to the acoustic response function involving, perhaps, the carrying through of the formulation of appendix D.

Boeing Commercial Airplane Company
P.O. Box 3707
Seattle, Washington 98124, May 31, 1974.

APPENDIX A

In this report, the temporal Fourier transform of a real function f(t) is referred to as the spectral density of f and is defined by

$$\hat{f}(\omega) = \int_{-\infty}^{\infty} f(t)\, e^{i\omega t}\, dt \tag{A1}$$

so that

$$f(t) = \frac{1}{2\pi} \int_{-\infty}^{\infty} \hat{f}(\omega)\, e^{-i\omega t}\, d\omega \tag{A2}$$

A function that is periodic has a spectral density that is a sum of Dirac delta functions, or frequency spikes, i.e., if

$$f(t) = \frac{1}{2\pi} \sum_{n=-\infty}^{\infty} f_n\, e^{-i\omega_n t} \tag{A3}$$

then

$$\hat{f}(\omega) = \sum_{n=-\infty}^{\infty} f_n\, \delta(\omega-\omega_n) \tag{A4}$$

All complex functions will obey a symmetry principle in ω (when $\omega \to -\omega$) so that only positive frequencies need to be considered in the final calculations, i.e.,

$$f(t) = \frac{1}{2\pi} \int_{o}^{\infty} 2 \text{ Real } \left(\hat{f}(\omega) e^{-i\omega t} \right) d\omega \tag{A5}$$

Spatial Fourier transforms are defined by

$$\bar{g}(K) = \int_{-\infty}^{\infty} g(x)\ e^{-iKx} dx \tag{A6}$$

with

$$g(x) = \frac{1}{2\pi} \int_{-\infty}^{\infty} \bar{g}(K) e^{iKx} dK \tag{A7}$$

and Fourier series, such as on the interval 0 to 2π,

$$W_{\ell} = \int_{o}^{2\pi} W(\phi)\ e^{-i\ell\phi}\ d\phi \tag{A8}$$

with

$$W(\phi) = \frac{1}{2\pi} \sum_{\ell=-\infty}^{\infty} W_{\ell}\ e^{i\ell\phi} \tag{A9}$$

The linearized differential equations of an inviscid, compressible fluid in which isentropic perturbations from equilibrium can take place are assumed to be sufficient for the analysis. The speed of sound is then taken to be a constant, with

$$\text{speed of sound} = a_o = \sqrt{\frac{p}{\delta}} \qquad \text{(A10)}$$

where p is the pressure perturbation and δ is the density perturbation. It is assumed that for computing the perturbation variables the mean velocity can be taken uniform and constant. Since everything will take place in a duct, the duct outer radius will occur often as a factor multiplying an inverse length type quantity.

The choice is made then to nondimensionalize all quantities from the beginning, choosing the duct outer radius, the speed of sound, and the mean fluid density as the basic scale factors. Letting these be, respectively, r_o, a_o, and d_o, and letting primed quantities be dimensional, then the nondimensional quantities of interest are

$$\delta = \delta' / d_o \qquad \text{density perturbation} \qquad \text{(A11)}$$

$$p = p' / d_o a_o^2 \qquad \text{pressure perturbation} \qquad \text{(A12)}$$

$$v = v' / a_o \qquad \text{velocity perturbation} \qquad \text{(A13)}$$

$$V = M = V' / a_o \qquad \text{mean velocity} \qquad \text{(A14)}$$

$$x = x' / r_o \qquad \text{length} \qquad \text{(A15)}$$

$$t = t' a_o / r_o \qquad \text{time} \tag{A16}$$

$$\omega = \omega' r_o / a_o \qquad \text{frequency} \tag{A17}$$

The nondimensionalized basic equations are

$$\frac{\vec{Dv}}{Dt} + \vec{\nabla} p = 0 \tag{A18}$$

$$\frac{D\delta}{Dt} + \vec{\nabla} \cdot \vec{v} = 0 \tag{A19}$$

$$\delta = p \tag{A20}$$

with

$$\frac{D}{Dt} = \frac{\partial}{\partial t} + \vec{M} \cdot \vec{\nabla} \tag{A21}$$

and $\vec{M}$ is a constant vector. For computing sound pressures, $\vec{M}$ is taken to be axial and positive in the positive z direction, where the z-axis of the coordinate system is coincident with the duct axis. Substituting for δ in equation (A19) and decoupling v from p by applying $\vec{\nabla}\cdot$ to equation (A18) and D/Dt to equation (A19), the convective wave equation for p is arrived at:

$$-\Box_c p = \nabla^2 p - \frac{D^2 p}{Dt^2} = 0 \tag{A22}$$

This is the basic, nondimensionalized equation for this analysis.

APPENDIX B

The required particular integral to the inhomogenous equation, equation (2.1.10), is the familiar Helmholtz equation Green's function for outgoing waves:

$$\hat{\gamma}_{FF}\left(\vec{r^*}\ \vec{r_o^*},\omega^*\right) = -\frac{e^{i\omega^* R^*}}{4\pi R^*} \tag{B1}$$

with

$$R^* = \sqrt{\rho^2+\rho_o^2-2\rho\rho_o\cos\left(\phi-\phi_o\right)+\left(Z^*-Z_o^*\right)^2} \tag{B2}$$

It is more convenient in cylindrical coordinates to express this solution in a combined Fourier series-Fourier transform form,

$$\hat{\gamma}_{FF} = -\frac{i}{8\pi}\sum_{m=-\infty}^{\infty} e^{im\left(\phi-\phi_o\right)} \int_{-\infty}^{\infty} \hat{H}_m^{(1)}\left(\mu\rho_>\right)\cdot J_m\left(\mu\rho_<\right) e^{is\left(Z^*-Z_o^*\right)} ds \tag{B3}$$

(see, e.g., Levine and Schwinger, ref. 44)

$$\mu = \sqrt{\omega^{*2}-s^2} \quad = \sqrt{s^2-\omega^{*2}} \tag{B4}$$

and

$$\rho_> = \begin{cases} \rho & \text{IF } \rho > \rho_o \\ \rho_o & \text{IF } \rho < \rho_o \end{cases} \tag{B5}$$

$$\rho_{<} = \begin{cases} \rho & \text{IF } \rho < \rho_o \\ \rho_o & \text{IF } \rho > \rho_o \end{cases} \tag{B5}$$

and $H_m^{(1)}$ is the Hankel function of the first kind, of order m, and J_m is the Bessel function of order m. By separation of variables, the general solution to the homogenous Helmholtz equation in cylindrical coordinates can be similarly expressed,

$$\hat{\gamma}_B = \frac{i}{8\pi} \sum_{m=-\infty}^{\infty} e^{im\left(\phi-\phi_o\right)} \int_{-\infty}^{\infty} \left\{ A_m J_m\left(\mu\rho\right) + B_m Y_m\left(\mu\rho\right) \right\} e^{is(Z^*-Z_o^*)} \, ds \tag{B6}$$

with Y_m the Neumann function of order m, with A_m and B_m undetermined, and the subscript on $\hat{\gamma}_B$ intended to convey the use to which the general solution will be put, i.e., as a boundary effect. It is by adding $\hat{\gamma}_B$ to $\hat{\gamma}_{FF}$ and solving for A_m and B_m from the boundary conditions that the boundary effects are included in $\hat{\gamma}$. Adding them gives

$$\begin{aligned} \hat{\gamma} &= \hat{\gamma}_{FF} + \hat{\gamma}_B \\ &= \frac{i}{8\pi} \sum_{m=-\infty}^{\infty} e^{im\left(\phi-\phi_o\right)} \int_{-\infty}^{\infty} \left\{ A_m J_m(\mu\rho) + B_m Y_m(\mu\rho) - H_m^{(1)}(\mu\rho_>) J_m(\mu\rho_<) \right\} \\ &\qquad * e^{is(Z^*-Z_o^*)} \, ds \end{aligned} \tag{B7}$$

Employing the boundary conditions of equation (2.1.11),

$$\frac{\partial \hat{\gamma}}{\partial \rho} = o \quad \text{AT} \quad \rho = 1 \quad , \quad \rho = \eta \quad ,$$

gives the simultaneous equations for A_m and B_m,

$$A_m J_m'(\mu) + B_m Y_m'(\mu) = J_m(\mu\rho_o) H_m^{(1)}(\mu)$$

$$A_m J_m'(\mu\eta) + B_m Y_m'(\mu\eta) = J_m'(\mu\eta) H_m^{(1)}(\mu\rho_o) \tag{B8}$$

where the prime denotes differentiation with respect to the argument. The solutions to these equations are

$$A_m = J_m(\mu\rho_o) + i Y_m'(\mu) \frac{J_m(\mu\rho_o) Y_m'(\mu\eta) - Y_m(\mu\rho_o) J_m'(\mu\eta)}{\Delta_m(\mu)} \tag{B9}$$

and

$$B_m = -i J_m'(\mu\eta) \frac{J_m(\mu\rho_o) Y_m'(\mu) - Y_m(\mu\rho_o) J_m'(\mu)}{\Delta_m(\mu)} \tag{B10}$$

with

$$\Delta_m(\mu) = J_m'(\mu) Y_m'(\mu\eta) - J_m'(\mu\eta) Y_m'(\mu) \tag{B11}$$

Substituting these results into equation (B7) and performing the algebra gives for $\hat{\gamma}$,

$$\hat{\gamma} = \frac{1}{2\pi} \sum_{m=-\infty}^{\infty} e^{im\left(\phi-\phi_o\right)} \hat{I}_m\left(\rho,\rho_o,Z^*-Z_o^*,\omega^*\right) \tag{B12}$$

where

$$\hat{I}_m = -\frac{1}{4}\int_{-\infty}^{\infty} \frac{\chi_m(\mu)}{\Delta_m(\mu)}\, e^{is(Z^*-Z_o^*)}\, ds \tag{B13}$$

and

$$\chi_m = \left\{ J_m(\mu\rho_>)\, Y'_m(\mu) - Y_m(\mu\rho_>)\, J'_m(\mu) \right\} \quad \left\{ J_m(\mu\rho_<)\, Y'_m(\mu\eta) - Y_m(\mu\rho_<)\, J'_m(\mu\eta) \right\} \tag{B14}$$

χ_m and Δ_m, when analytically continued into the complex s-plane, are regular functions of the complex variable s. This can be seen by considering Δ_m and letting ω^* have a small positive imaginary part:

$$\omega^* = \omega_R^* + i\varepsilon \ , \ \varepsilon > 0. \tag{B15}$$

Then the branch points of μ are raised off the real s-axis, as in figure 14. The phases of μ are indicated in this figure as well. Across the cut for μ, the following relations hold:

$$J_m(\mu^+) = (-1)^m\, J_m(\mu^-)$$

$$Y_m(\mu^+) = (-1)^m \left[Y_m(\mu^-) + 2\, i\, J_m(\mu^-) \right] \tag{B16}$$

Then, using the relationships

$$2\, J'_m(\mu) = J_{m-1}(\mu) - J_{m+1}(\mu) \tag{B17}$$

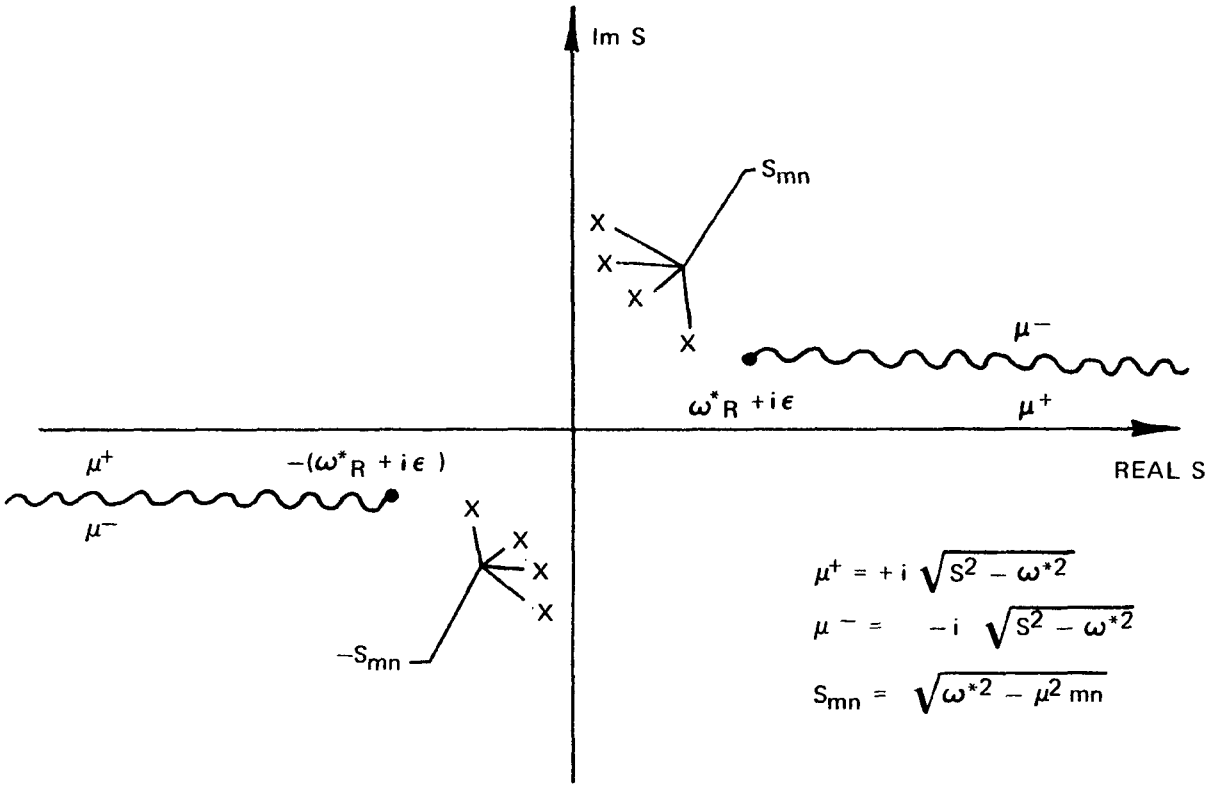

FIGURE 14. — COMPLEX S PLANE

$$2\,Y'_m(\mu) = Y_{m-1}(\mu) - Y_{m+1}(\mu)\ , \tag{B17}$$

it follows that

$$\Delta_m(\mu^+) = 4\left[\left(J_{m-1}(\mu^+) - J_{m+1}(\mu^+)\right)\left(Y_{m-1}(\eta\mu^+) - Y_{m+1}(\eta\mu^+)\right)\right.$$
$$\left. - \left(J_{m-1}(\eta\mu^+) - J_{m+1}(\eta\mu^+)\right)\left(Y_{m-1}(\mu^+) - Y_{m+1}(\mu^+)\right)\right]$$
$$= \Delta_m(\mu^-) \tag{B18}$$

from equation (B16). Similarly for χ_m.

Then, since the zeros of Δ_m are not coincident with the zeros of χ_m, the integrand of the integral for $\hat{I}_m$ is meromorphic in the finite complex s-plane. For $z^* - z_o^* > 0$, the contour can be closed in the upper half-plane to encircle the poles at the zeros of Δ_m. If these zeros (an infinite number, since Δ_m is transcendental) occur at s_{mn}, $n = 0, 1, 2, \ldots$, then

$$\hat{I}_m = -\frac{i\pi}{2}\sum_{n=o}^{\infty} \text{RES}\left[(s-s_{mn})\,\frac{\chi_m}{\Delta_m}\,e^{is(Z^*-Z_o^*)}\right]_{s\to s_m} \tag{B19}$$

The zeros in the lower half-plane occur at $s = -s_{mn}$, $n = 0, 1, 2, \ldots$ (see fig. 15), so that when $z^* - z_o^* < 0$, and the contour is closed in the lower half-plane,

$$\hat{I}_m = + \frac{i\pi}{2} \sum_{n=o}^{\infty} \text{RES} \left[(s + s_{mn}) \frac{\chi_m}{\Delta_m} e^{is(Z^*-Z_o^*)} \right]_{s \to -s_{mn}} \qquad \text{(B20)}$$

Since Δ_m is a function of μ, the zeros of Δ_m are $\mu = \mu_{mn}$, $n = 0, 1, 2, \ldots$, real, nonnegative numbers, and since

$$\Delta_m = - \Delta_m \quad , \quad \mu_{mn} = \mu_{-mn}$$

This gives for s_{mn},

$$s_{mn} = \sqrt{\omega^{*2} - \mu_{mn}^2} \qquad \text{(B21)}$$

See appendix J for a discussion of the numerical scheme used to calculate these zeros.

Near a zero in the upper half-plane,

$$\begin{aligned} \Delta_m(\mu) &\approx \Delta_m(\mu_{mn}) + (s-s_{mn}) \left. \frac{d\mu}{ds} \right|_{s = s_{mn}} \Delta'_m(\mu_{mn}) \\ &= (s-s_{mn}) \left. \frac{d\mu}{ds} \right|_{s = s_{mn}} \Delta'_m(\mu_{mn}) \quad , \end{aligned} \qquad \text{(B22)}$$

$$\text{RES}\left[\ \right] = \frac{\chi_m(\mu_{mn})}{\left. \frac{d\mu}{ds} \right|_{s=s_{mn}} \Delta'_m(\mu_{mn})} e^{i\, s_{mn}(Z^*-Z_o^*)} \qquad \text{(B23)}$$

From equation (B4),

$$\left.\frac{d\mu}{ds}\right|_{s=s_{mn}} = -\frac{s_{mn}}{\mu_{mn}} \quad , \tag{B24}$$

and

$$\Delta'_m(\mu_{mn}) = \Big[\, J''_m(\mu)\, Y'_m(\mu\eta) + \eta\, J'_m(\mu)\, Y''_m(\mu\eta) - \eta\, J''_m(\mu\eta)\, Y'_m(\mu)$$

$$-J'_m(\mu\eta)\, Y''_m(\mu)\Big]_{\mu=\mu_{mn}}$$

$$= -\left(1-\frac{m^2}{\mu_{mn}^2}\right) Y'_m\left(\eta\mu_{mn}\right)\, R_m\left(\mu_{mn}\right) + \eta\left(1-\frac{m^2}{\eta^2\mu_{mn}^2}\right) Y'_m\left(\mu_{mn}\right)\, R_m\left(\eta\mu_{mn}\right) \tag{B25}$$

with

$$R_m\left(\mu_{mn}\rho\right) = J_m\left(\mu_{mn}\rho\right) - \frac{J'_m\left(\eta\mu_{mn}\right)}{Y'_m\left(\eta\mu_{mn}\right)}\, Y_m\left(\mu_{mn}\rho\right) \tag{B26}$$

and use has been made of the result from $\Delta_m = 0$,

$$\frac{J'_m\left(\eta\mu_{mn}\right)}{Y'_m\left(\eta\mu_{mn}\right)} = \frac{J'_m\left(\mu_{mn}\right)}{Y'_m\left(\mu_{mn}\right)} \tag{B27}$$

Also,

$$\chi_m\left(\mu_{mn}\right) = Y'_m\left(\mu_{mn}\right) Y'_m\left(\eta\mu_{mn}\right) R_m\left(\mu_{mn}\rho\right) R_m\left(\mu_{mn}\rho_o\right) \tag{B28}$$

so that

$$RES = \frac{Y'_m\left(\mu_{mn}\right) Y'_m\left(\eta\mu_{mn}\right) R_m\left(\mu_{mn}\rho\right) R_m\left(\mu_{mn}\rho_o\right) e^{is_{mn}\left(Z^*-Z_o^*\right)}}{\frac{s_{mn}}{\mu_{mn}}\left\{\left(1-\frac{m^2}{\mu_{mn}^2}\right) Y'_m\left(\eta\mu_{mn}\right) R_m\left(\mu_{mn}\right) - \eta\left(1-\frac{m^2}{\eta^2\mu_{mn}^2}\right) Y'_m\left(\mu_{mn}\right) R_m\left(\mu_{mn}\eta\right)\right\}} \tag{B29}$$

Dividing top and bottom of this expression by $Y'_m\left(\mu_{mn}\right) Y'_m\left(\eta\mu_{mn}\right)$

gives

$$RES = \frac{R_m\left(\mu_{mn}\rho\right) R_m\left(\mu_{mn}\rho_o\right)}{\frac{1}{\mu_{mn}}\left\{\left(1-\frac{m^2}{\mu_{mn}^2}\right)\frac{R_m\left(\mu_{mn}\right)}{Y'_m\left(\mu_{mn}\right)} - \eta\left(1-\frac{m^2}{\eta^2\mu_{mn}^2}\right)\frac{R_m\left(\eta\mu_{mn}\right)}{Y'_m\left(\eta\mu_{mn}\right)}\right\}} \frac{e^{is_{mn}\left(Z^*-Z_0^*\right)}}{s_{mn}} \tag{B30}$$

Then,

$$\frac{R_m\left(\mu_{mn}\right)}{Y'_m\left(\mu_{mn}\right)} = \frac{R_m^2\left(\mu_{mn}\right)}{Y'_m\left(\mu_{mn}\right) J_m\left(\mu_{mn}\right) - J'_m\left(\mu_{mn}\right) Y_m\left(\mu_{mn}\right)}$$

$$= \frac{\pi}{2}\mu_{mn} R_m^2\left(\mu_{mn}\right) \tag{B31}$$

and

$$\frac{R_m\left(\eta\mu_{mn}\right)}{Y'_m\left(\eta\mu_{mn}\right)} = \frac{\pi}{2}\,\mu_{mn}\,\eta\,R_m^2\left(\eta\mu_{mn}\right) \tag{B32}$$

Thus,

$$\text{RES.} = \frac{1}{\pi}\,\frac{R_m\left(\mu_{mn}\rho\right)\;R_m\left(\mu_{mn}\rho_o\right)}{\frac{1}{2}\left\{\left(1-\frac{m^2}{\mu_{mn}^2}\right)R_m^2\left(\mu_{mn}\right)-\eta^2\left(1-\frac{m2}{\eta^2\mu_{mn}^2}\right)R_m^2\left(\eta\mu_{mn}\right)\right\}}\,\frac{e^{is_{mn}\left(Z^*-Z_o^*\right)}}{s_{mn}}$$

$$= \frac{1}{\pi}\,\mathcal{R}_m\left(\mu_{mn}\rho\right)\;\mathcal{R}_m\left(\mu_{mn}\rho_o\right)\frac{e^{is_{mn}\left(Z^*-Z_o^*\right)}}{s_{mn}} \tag{B33}$$

where

$$\mathcal{R}_m\left(\mu_{mn}\rho\right) = \frac{R_m\left(\mu_{mn}\rho\right)}{N_{mn}} \tag{B34}$$

and

$$N_{mn}^2 = \frac{1}{2}\left\{\left(1-\frac{m^2}{\mu_{mn}^2}\right)R_m^2\left(\mu_{mn}\right)-\eta^2\left(1-\frac{m^2}{\eta^2\mu^2{}_{mn}}\right)R_m^2\left(\eta\mu_{mn}\right)\right\} \tag{B35}$$

This is a convenient form for the result since N_{mn} is the normalization of the $R_m(\mu_{mn}\rho)$ function, i.e.,

$$\int_{\eta}^{1} \mathcal{R}_m\left(\mu_{mn}\rho\right)\ \mathcal{R}_m\left(\mu_{m\ell}\rho\right)\ \rho d\rho = \delta_{n\ell} \tag{B36}$$

Then, for $Z^* - Z_o^* > 0$,

$$\hat{I}_m = \sum_{n=o}^{\infty} \mathcal{R}_m\left(\mu_{mn}\rho\right)\ \mathcal{R}_m\left(\mu_{mn}\rho_o\right)\ \frac{e^{is_{mn}\left(Z^*-Z_o^*\right)}}{2\,is_{mn}} \tag{B37}$$

For For $Z^* - Z_o^* < 0$,

$$\left.\frac{d\mu}{ds}\right|_{s=-s_{mn}} = -\frac{s}{\mu}\Bigg|_{s=-s_{mn}} = \frac{s_{mn}}{\mu_{mn}} \tag{B38}$$

So that, following the same algebra, from equation (B20),

$$\hat{I}_m = \sum_{n=o}^{\infty} \mathcal{R}_m\left(\mu_{mn}\rho\right)\ \mathcal{R}_m\left(\mu_{mn}\rho_o\right)\ \frac{e^{-is_{mn}\left(Z^* - Z_o^*\right)}}{2is_{mn}} \tag{B39}$$

Finally, the result for $\hat{I}_m$ is

$$\hat{I}_m\left(\rho,\rho_o,\ Z^*-Z_o^*,\ \omega^*\right) = \sum_{n=o}^{\infty} \mathcal{K}_m\left(\mu_{mn}\rho\right) \mathcal{K}\left(\mu_{mn}\rho_o\right)\ \hat{d}_{mn}\left(Z^*-Z_o^*,\omega^*\right)$$

(B40)

with

$$\hat{d}_{mn}\left(Z^*-Z_o^*,\omega^*\right) = \frac{e^{is_{mn}\left|Z^*-Z_o^*\right|}}{2is_{mn}}$$

(B41)

Substituting this result into equation (B12) gives the final result, the solution for $\hat{\gamma}$:

$$\hat{\gamma} = \frac{1}{2\pi}\sum_{m=-\infty}^{\infty}{}' e^{im\left(\phi-\phi_o\right)}\sum_{n=o}^{\infty}\mathcal{K}_m\left(\mu_{mn}\rho\right)\mathcal{K}_m\left(\mu_{mn}\rho_o\right)\hat{d}_{mn}\left(Z^*-Z_o^*,\omega^*\right)$$

(B42)

Considering ω^* to be a complex variable, then s_{mn} as a function of the complex ω^* has the branch line and phases as indicated in figure 15. Hence, for $\omega^* > \mu_{mn}$, $s_{mn}(-\omega^*) = -s_{mn}(\omega^*)$, and when $\omega^* < \mu_{mn}$, $s_{mn} = i\sqrt{\mu_{mn}^2 - \omega^{*2}}$ when ω^* approaches the real axis from above it. The region of the real axis outside the branch points at $\pm\mu_{mn}$ is referred to as the propagation (or "cut-on") region. It is seen that

$$\hat{d}_{mn}\left(Z^*-Z_o^*,-\omega^*\right) = \hat{d}_{mn}^{\dagger}\left(Z^*-Z_o^*,\omega^*\right)$$

(B43)

where $\dagger$ means complex conjugation. This ensures that $\hat{\gamma}(-\omega^*) = \hat{\gamma}^{\dagger}(\omega^*)$. Finally, just above the real axis in the propagating region, s_{mn} has a

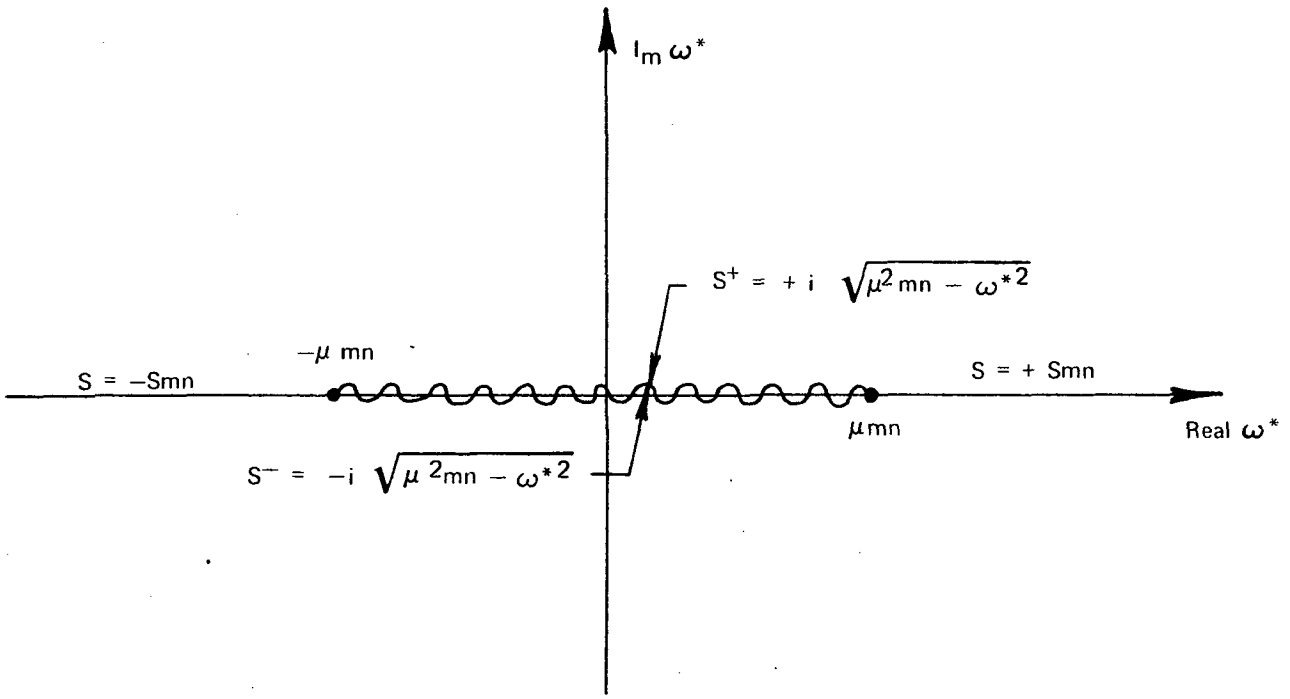

FIGURE 15. – COMPLEX ω PLANE*

positive imaginary part greater than that of ω^* so that for $|z^* - z_o^*| \to \infty$,

$$\hat{\gamma} \sim e^{-a\ \mathrm{Im}\,(\omega^*)\ |Z^* - Z_o^*|} \tag{B44}$$

APPENDIX C

The evaluation of equation (2.2.7) is done using the transforms of F and D_{mn}. Letting

$$F\left(t_o\right) = \frac{1}{2\pi}\int_{-\infty}^{\infty} \hat{F}(\omega)\, e^{-i\omega t_o}\, d\omega \tag{C1}$$

and

$$D_{mn}\left(Z-Z_o,\tau\right) = \frac{1}{2\pi}\int_{-\infty}^{\infty} \hat{D}_{mn}\left(Z-Z_o,\omega\right)\, e^{-i\omega\tau}\, d\omega \tag{C2}$$

with $\tau = t - t_o$, then

$$p(\vec{r},t) = -\frac{1}{2\pi}\sum_{m=-\infty}^{\infty}\sum_{n=o}^{\infty} \mathcal{R}_m\left(\mu_{mn}\rho\right)\mathcal{R}_m\left(\mu_{mn}\rho_s\right) e^{im\phi} \tag{C3}$$

$$\cdot\int_{-\infty}^{\infty}\int \frac{d\omega}{2\pi}\frac{d\omega'}{2\pi}\left[\frac{m}{\rho_s}\, e_\phi + K_{mn}^{\pm} e_z\right]\, \hat{F}(\omega)\, e^{i\omega' t}$$

$$\cdot\hat{D}_{mn}\left(Z-Z_s,\omega'\right)\sum_{\ell=-\infty}^{\infty}\int_{-\infty}^{\infty}\int_{o}^{2\pi}\delta\left(\phi_o - \bar{\phi} + 2\pi\ell - \Omega t_o\right)\, e^{-im\phi_o} e^{-i(\omega-\omega')t_o}\, dt_o d\phi_o$$

Considering the t_o and ϕ_o integration, the delta function gives

$$\sum_{\ell=-\infty}^{\infty} \int_{-\infty}^{\infty} \int_{0}^{\pi} \delta\left(\phi_o - \bar{\phi} + 2\pi\ell - \Omega t_o\right) e^{i(\omega-\omega')t_o} e^{-im\phi_o} \, dt_o d\phi_o \tag{C4}$$

$$= \left(\sum_{\ell=-\infty}^{\infty} \frac{1}{\Omega} e^{-2\pi i \ell \frac{\omega-\omega'}{\Omega}}\right) e^{i\frac{\omega-\omega'}{\Omega}\bar{\phi}} \int_{0}^{2\pi} e^{-i\frac{\omega-\omega'+m\Omega}{\Omega}\phi} d\phi_o$$

$$= \sum_{\ell=-\infty}^{\infty} \frac{1}{\Omega} \int_{0}^{2\pi} e^{-i\left(\frac{\omega-\omega'}{\Omega}\right)\left(\phi_o - \bar{\phi} + 2\pi\ell\right)} e^{-im\phi_o} d\phi_o$$

Then, using Poisson's sum rule, and doing the ϕ_o integration, gives

$$\text{R.H.S.} = \sum_{\sigma=-\infty}^{\infty} \delta\left(\sigma\Omega - (\omega-\omega')\right) e^{i\sigma\bar{\phi}} \frac{i\Omega}{\omega-\omega' + m\Omega} \left(e^{-2\pi i \frac{\omega-\omega' + m\Omega}{\Omega}} - 1\right)$$

$$= \sum_{\sigma=-\infty}^{\infty} \delta\left(\sigma\Omega - (\omega-\omega')\right) e^{i\sigma\bar{\phi}} \frac{i}{\sigma + m} \left(e^{-2\pi i(\sigma + m)} - 1\right)$$

$$= \sum_{\sigma=-\infty}^{\infty} \delta\left(\sigma\Omega - (\omega-\omega')\right) e^{i\sigma\bar{\phi}} 2\pi \, \delta_{\sigma,-m} \tag{C5}$$

$$= 2\pi\ \delta(\omega-\omega' + m\Omega)\ e^{-im\bar{\phi}}$$

$$\hat{p}^{\pm}(\vec{r},\omega) = -\frac{1}{2\pi}\sum_{m=-\infty}^{\infty}\sum_{n=0}^{\infty}\mathcal{R}_m\left(\mu_{mn}\rho\right)\ \mathcal{R}_m\left(\mu_{mn}\rho_o\right)e^{im\phi}\ e^{iK^{\pm}_{mn}Z}$$

$$\cdot\left[\frac{\frac{m}{\rho_s}e_\phi + K^{\pm}_{mn}\,e_\phi}{2\beta_{mn}}\right]e^{-im\bar{\phi}}e^{-iK^{\pm}_{mn}Z_s}\cdot\int_{-\infty}^{\infty}d\omega'\delta(\omega'-\omega + m\Omega)\ \hat{F}(\omega')$$

$$= \frac{1}{2\pi}\sum_{m=-\infty}^{\infty}\sum_{n=0}^{\infty}A^{\pm}_{mn}(\omega)\ \mathcal{R}_m\left(\mu_{mn}\rho\right)e^{i\left(m\phi + K^{\pm}_{mn}Z\right)} \qquad (C6)$$

$$A^{\pm}_{mn}(\omega) = -\hat{F}(\omega-m\Omega)\ \frac{\frac{m}{\rho_s}e_\phi + K^{\pm}_{mn}\,e_z}{2\beta_{mn}}\ \mathcal{R}_m\left(\mu_{mn}\rho_s\right)e^{-i\left(m\bar{\phi} + K^{\pm}_{mn}Z_s\right)} \qquad (C7)$$

APPENDIX D

The geometry is shown in figure 16, assuming for this discussion a stationary row. The blades are unstaggered, flat-plate, constant chord airfoils, so that $e_\phi = 1$ and $e_z = 0$. Letting $z_{M.C.} = 0$, then when points within the blade row are to be considered, the pressure spectral density resulting from the airfoils being dipole surfaces is

$$\hat{p}\ (\vec{r},\omega) = -\frac{c}{8\pi}\sum_{m=-\infty}^{\infty}\sum_{n=o}^{\infty}\sum_{j=o}^{N-1} \mathcal{R}_m\left(\mu_{mn}\rho\right) e^{im\phi}\ \frac{m}{\beta_{mn}}\int_{\eta}^{1}\frac{d\rho_s}{\rho_s}\,\mathcal{R}_m\left(\mu_{mn}\rho_s\right)$$

$$\cdot\int_{-1}^{1}\hat{F}_j\left(\rho_s,\xi';\omega\right)\left\{\varepsilon\left(\bar{Z}'-\xi'\right)\ e^{i\kappa^{+}_{mn}\left(\bar{Z}'-\xi'\right)}+\varepsilon\left(\xi'-\bar{Z}'\right)\ e^{i\kappa^{-}_{mn}\left(\bar{Z}'-\xi'\right)}\right\}d\xi' \tag{D1}$$

with

$$\bar{Z}' = \frac{Z'}{\frac{c}{2}} \tag{D2}$$

and

$$\kappa^{\pm}_{mn} = \frac{c}{2}\,K^{\pm}_{mn} \tag{D3}$$

The ϕ-component of the velocity spectral density associated with this pressure field is, from equation (A18).

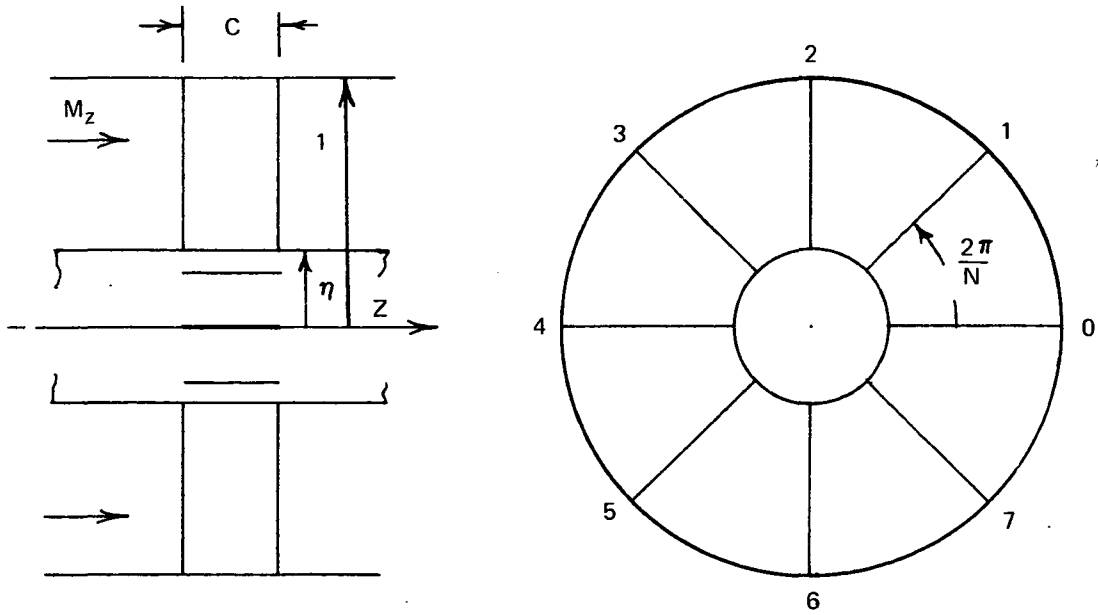

FIGURE 16. – UNSTAGGERED BLADES IN ANNULUS

$$\hat{v}_\phi(\rho,\phi,Z,\omega) = \hat{v}_\phi(\rho,\phi,Z=-\infty,\omega) - \frac{1}{M}\int_{-\infty}^{Z} e^{i\frac{\omega}{M}(Z-Z')} \frac{1}{\rho}\frac{\partial \hat{p}(\rho,\phi,Z',\omega)}{\partial \phi} dZ$$

$$= \hat{v}_\phi(\rho,\phi,Z=-\infty,\omega) + \frac{c^2}{16\pi i M\rho}\sum_{m=-\infty}^{\infty}\sum_{n=o}^{\infty}\sum_{j=o}^{N-1}\frac{m^2}{\beta_{mn}}\mathcal{R}_m\left(\mu_{mn}\rho\right)$$

$$\cdot e^{im\left(\phi-\frac{2\pi j}{N}\right)}\int_{-1}^{1}\hat{f}_{mnj}(\xi',\omega)\Delta_{mn}(\xi',Z)\,d\xi' \qquad \text{(D4)}$$

with

$$\hat{f}_{mnj}(\xi',\omega) = \int_{\eta}^{1}\mathcal{R}_m\left(\mu_{mn}\rho_s\right)\hat{F}_j\left(\rho_s,\xi',\omega\right)\frac{d\rho_s}{\rho_s} \qquad \text{(D5)}$$

and

$$\Delta_{mn}(\xi',Z) = \int_{-\infty}^{Z}\left\{\varepsilon\left(\bar{Z}'-\xi'\right)e^{i\kappa^{+}_{mn}(\bar{Z}'-\xi')} + \varepsilon\left(\xi'-\bar{Z}'\right)e^{i\kappa^{-}_{mn}\left(\bar{Z}'-\xi'\right)}\right\}d\bar{Z}' \qquad \text{(D6)}$$

The boundary conditions at the airfoils are that this induced velocity cancels the "incident" velocity normal to the airfoil,

$$\hat{u}\ , \text{ FOR } k = 0,1,\cdots,N-1,\quad \phi_k = \frac{2\pi k}{N}\ ,$$

$$\hat{u}_k(\rho,Z,\omega) = \hat{u}(\rho,\phi_k,Z,\omega) = -\hat{v}_\phi\left(\rho,\phi_k,Z,\omega\right) \qquad \text{(D7)}$$

with

$$\eta < \rho < 1 \quad \text{AND} \quad -\frac{c}{2} \leq Z \leq \frac{c}{2} \quad ,$$

and that the pressure difference or dipole density vanishes at the trailing edge (the Kutta condition). These conditions turn equation (D4) into the system of equations for $\hat{f}_{mnj}$

$$-\hat{u}_k(\rho,Z,\omega) = \hat{v}_{\phi k}(\rho,Z=-\infty,\omega) + \frac{c^2}{16\pi i M\rho} \sum_{m=-\infty}^{\infty} \sum_{n=o}^{\infty} \frac{m^2}{\beta_{mn}} \mathcal{R}_m(\mu_{mn}\rho)$$

$$\cdot \int_{-1}^{1} \left\{ \sum_{j=o}^{N-1} e^{2\pi i m \frac{k-j}{N}} \hat{f}_j(\xi',\omega) \right\} \Delta_{mn}(\xi',Z)\, d\xi' \qquad \text{(D8)}$$

for $k = 0, 1, \ldots N-1$, and ρ,z on the k^{th} airfoil. The state of affairs in solving this problem seems to be as follows: writing equation (D1) in the form

$$\hat{p}(r,\omega) = \sum_{j=o}^{N-1} \iint \hat{F}_j(\rho_s,Z_s,\omega) \frac{\partial \hat{\Gamma}}{\partial n_s} da_s \qquad \text{(D9)}$$

with da_s a surface area element, and using $\hat{\Gamma} = \hat{\Gamma}_{FF} + \hat{\Gamma}_B$ (see appendix B), with $\hat{\Gamma}_{FF}$ the free-field propagator and $\hat{\Gamma}_B$ the "duct wall effects" function, gives

$$\hat{P} = \hat{P}_{FF} + \hat{P}_B \qquad \text{(D10)}$$

with $\hat{p}_{FF}$ and $\hat{p}_B$ given by equation (D9), with $\hat{\Gamma}_{FF}$ and $\hat{\Gamma}_B$ in place of $\hat{\Gamma}$, respectively. The term $\hat{p}_B$ is then neglected for the purpose of solving for $\hat{F}_j$. Further, the three-dimensional problem remaining is converted to a two-dimensional cascade problem by taking the airfoils to be infinite and parallel (see Kaji and Okazaki, [ref. 45] and Mani [ref. 46]).

APPENDIX E

The phase factor

$$e^{-in N_1 \frac{d}{\rho} \text{ TAN } \psi} \tag{E1}$$

in equation (3.1.9) accounts for the relative phase of the wake at the downstream row for different span positions. If tan ψ is not proportional to ρ, then the wake will be skewed, i.e., nonradial, and the relative phase will be different for different span positions. Three-dimensional flow effects might also cause skewness in the wakes. A crude model to account for some of this extra skewness is the following: assume that the major three-dimensional correction will be in the tip region and consider the linear adjustment

$$\frac{d}{\rho} \text{ TAN } \psi \longrightarrow \frac{d}{\rho} \text{ TAN}\psi \; -\phi \frac{\rho-\eta}{1-\eta} \tag{E2}$$

where ϕ and this linear phase adjustment is illustrated in figure 17.

This correction is included in the computer subprogram but has no other justification than that it was a part of a study to understand the effects of wake skewness on tone noise. The correction was not itself developed from theory.

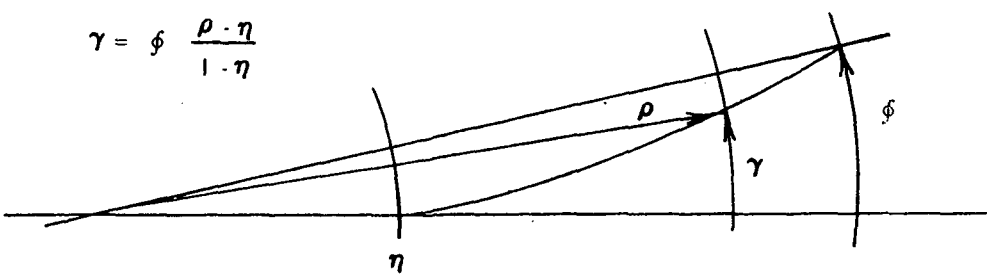

FIGURE 17. — VISCOUS WAKE SKEWNESS CORRECTION

APPENDIX F

The equations for the mode amplitudes of the four potential flow field interactions are very similar. They only differ in signs and indexes. All four interactions are therefore represented by the same set of equations. Modifications to the signs in the equations are done with switches C3 to C14, defined in the table following the equations.

$$\gamma_K = \left| \text{arc} \cos\left(\frac{M_{Z,K}}{M_{M,K}}\right) \right| \tag{F1}$$

$$M_{M,K} = \sqrt{\left(\sqrt{M_{I,K}^2 - M_{Z,K}^2} + \sqrt{M_{E,K}^2 - M_{Z,K}^2}\right)^2 \frac{1}{4} + M_{Z,K}^2} \tag{F2}$$

$$\Gamma_{K2} = \pi \cdot C_{K2} \cdot M_{M,K2} \left(A_{o,K2} + A_{1,K2}\right) \tag{F3}$$

$$G_{\kappa,K1} = C_6 \cdot \frac{C_{K1}}{2\rho} N_{K2} \; e^{-C_7 \frac{d}{\rho} N_{K2}^{\kappa}} \; H_{\kappa,K2} \; e^{-i\left[C_8 \gamma_{K1} + C_9 N_{K2}^{\kappa}\left(\frac{d}{\rho}\tan\gamma_{K1} + \frac{M_t C_{K2}}{2M_{M,K2}}\right)\right]} \tag{F4}$$

$$H_{\kappa,K2} = J_o\left(\left(C_{12}^{\kappa} \frac{C_{K2}}{2\rho} N_{K2} \; e^{iC_{13}\left(\frac{\pi}{2} - C_{14}\gamma_{K2}\right)}\right) + \sum_{n=1}^{\infty}\left[\left(C_{11} i\right)^n \frac{A_{n+1,K2} - A_{n-1,K2}}{A_{o,K2} + A_{1,K2}} J_n\left(C_{12}^{\kappa} \frac{C_{K2}}{2\rho} N_{K2} \; e^{iC_{13}\left(\frac{\pi}{2} - C_{14}\gamma_{K2}\right)}\right)\right]\right) \tag{F5}$$

$$K_{\kappa,K1} = \begin{cases} \left[K_L \left(\nu_{\kappa,K1}, \lambda_{\kappa,K1}\right)\right]^* & \nu_{\kappa,K1} > 0 \\ \left[K_L \left(-\nu_{\kappa,K1}, -\lambda^*_{\kappa,K1}\right)\right] & \nu_{\kappa,K1} < 0 \end{cases} \tag{F6}$$

$$K_L(\nu,\lambda) = \left[J_o(\lambda) - i\, J_1(\lambda)\right] \frac{H_1^{(2)}(\nu)}{H_1^{(2)}(\nu) + iH_o^{(2)}(\nu)} + i\,\frac{\nu}{\lambda}\, J_1(\lambda) \tag{F7}$$

$$\nu_{\kappa,K1} = C_6 \frac{M_t \cdot N_{K2} \cdot C_{K1}}{2 \cdot M_{M,K1}}\, \kappa \tag{F8}$$

$$\lambda_{\kappa,K1} = C_6\, \kappa\, \frac{C_{K1}}{2\rho}\, N_{K2}\, e^{C_3\, i \left(\frac{\pi}{2} - \gamma_{K1}\right)} \tag{F9}$$

$$\sum_{j=o}^{N_1-1} e^{-im\frac{2\pi_j}{N_1}} \cdot \hat{L}_j(\rho,\omega) = N_{K1} \cdot \Gamma_{K2} \cdot M_{M,K1} \cdot \frac{1}{2} \left(\frac{dC_L}{d\alpha}\right)_{K1} G_{\kappa,K1}\, K_{\kappa,K1}\, \delta\left(\omega_{\kappa,K1} - \omega\right) \tag{F10}$$

$$A^{\pm}_{mn}(\omega) = - \frac{e^{-iK^{\pm}_{mn} Z_{M.C.}}}{2\beta_{mn}} \cdot$$

$$\int_{\eta}^{1} \left[\frac{me_{\phi}}{\rho} + K^{\pm}_{mn} e_Z\right] \mathcal{R}_m\left(\mu_{mn}\rho\right) \sum_{j=0}^{N_{K1}-1} e^{-im\frac{2\pi j}{N_{K1}}}\, \hat{L}_j(\rho,\omega)\, d\rho \tag{F11}$$

The following table gives the values of the switches required in the previous equations to make the equations represent a specific interaction. For an interaction specified by a column in the upper box, the corresponding column in the lower box gives the appropriate value of the switches. The abbreviations and indexes used in the table are as follows:

Component	Index	Abbreviation
Inlet stator	1	IS
Rotor	2	R
Outlet stator	3	OS

Velocity-inducing component	IS	R	OS	R	IS	R	OS	R
Lift-producing component	R	OS	R	IS	R	OS	R	IS
Subscript of velocity-inducing component, K2	1	2	3	2	1	2	3	2
Subscript of sound-producing component, K1	2	3	2	1	2	3	2	1
Sign of κ	<o				>o			
κ	ℓ	σ	ℓ	σ	ℓ	σ	ℓ	σ
C3	-1	1	1	-1	1	-1	-1	1
C6	-1	1	-1	1	-1	1	-1	1
C7	-1	-1	-1	-1	1	1	1	1
C8	1	-1	-1	1	-1	1	1	-1
C9	1	-1	-1	1	1	-1	-1	1
C11	1	1	-1	-1	-1	-1	1	1

C12	-1	-1	-1	-1	1	1	1	1
C13	-1	-1	-1	-1	1	1	1	1
C14	1	-1	-1	1	1	-1	-1	1

APPENDIX G

Figure 18 illustrates the rotor blades as a two-dimensional cascade and defines the blade coordinates. It is seen that a point in the velocity field is given in terms of the blade-fixed coordinates of the j^{th} blade by

$$Z = \bar{Z}'_j \text{ COS } \gamma + \bar{Y}'_j \text{ SIN } \gamma + Z_{M.C.}$$

$$Y = -\bar{Z}'_j \text{ SIN}\gamma + \bar{Y}'_j \text{ COS } \gamma + jb + Ut - \ell 2\pi\rho \qquad \text{(G1)}$$

where the $\ell 2\pi\rho$ term results from the periodicity on $2\pi\rho$ of the distortion (this must be modified if there is preswirl to the rotor). Assuming the two-dimensional representation of the distortion, then the magnitude of the velocity disturbance at the j^{th} rotor blade on the ℓ^{th} revolution is, at $\bar{Y}'_j = 0$

$$W_\ell(Y,Z,t) = \int_{-\infty}^{\infty}\int\int \frac{d\lambda}{2\pi}\,\frac{dK}{2\pi}\,\frac{d\omega}{2\pi}\,\hat{\hat{W}}\,(K,\lambda,\omega)\; e^{i(KY+\lambda Z-\omega t)}$$

$$= \int_{-\infty}^{\infty}\int\int \frac{d\lambda}{2\pi}\,\frac{dK}{2\pi}\,\frac{d\omega}{2\pi}\,\hat{\hat{W}}\, e^{-2\pi i\ell K\rho}\, e^{i(KU-\omega t)}\, e^{ijKb}$$

$$\cdot\; e^{-i(K\text{SIN}\gamma-\lambda\text{COS}\gamma)\bar{Z}'_j}\, e^{i\lambda Z_{M.C.}} \qquad \text{(G2)}$$

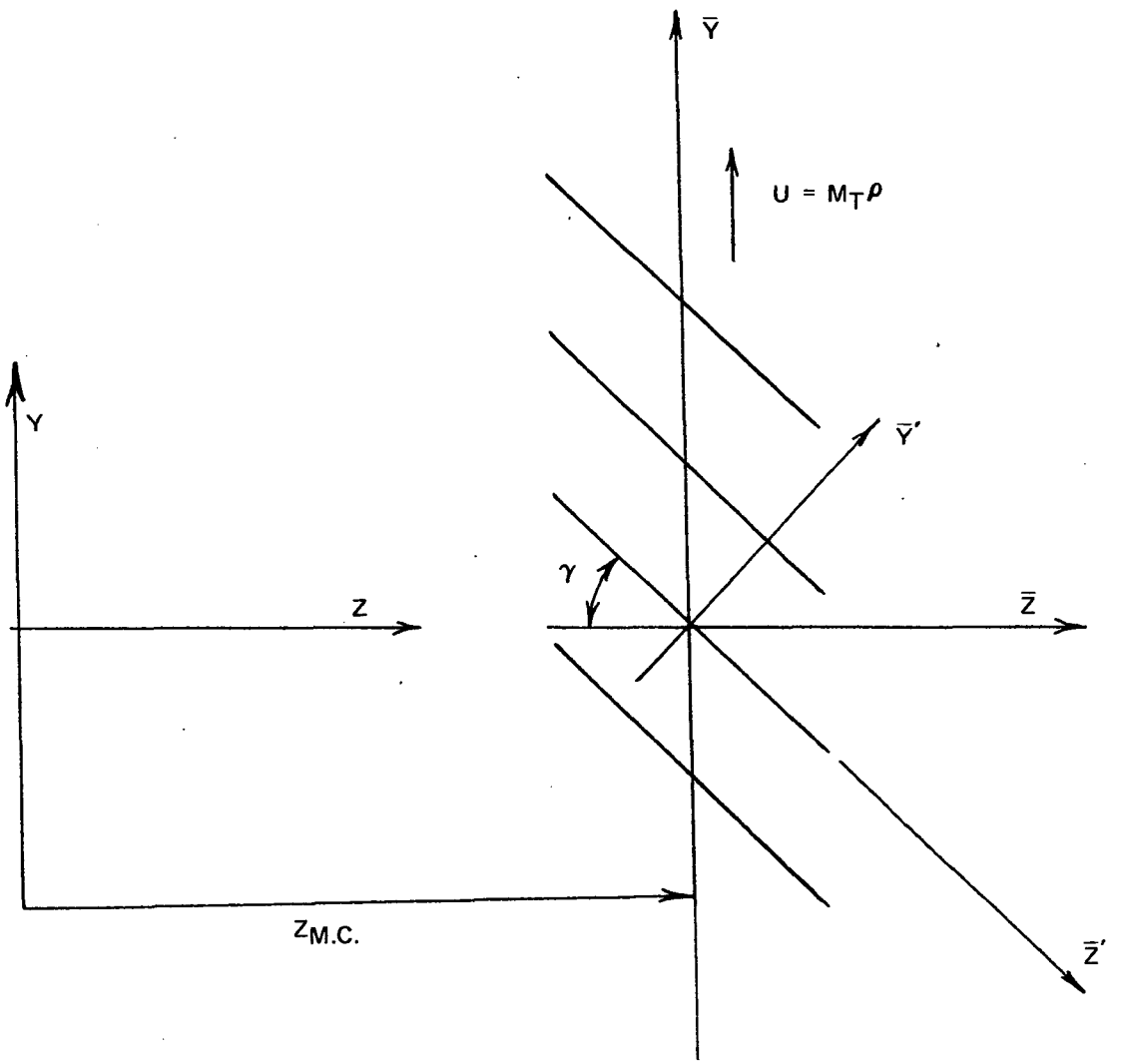

FIGURE 18. – CASCADE REPRESENTATION OF ROTOR ALONE

The sum over all the periods gives the velocity

$$W = \sum_{\ell=-\infty}^{\infty} W_\ell \tag{G3}$$

From the Poisson sum rule,

$$\sum_{\ell=-\infty}^{\infty} e^{-2\pi i \ell K \rho} = \frac{1}{\rho} \sum_{n=-\infty}^{\infty} \delta\left(K - \frac{n}{\rho}\right), \tag{G4}$$

so that, using $b = 2\pi\rho/N$ and $U = M_T\rho$,

$$W = \frac{1}{2\pi\rho} \sum_{n=-\infty}^{\infty} e^{in\frac{2\pi j}{N}} \iint_{-\infty}^{\infty} \frac{d\lambda}{2\pi} \frac{d\omega}{2\pi} \hat{\bar{\bar{W}}}\left(\frac{n}{\rho}, \lambda, \omega\right) e^{i\lambda Z_{M.C.}} \tag{G5}$$

$$\cdot\, e^{i\left[(\lambda \text{COS } \gamma - \frac{n}{\rho} \text{ SIN } \gamma)\, \bar{Z}' - (nM_T - \omega)t\right]}$$

Assuming the distortion is frozen convected with the mean axial velocity in the duct, then

$$W(Y,Z,t) = W(Y,Z - M_z t) \tag{G6}$$

$$= \iint_{-\infty}^{\infty} \frac{d\lambda}{2\pi} \frac{dK}{2\pi} \bar{\bar{W}}(\kappa,\lambda)\, e^{iKY}\, e^{i\lambda\left(Z - M_z t\right)}$$

giving

$$\hat{\bar{\bar{W}}}\left(\frac{n}{\rho},\lambda,\omega\right) = \hat{\bar{\bar{W}}}\left(\frac{n}{\rho},\lambda\right) 2\pi\delta\left(\omega - \lambda M_z\right) \tag{G7}$$

and, from equation (G5),

$$W = \frac{1}{2\pi\rho} \sum_{n=-\infty}^{\infty} e^{in\frac{2\pi j}{N}} \int_{-\infty}^{\infty} \frac{d\lambda}{2\pi} \bar{\bar{W}}\left(\frac{n}{\rho},\lambda\right) e^{-i\nu_n(\lambda)\left[Z-V't'\right]} e^{i\lambda Z_{M.C.}} \tag{G8}$$

with $t' = \dfrac{t}{\frac{c}{2}}$, $\bar{Z}'' = \dfrac{\bar{Z}'}{\frac{c}{2}}$, AND (G9)

$$V = \frac{M_T\rho - \lambda\frac{\rho}{n}\,\mathrm{SIN}\,\gamma}{\mathrm{SIN}\,\gamma - \lambda\frac{\rho}{n}\,\mathrm{COS}\gamma}$$

and

$$\nu_n(\lambda) = \frac{nM_T - \lambda M_z}{V'}\frac{c}{2} \tag{G10}$$

Finally, from the periodicity in y,

$$\begin{aligned}\bar{\bar{W}}\left(\frac{n}{\rho},\lambda\right) &= \int_0^{2\pi\rho} \bar{W}(Y,\lambda)\, e^{-i\frac{n}{\rho}Y} dY \\ &= \rho\int_0^{2\pi} \bar{W}(\phi,\lambda)\, e^{-in\phi}\, d\phi \\ &= \rho\,\bar{W}_n(\lambda),\end{aligned} \tag{G11}$$

so that

$$\bar{W}\ (\phi,\lambda) = \frac{1}{2\pi} \sum_{n=-\infty}^{\infty} \bar{W}_n(\lambda)\ e^{in\phi} \tag{G12}$$

This gives for W, letting $\phi_j = 2\pi j/N$,

$$W = \frac{1}{2\pi} \sum_{n=-\infty}^{\infty} W_n\left(Z - M_z t\right) e^{in\phi_j} \tag{G13}$$

with

$$W_n\left(Z - M_z t\right) = \int_{-\infty}^{\infty} \frac{d\lambda}{2\pi}\ \bar{W}_n\ (\lambda)\ e^{-i\nu_n(\lambda)} \left[\bar{Z}'' - V't'\right] e^{i\lambda Z_{M.C.}} \tag{G14}$$

When the distortion is steady,

$$\bar{W}_n\ (\lambda) = 2\pi\delta(\lambda)\ W_n \tag{G15}$$

so that

$$W = \frac{1}{2\pi} \sum_{n=-\infty}^{\infty} W_n e^{in\phi_j}\ e^{-i\nu_n}\left[\bar{Z}'' - Vt'\right] \tag{G16}$$

with

$$\nu_n = \frac{nM_T}{V}\frac{c}{2} \tag{G17}$$

and

$$V = \frac{M_T \rho}{SIN\gamma} \tag{G18}$$

If the distortion is strictly axial, then the spectral density of the normal component of the velocity perturbation on the j^{th} blade required in equation (2.3.1) is

$$\hat{u}_j = SIN\ \gamma \int_{-\infty}^{\infty} W(\bar{\bar{Z}}''=0)\ e^{+i\omega t}\ dt \tag{G19}$$

$$= SIN\ \gamma \sum_{n=-\infty}^{\infty} W_n\ e^{in\phi}\, j\delta(\omega + nM_t)$$

When the distortion is nonsteady, the assumption is that it is the quasi-steady disturbance resulting from the convection with the flow of stretched eddies. Thus, the factorization can be made

$$W = W(\phi)\Delta(\xi - \xi_o) \tag{G20}$$

where:

$\xi = z - M_z t$

$\xi_o = z_{M.C.} - M_z \tau$,

τ = time at which the center of eddy is coincident with the midchord plane of the rotor

Choosing to represent $\Delta(\xi-\xi_o)$ by a Gaussian distribution,

$$\Delta\ (\xi\ -\ \xi_o) = e^{-\frac{(\xi\ -\xi_o)^2}{2L^2}}$$

(G21)

with L the "axial length scale" of the eddy, then

$$\bar{\Delta}(\lambda) = \sqrt{2\pi}\ Le^{i\lambda\xi_o}\ \bar{e}\ \frac{1}{2}L^2\lambda^2$$

$$\xrightarrow[L\to\infty]{} 2\pi\delta(\lambda)$$

(G22)

If the eddy velocity disturbance has both axial (W_z) and circumferential (W_ϕ) components, then the spectral density of the normal component of the velocity perturbation on the j^{th} blade is

$$\hat{u}_j = \int_{-\infty}^{\infty} \left\{ \text{SIN}\gamma\ W_z(\bar{z}'=0) + \text{COS}\gamma\ W_\phi(\bar{z}'=0) \right\} e^{i\omega t}\, dt$$

$$= \sum_{n=-\infty}^{\infty} e^{in\phi_j} \left\{ W_{zn}\text{SIN}\ \gamma \int_{-\infty}^{\infty} \frac{d\lambda}{2\pi}\ \bar{\Delta}_z(\lambda)\,\delta\left(\lambda M_z\ -nM_T\ -\omega\right) \right.$$

$$\left. +W_{\phi n}\ \text{COS}\gamma \int_{-\infty}^{\infty} \frac{d\lambda}{2\pi}\ \ \bar{\Delta}_\phi(\lambda)\,\delta\left(\lambda M_z\ -\ nM_T\ -\omega\right) \right\}$$

$$= \sum_{n=-\infty}^{\infty}\ e^{in\phi_j} \left\{ W_{zn}\ \text{SIN}\gamma\ \frac{\bar{\Delta}_z\left(\frac{nM_T\ +\omega}{M_z}\right)}{2\pi\ M_z} + W_{\phi n}\ \text{COS}\gamma\ \frac{\bar{\Delta}_\phi\left(\frac{nM_T\ +\omega}{M_z}\right)}{2\pi\ M_z} \right\}$$

(G23)

From equations (G9) and (G10) it is seen that when the distortion is nonsteady, the harmonic gusts at the blades have phase velocities differing from the relative mean flow velocity, i.e., the harmonic gusts are not "frozen" in the fluid. It is only when $\Delta_z/2\pi M_z$ and $\Delta_\phi/2\pi M_z$ approach being delta functions that these gusts became frozen convected.

APPENDIX H

Figure 12 illustrates the oblique gust geometry. Filotas (ref. 36) developed an approximate solution for the lift response of a thin airfoil to such a gust. His results were in a form containing an infinite series,

$$T(h,\psi) = \frac{1}{\frac{\pi}{2} h + F(h,\psi)} \frac{I_o(h_2) + I_1(h_2)}{J_o\left(h_1 - ih_2\right) + iJ_1\left(h_1 - ih_2\right)} \tag{H1}$$

where $h_1 = h \sin \psi$ and $h_2 = h \cos \psi$ (equation [64] of ref. 36 with his $k \to h$ and $\beta \to \psi$). In this equation, I_0 and I_1 are modified Bessel functions of the first kind, J_0 and J_1 are Bessel functions, and F is given in terms of an infinite series involving modified Bessel functions of the second kind (equations [21] and [22] of ref. 36). A generally good approximate form to equation (H1) was also developed:

$$T = \frac{e^{-ih\left[\mathrm{SIN}\psi - \frac{\pi\psi\left(1+.5\ \mathrm{COS}\psi\right)}{1+2\pi h\left(1+\frac{1}{2}\mathrm{COS}\psi\right)}\right]}}{\sqrt{1+\pi h\left(1+\mathrm{SIN}^2\psi + \pi h\ \mathrm{COS}\psi\right)}} \tag{H2}$$

Both equations (H1) and (H2) have been programmed for use in subprogram BBCAA. Figure 19 is a plot of $|T|$ versus h for different ψ values. When $\psi = \pi/2$, the gust is no longer oblique and T then approximates the Sears function.

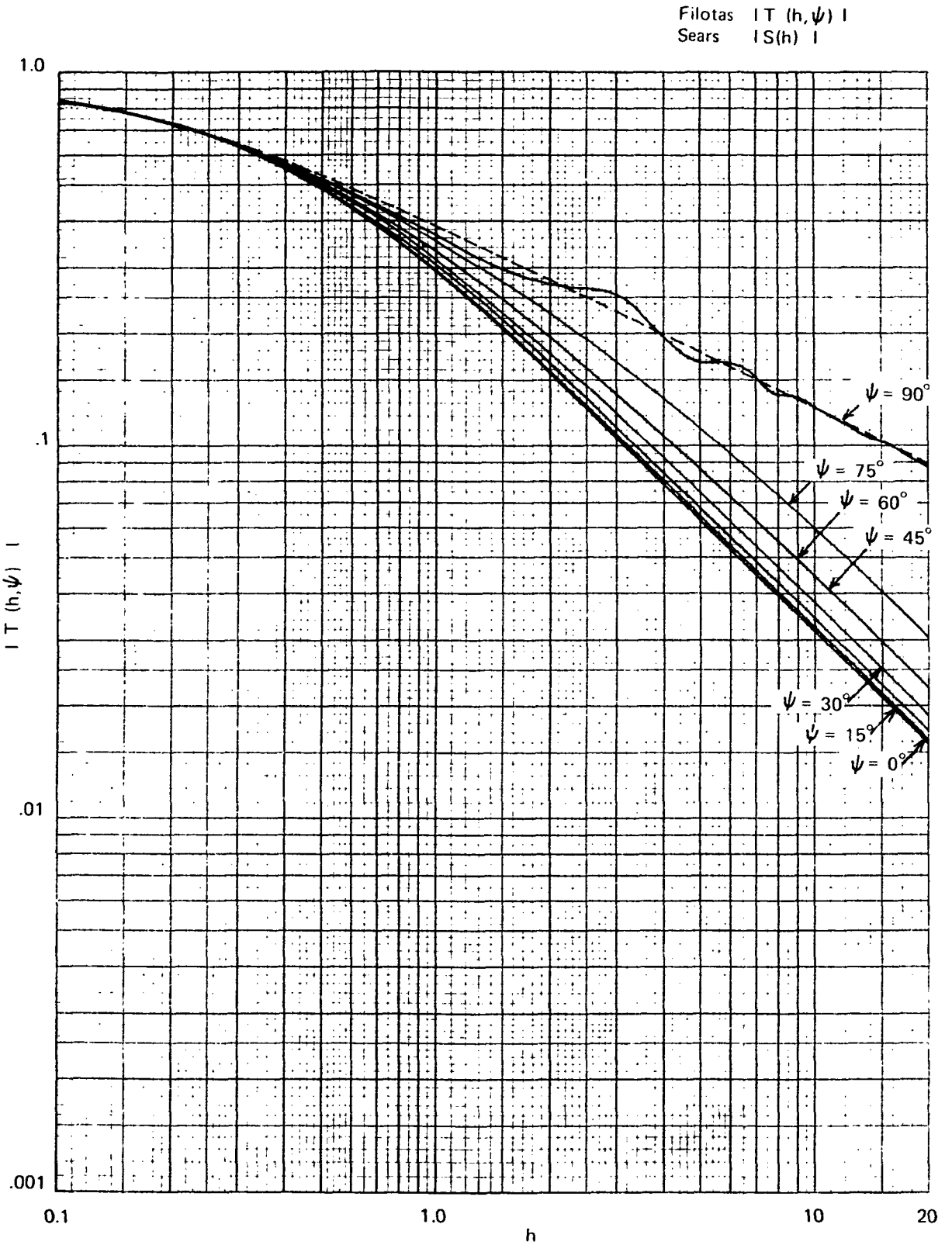

FIGURE 19. – MAGNITUDE OF OBLIQUE GUST LIFT RESPONSE FUNCTION

APPENDIX I

This appendix contains the list of equations used in the analysis that are referenced in the FORTRAN variable dictionary and the subprogram descriptions.

1. $$\beta_{mn} = \sqrt{(\sigma N_R M_T)^2 - (1-M)^2 \mu_{mn}^2}$$

2. $$K_{mn}^{\pm} = \frac{-(\sigma N_R M_T)\cdot M \pm \beta_{mn}}{1-M^2}$$

3. $$\mu_{mn} \leq \frac{\sigma N_R M_T}{\sqrt{1-M^2}} = E_B$$

4. $$J_m'(X) - \frac{J_m'(\eta X)}{Y_m'(\eta X)} Y_m'(X) = 0$$

5. $$Y_m'(\eta X) \left\{ J_m'(X) - \frac{J_m'(\eta X)}{Y_m'(\eta X)} Y_m'(X) \right\} = 0$$

6. $$R(\mu_{mn}\rho) = J_m(\mu_{mn}\rho) - \frac{J_m'(\mu_{mn}\eta)}{Y_m'(\mu_{mn}\eta)} Y_m(\mu_{mn}\rho)$$

7. $$N_{mn} = \left[\frac{1}{2} \left(1 - \frac{m^2}{\mu_{mn}^2} \right) R_m^2 \left(\mu_{mn} \right) - \frac{1}{2} \left(\eta^2 - \frac{m^2}{\mu_{mn}^2} \right) R_m^2 \left(\mu_{mn}\eta \right) \right]^{\frac{1}{2}}$$

8. $$\mathcal{R}_m(\mu_{mn}\rho) = R_m(\mu_{mn}\rho) \Big/ N_{mn}$$

9. $$A^{\pm}_{mn\sigma} = \left\{\begin{matrix}\text{CONSTANT}\\ \text{FACTOR}\end{matrix}\right\} * \sum_{j=1}^{N_{SUB}} \left\{\begin{matrix}\text{AVERAGE OF}\\ \text{NON-OSCILLATORY}\\ \text{FACTOR}\end{matrix}\right\}_j * \int_{aj}^{bj} \left\{\begin{matrix}\text{OSCILLATORY}\\ \text{FACTOR}\end{matrix}\right\}$$

10. $$M_M(\rho) = \sqrt{\left(\sqrt{M_I^2(\rho) - M_Z^2(\rho)} + \sqrt{M_E^2(\rho) - M_Z^2(\rho)}\right)^2 \frac{1}{4} + M_Z^2(\rho)}$$

11. $$\gamma(\rho) = \left| \text{ARC COS } \frac{M_Z(\rho)}{M_M(\rho)} \right|$$

12. $$e_\phi(\rho) = \text{COS}\left(\gamma(\rho)\right) = \frac{M_Z(\rho)}{M_M(\rho)}$$

13. $$e_Z(\rho) = \text{SIN}\left(\gamma(\rho)\right) = \sqrt{1 - e_\phi^2(\rho)}$$

14. $$\kappa^{\pm}_{mn\sigma}(\rho) = \frac{C(\rho)}{2}\left[K^{\pm}_{mn} \cdot e_\phi(\rho) - \frac{m}{\rho} e_Z(\rho)\right]$$

15. $$S(\nu) = \frac{1}{\frac{\pi\nu}{2}\left(H_o^{(2)}(\nu) - iH_1^{(2)}(\nu)\right)}$$

16. $$F_{\alpha}(\nu) = J_{o}(\nu) + iJ_{1}(\nu)$$

17. $$T(\nu) = \frac{H_{o}^{(2)}(\nu) + iH_{1}^{(2)}(\nu)}{-H_{o}^{(2)}(\nu) + iH_{1}^{(2)}(\nu)}$$

18. $$J(X) = J_{o}(X) + i\, J_{1}(X)$$

19. $$F(X) = T(X) \cdot \left[J^{*}(X) - \frac{1}{X} J_{1}(X)\right] - \left[J(X) - \frac{1}{X} J_{1}(X)\right]$$

20. $$F_{f}(\nu) = F(\nu) + \frac{4}{\nu} J(\nu)$$

21. $$L(\nu) = b_{1} \cdot S(\nu) + b_{2} \cdot F_{\alpha}(\nu) + b_{3}\, F_{f}(\nu)$$

22. $$L'(\nu) = b_{1} \cdot S(\nu) \cdot J\left(\kappa_{mn\sigma}^{\pm}\right) + b_{2} \cdot J\left(\nu + \kappa_{mn\sigma}^{\pm}\right) + b_{3} F_{f}'\left(\nu, \kappa_{mn\sigma}^{\pm}\right)$$

23. $$F_{f}'\left(\nu, \kappa_{mn\sigma}^{\pm}\right) = \left[J\left(\kappa_{mn\sigma}^{\pm}\right) \cdot F(\nu) + \frac{2 \cdot J_{1}\left(\nu + \kappa_{mn\sigma}^{\pm}\right)}{\left(\nu + \kappa_{mn\bar{\sigma}}^{\pm}\right)} - \frac{2}{\nu} \sum_{j=1}^{J_{MAX}} (-1)^{j} \cdot J_{j}(\nu) \left[J_{j+1}\left(\kappa_{mn\sigma}^{\pm}\right) + J_{j-1}\left(\kappa_{mn\sigma}^{\pm}\right)\right]\right]$$

24.

$$K_L(\nu,\lambda) = \begin{cases} \left[J_o(\lambda) - i\,J_1(\lambda)\right] \dfrac{H_1^{(2)}(\nu)}{H_1^{(2)}(\nu) + iH_o^{(2)}(\nu)} + i\nu/\lambda\, J_1(\lambda) & \text{IF } \nu\lambda \neq 0 \\ \dfrac{H_1^{(2)}(\nu)}{H_1^{(2)}(\nu) + iH_o^{(2)}(\nu)} + i\,\dfrac{\nu}{2} & \text{IF } \nu \neq 0, \lambda = 0 \\ \left[J_o(\lambda) - i\,J_1(\lambda)\right] & \text{IF } \nu = 0,\ \lambda \neq 0 \\ 1 & \text{IF } \nu = 0,\ \lambda = 0 \end{cases}$$

25.

$$T(\nu,\Theta) = \frac{e^{-i\nu\left[\mathrm{SIN}\Theta - \frac{\pi\Theta\left(1+\frac{1}{2}\mathrm{COS}\Theta\right)}{1+2\pi\nu\left(1+\frac{1}{2}\mathrm{COS}\Theta\right)}\right]}}{\left[1+\pi\nu\left(1+\mathrm{SIN}^2\,\Theta+\pi\nu\,\mathrm{COS}\Theta\right)\right]^{\frac{1}{2}}}$$

Additional equations for the viscous wakes interaction model:

26.

$$\mathrm{COS}(\psi) = \frac{M_{2Z}(\rho)}{M_{1E}(\rho)}$$

27.

$$\beta(\rho) = \gamma(\rho) + \psi(\rho)$$

28.
$$T_1 = \frac{\text{SIGOL} \cdot Y_o \cdot N_1}{2\,\pi\rho\cos\psi}$$

29.
$$Y_o = 1.36 \cdot C_1\sqrt{\frac{X}{C_1} - .35}$$

30.
$$\Lambda_\sigma = \frac{\sin \pi T_1}{\pi T_1}\left(\frac{1}{1-T_1^2}\right)$$

31.
$$\Delta_o = 1.65\ C_{D_1}\sqrt{\left(\frac{1}{\frac{X}{C_1} - .2}\right) - \left(\frac{.15}{\frac{X}{C_1} - .2}\right)^2}$$

32.
$$V_\sigma = \text{SIGN} \cdot \frac{\text{SIGOL} \cdot N_1 \cdot C_2\ M_t}{2 \cdot M_{M,2}}$$

ISOROS	1	2
SIGOL	ℓ	σ
q	$-\ell$	σ
SIGN	1	-1

33.
$$\left\{\begin{matrix}\text{Constant} \\ \text{factor}\end{matrix}\right\} = -\frac{N_1 N_2}{8\beta_{mn}}\ e^{-iK_{mn}^{\pm} Z_2}$$

34. $$\left\{\begin{array}{l}\text{Average of}\\ \text{non oscillatory}\\ \text{factor}\end{array}\right\}_{\substack{\text{COMPACT}\\ \text{SOURCE}}} = C_1 \cdot C_2 \cdot \left(\frac{dC_L}{d\alpha}\right) \cdot M_{M,2} \cdot M_{E,1} \frac{\text{SIN } \beta}{\rho \cdot \text{COS}\psi} \Delta_o \cdot \Lambda_\sigma$$

$$\cdot \left[S(\nu_\sigma) - \alpha \text{ COT}\beta \cdot F_\alpha(\nu_\sigma) - f \cdot \text{COT}\beta \cdot F_f(\nu_\sigma)\right] \cdot \left[\frac{me_\phi}{\rho} + K_{mn}^{\pm} e_Z\right]$$

35. $$\left\{\begin{array}{l}\text{Average of}\\ \text{non oscillatory}\\ \text{factor}\end{array}\right\}_{\substack{\text{NON-COMPACT}\\ \text{SOURCE}}} = C_1 \cdot C_2 \left(\frac{dC_L}{d}\right) \cdot M_{M,2} \cdot M_{E,1} \frac{\text{SIN } \beta}{\rho \cdot \text{COS}\psi} \cdot \Delta_o \cdot \Lambda_\sigma \cdot$$

$$\cdot \left[\frac{me_\phi}{\rho} + K_{mn}^{\pm} e_Z\right] \cdot \left[S(\nu_\sigma) \cdot J\left(\kappa_{mn\sigma}^{\pm}\right) - \text{COT}\beta \cdot \alpha \cdot J\left(\nu_\sigma \kappa_{mn\sigma}^{\pm}\right) + \text{COT}\beta \, f F_f'(\nu_\sigma)\right]$$

36. $$\left\{\begin{array}{l}\text{Oscillatory}\\ \text{factor}\end{array}\right\} = e^{iqN_1\Theta_2} \cdot e^{i \, \text{SIGOL} \cdot N_1 \frac{d \cdot \text{SIN}\psi}{\rho \cdot \text{COS}\,\psi}} \cdot \mathcal{R}_m\left(\mu_{mn}\rho\right)$$

Additional equations for the potential flow field interaction model:

37. $$\Gamma^{\circ}_{K2}(\rho) = \pi C_{K2}(\rho) \, M_{M,K2}(\rho) \left(A^{\circ}_{K2}(\rho) + A^{1}_{K2}(\rho)\right)$$

where A^{j}_{K2} = Glauert coefficient of j^{th} order of component K2

38.
$$a_{\kappa,K1}(\rho) = \frac{C_6 C_{K1}(\rho)\, N_{K2}}{2\rho}\; e^{-C_7 \kappa \left(b/\rho\right) N_{K2}}$$

39.
$$g_{n,K2}(\rho) = \frac{A_{K2}^{n+1}(\rho) - A_{K2}^{n-1}(\rho)}{A_{K2}^{\circ}(\rho) + A_{K2}^{1}(\rho)}$$

where

$A_{K2}^{\circ}(\rho)$, $A_{K2}^{1}(\rho), \cdots, A_{K2}^{N}(\rho)$ ARE INPUT,

$A_{K2}^{N+1}(\rho) = A_{K2}^{N+2}(\rho) = 0$ AND $n=1,2,\cdots,N+1$

40.
$$h_{K2}(\rho) = \frac{C_{12} \kappa N_{K2} C_{K2}(\rho)}{2\rho}\; e^{iC_{13}\left[\frac{\pi}{2} - C_{14}\Theta_{K2}(\rho)\right]}$$

41.
$$H_{\kappa,K2}(\rho) = J_{\circ}\left(h_{K2}(\rho)\right) + \sum_{n=1}^{N+1} \left(C_{11} \cdot i\right)^{n} g_{n,K2}(\rho) \cdot J_n\left(h_{K2}(\rho)\right)$$

42.
$$d_{\kappa,K1}(\rho) = C_8 \Theta_{K1}(\rho) + C_9 \kappa N_{K2} \left[\left(b/\rho\right) \mathrm{TAN}\Theta_{K1}(\rho) + \frac{M_T C_{K2}(\rho)}{2M_{M,K2}(\rho)}\right]$$

43.
$$\nu_{\kappa,K1}(\rho) = C_6 \frac{M_T N_{K2} C_{K1}(\rho)}{2M_{M,K1}(\rho)}\; \kappa$$

44. $$\lambda_{\kappa,K1}(\rho) = C_6 \frac{\kappa N_{K2} C_{K1}(\rho)}{2\rho} \kappa\, e^{iC_3\left[\frac{\pi}{2} - \Theta_{K1}(\rho)\right]}$$

45. $$\left\{\begin{matrix}\text{Constant} \\ \text{factor}\end{matrix}\right\} = -\frac{N_{K1}}{4\beta_{mn}} \cdot e^{-iK^{\pm}_{mn} Z_{K1}} \cdot 2\pi$$

46. $$\left\{\begin{matrix}\text{Non-oscillatory} \\ \text{factor}\end{matrix}\right\}_j = 1.$$

47. $$\left\{\begin{matrix}\text{Oscillatory} \\ \text{factor}\end{matrix}\right\} = M_{M,K1}(\rho)\Gamma^{\circ}_{K2}(\rho)\, a_{\kappa,K1}(\rho)\, H_{\kappa,K2}(\rho)\, e^{-id_{\kappa,K1}(\rho)} \cdot$$

$$\cdot \frac{\left(\frac{dC_L}{d\alpha}\right)_{K1}}{2\pi} \cdot \left[\frac{me_{\phi}}{\rho} + K^{\pm}_{mn} e_Z\right] \mathcal{R}_m\left(\mu_{mn}\rho\right) K_{\kappa,K1}(\rho)$$

Additional equations for the rotor-steady velocity distortion interaction model:

48. $$W_{\ell}(\rho) = \int_{\circ}^{2\pi} W(\rho,\phi)\, e^{-i\ell\phi}\, d\phi$$

where

$$W(\rho,\phi) = \frac{\left(1-V_A/V_1\right)}{1-A^2}\left[1-A\rho\ \cos\ \phi - \sqrt{\left(A\rho\cos\phi-1\right)^2 - \left(A^2-1\right)\left(\rho^2-1\right)}\right]$$

49.
$$W_{\ell}(\rho) = \frac{1}{2}\, a_1(\rho) \cdot 1^{-q}$$

50.
$$W_{\ell}(\rho) = \begin{cases} \frac{1}{2}\left(a_{\ell}(\rho) + ib_{\ell}(\rho)\right) & \text{IF } \ell>0 \\ \frac{1}{2}\left(a_{\ell}(\rho) - ib_{\ell}(\rho)\right) & \text{IF } \ell<0 \end{cases}$$

51.
$$\nu_{\ell}(\rho) = \ell\, \frac{C_2(\rho)\cdot M_t}{2M_M(\rho)}$$

52.
$$\mathrm{COT}(\beta) = \frac{M_Z(\rho)}{\sqrt{M_M^2(\rho) - M_Z^2(\rho)}}$$

53.
$$\left\{\begin{matrix}\text{Constant}\\ \text{factor}\end{matrix}\right\} = -\frac{N_R e^{-iK_{mn}^{\pm} Z_R}}{4\beta_{mn}}$$

54.
$$\left\{\begin{matrix}\text{Average of}\\ \text{non-oscillatory}\\ \text{factor}\end{matrix}\right\}_{\substack{\text{COMPACT}\\ \text{SOURCE}}} = C_R \cdot \left(\frac{dC_L}{d\alpha}\right) \cdot M_M \cdot M_Z \quad \mathrm{SIN}\beta \left[\frac{me_{\phi}}{\rho} + K_{mn}^{\pm} e_Z\right]$$

$$\cdot \left[S(\nu_{\ell}) - d \cdot \mathrm{COT}\beta \cdot F_{\alpha}(\nu_{\ell}) - f\ \mathrm{COT}\beta \cdot F_f(\nu_{\ell})\right]$$

55.
$$\cdot \left[S(\nu_\ell) \cdot J\left(\kappa^{\pm}_{mn\sigma}\right) - COT\beta \cdot \alpha \cdot J\left(\nu_\ell + \kappa^{\pm}_{mn\sigma}\right) + COT\beta \cdot f \cdot F'_f(\nu_\ell) \right]$$

$$\left\{ \begin{matrix} \text{Average of} \\ \text{non-oscillatory} \\ \text{factor} \end{matrix} \right\} = C_R\left(\frac{dC_L}{d\alpha}\right) \cdot M_M \cdot M_Z \cdot SIN\beta \cdot \left[\frac{me_\phi}{\rho} + K^{\pm}_{mn} e_Z \right] \cdot$$
NON COMPACT SOURCE

56.
$$\left\{ \begin{matrix} \text{Oscillatory} \\ \text{factor} \end{matrix} \right\} = W_\ell(\rho) \cdot \mathcal{R}_m(\mu_{mn}\rho)$$

Additional equations for the rotor nonsteady velocity distortion interaction model:

57.
$$\left\{ \begin{matrix} \text{Average of} \\ \text{non-oscillatory} \\ \text{factor} \end{matrix} \right\} = M_Z \cdot C\left(\frac{dC_L}{d\alpha}\right) \cdot \left[\frac{me_\phi}{\rho} + K^{\pm}_{mn} e_Z \right]$$

58.
$$\left\{ \begin{matrix} \text{Constant} \\ \text{factor} \end{matrix} \right\} = -\frac{N}{4} \cdot \frac{e^{-iK^{\pm}_{mn} Z}}{\beta_{mn}}$$

59.
$$\left\{ \begin{matrix} \text{Oscillatory} \\ \text{factor} \end{matrix} \right\} = \text{FACTIN4}$$

60.
$$T_j = \frac{L_j}{M_Z}$$

61.
$$P_j = U_j \begin{cases} e^{-\frac{1}{2}\left(\frac{\tau}{T_j}\right)^2} & \text{IF } BT_j > 10. \\ E_j & \text{IF } .1 \leq BT_j \leq 10. \\ \dfrac{2BT_j \cdot \mathrm{SIN}(B\tau)}{\sqrt{2\pi} \cdot B\tau} & \text{IF } BT_j < .1 \end{cases}$$

$$E_j = \frac{T_j}{\sqrt{2\pi}} \int_{-B}^{B} e^{-\frac{(\omega T_j)^2}{2}} \cdot \mathrm{COS}(\omega\tau)\, d\omega$$

If ARMISC(25) = 3:

62.
$$\text{FACTIN4} = \mathcal{R}_m\left(\mu_{mn}\rho\right) \cdot M_M(\rho) \cdot \mathrm{SIN}(\gamma) \left[g_{1\ell}(\rho) \cdot F_1(\rho) - g_{2\ell}(\rho) \cdot F_2(\rho)\right]$$

63.
$$\nu_\ell(\rho) = \ell \cdot \frac{C_2(\rho) \cdot M_t}{2\, M_M(\rho)}$$

64.
$$\left[F_1(\rho)\right]_{\substack{\text{COMPACT} \\ \text{SOURCE}}} = S(\nu_\ell) - \alpha(\rho) \cdot \mathrm{COT}(\gamma) \cdot F_\alpha(\nu_\ell) - f(\rho) \cdot \mathrm{COT}(\gamma) \cdot F_f(\nu_\ell)$$

65.
$$\left[F_1(\rho)\right]_{\substack{\text{NON-COMPACT} \\ \text{SOURCE}}} = S(\nu_\ell) \cdot J\left(\kappa^{\pm}_{mn\sigma}\right) - \alpha(\rho)\mathrm{COT}(\gamma) \cdot J\left(\nu_\ell + \kappa^{\pm}_{mn\sigma}\right) - f(\rho) \cdot \mathrm{COT}(\gamma) \cdot F'_f(\nu_\ell)$$

66.
$$\left[F_2(\rho)\right]_{\substack{\text{COMPACT} \\ \text{SOURCE}}} = \mathrm{COT}(\gamma) \cdot S(\nu_\ell) + \alpha(\rho) \cdot F_\alpha(\nu_\ell) + f(\rho) \cdot F_f(\nu_\ell)$$

67. $$\left[F_2(\rho)\right]_{\substack{\text{NON-COMPACT}\\ \text{SOURCE}}} = \text{COT}(\gamma)\cdot S(\nu_\ell)\cdot J\left(\kappa^{\pm}_{mn\sigma}\right) + \alpha(\rho)\cdot J\left(\nu_\ell + \kappa^{\pm}_{mn\sigma}\right) + f(\rho)\cdot F'_f(\nu_\ell)$$

68. $$g_{j_\ell}(\rho) = 2\pi\cdot P_j \cdot e^{-\frac{(\rho-R)^2}{2a_j^2}} \cdot I_\ell\left(\frac{R\rho}{a_j^2}\right)\cdot e^{-\frac{\rho R}{a_j^2}} e^{-i\ell\phi}$$

If ARMISC(25) = 4:

69. $$\text{FACTIN4} = 2\sqrt{2\pi}\, R_m\left(\mu_{mn}\rho\right) e^{-i\ell\phi} \left\{M_M(\rho)\ \text{SIN}\gamma(\rho)\ P_1 I_\ell\left(\frac{\rho R}{a_1^2}\right) e^{-\frac{\rho R}{a_1^2}} I_1 - M_Z(\rho)\ P_2 I_\ell\left(\frac{\rho R}{a_2^2}\right) e^{-\frac{\rho R}{a_2^2}} I_2\right\}$$

70. $$I_j = a_j\ \text{Re}\left\{\int_0^\infty e^{-i(\rho-R)k}\cdot T^*(h(\rho,k),\psi(\rho,k)) e^{-\frac{k^2a_j^2}{2}}\, dk\right\}$$

$$\approx \Delta\left[\frac{1}{2} + \sum_{K=1}^{KMAX} \text{Re}\left\{e^{-i(\rho-R)\frac{K\Delta}{a_j}}\cdot e^{-\frac{K\Delta^2}{2}}\cdot T^*\left[\left(\rho,\frac{K\Delta}{a_j},\ \psi\ \rho,\frac{K\Delta}{a_j}\right)\right]\right.\right.$$

where $\Delta = \frac{a_j}{R}$, KMAX $= \frac{20}{\Delta} + 1$

71. $h(\rho,k) = \frac{C(\rho)}{2} \sqrt{k^2 + \left[\frac{\lambda}{\rho} \text{ SIN}(\gamma)\right]^2}$

72. $\psi\ (\rho,k) = \text{TAN}^{-1}\left[\frac{\lambda}{k \cdot \rho} \text{ SIN}(\gamma)\right]$

APPENDIX J

The zeros of $\Delta_m(\mu)$ are symmetric under a change in sign of m, i.e., for

$$\Delta_m(\mu) = J'_m(\mu)\, Y'_m(\mu\eta) - J'_m(\mu\eta)\, Y'_m(\mu) \tag{J1}$$

$$\Delta_{-m}(\mu) = \Delta_m(\mu) \tag{J2}$$

Hence, the zeros are computed for $\Delta|_m|(\mu)$. All the zeros are nonnegative. They are computed by first approximating the zeros for m = 0 as follows:

1) For $\eta = 0$, use formula (9.5.13) of reference 30

2) For $.2 \leq \eta < 1$, use formulas (9.5.28) and (9.5.31) of reference 30

3) For $0 < \eta < .2$, use quadratic interpolation with the values for $\eta = 0$ in item 1 above and $\eta = .2$ and .3 in item 2

Using the approximation formulas in item 2 restricted to $\eta \geq .2$ yeilds a one-to-one correspondence with the eigenvalues (zeros) where the first several values are poor approximations. The approximations in item 2 get worse as η decreases and for $\eta < .2$ no longer give a one-to-one correspondence. For this reason, interpolation procedure 3 is used to obtain better values. For more accurate values for the zeros, an iteration method is applied with above approximations as starting values. Reference 47 gives an iterative procedure for computing a real zero of a real valued nonlinear function f(x) in which a rational function is fitted through previously computed values. The interaction formula is

$$X_{n+1} = X_n + \frac{(X_n - X_{n-1})(X_n - X_{n-2})\, f_n\, (f_{n-1} - f_{n-2})}{(X_n - X_{n-1})\, (f_{n-2} - f_n)\, f_{n-1} + (X_n - X_{n-2})\, (f_n - f_{n-1})\, f_{n-2}} \tag{J3}$$

where f_n if $f(x_n)$. Here, f is $\Delta_{|m|}$ and x is μ. One of the three starting values required is chosen form the approximations discussed above, with the other two that approximation $\pm \varepsilon$ where ε is chosen to "surround" the zero.

Applying the iteration until $f(x_n)$ is small provides zeros with accuracy limited by the evaluation of f itself. In this case this accuracy is that of the Bessel and Neumann function evaluators. Do this for $m = 0$, use the $m = 0$ zeros as starting values for the $m = 1$ zeros, etc. Examples of the zeros used as eigenvalues in the analysis are plotted in figures 20, 21, and 22, each figure corresponding to a different value of η.

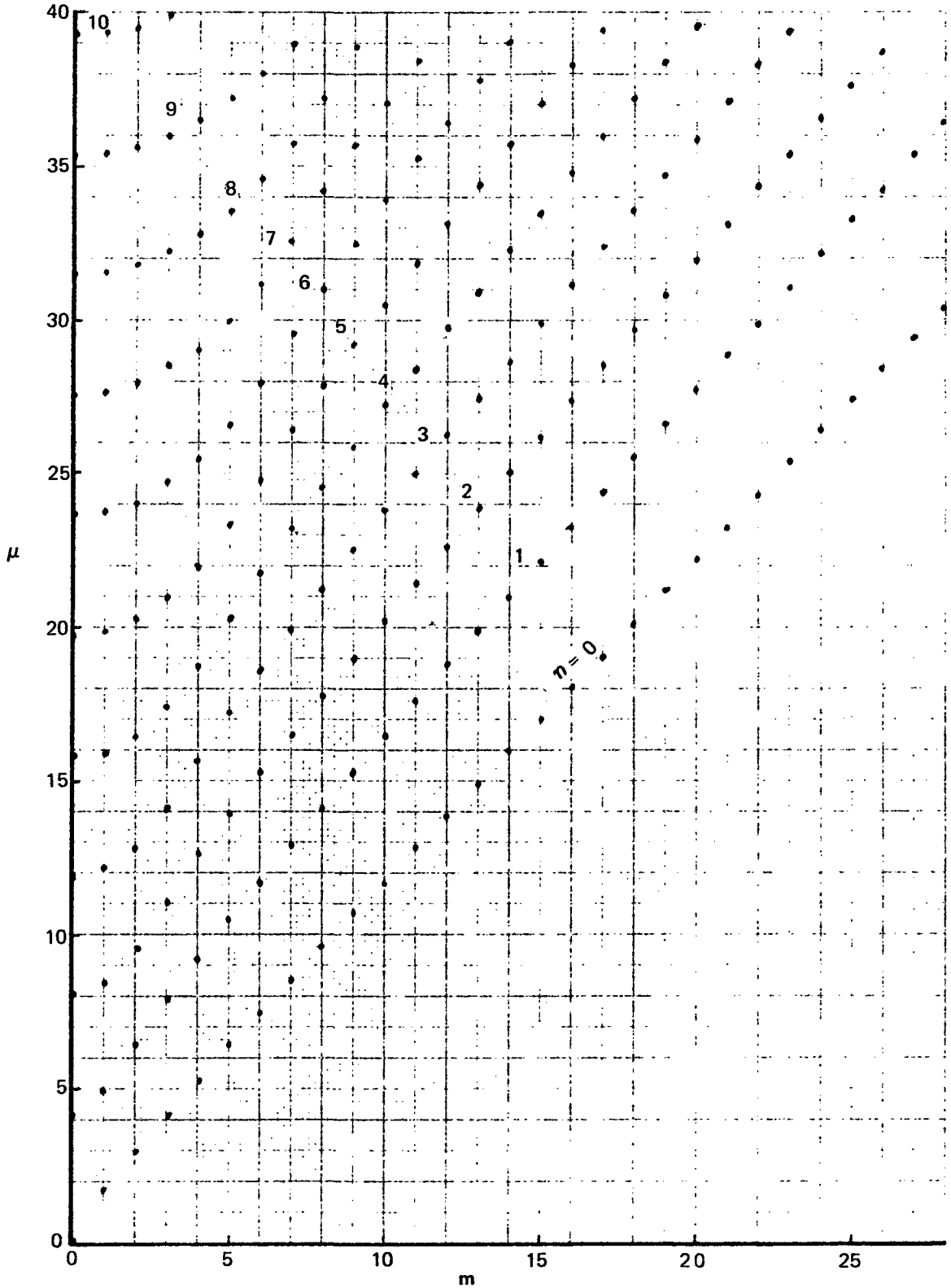

FIGURE 20. — ZEROS OF $\Delta_m(\mu)$, $\mu = \mu_{mn}$, $n = 0, 1, 2, \ldots$ NON-DIMENSIONAL INNER DUCT RADIUS OF $\eta = .2$

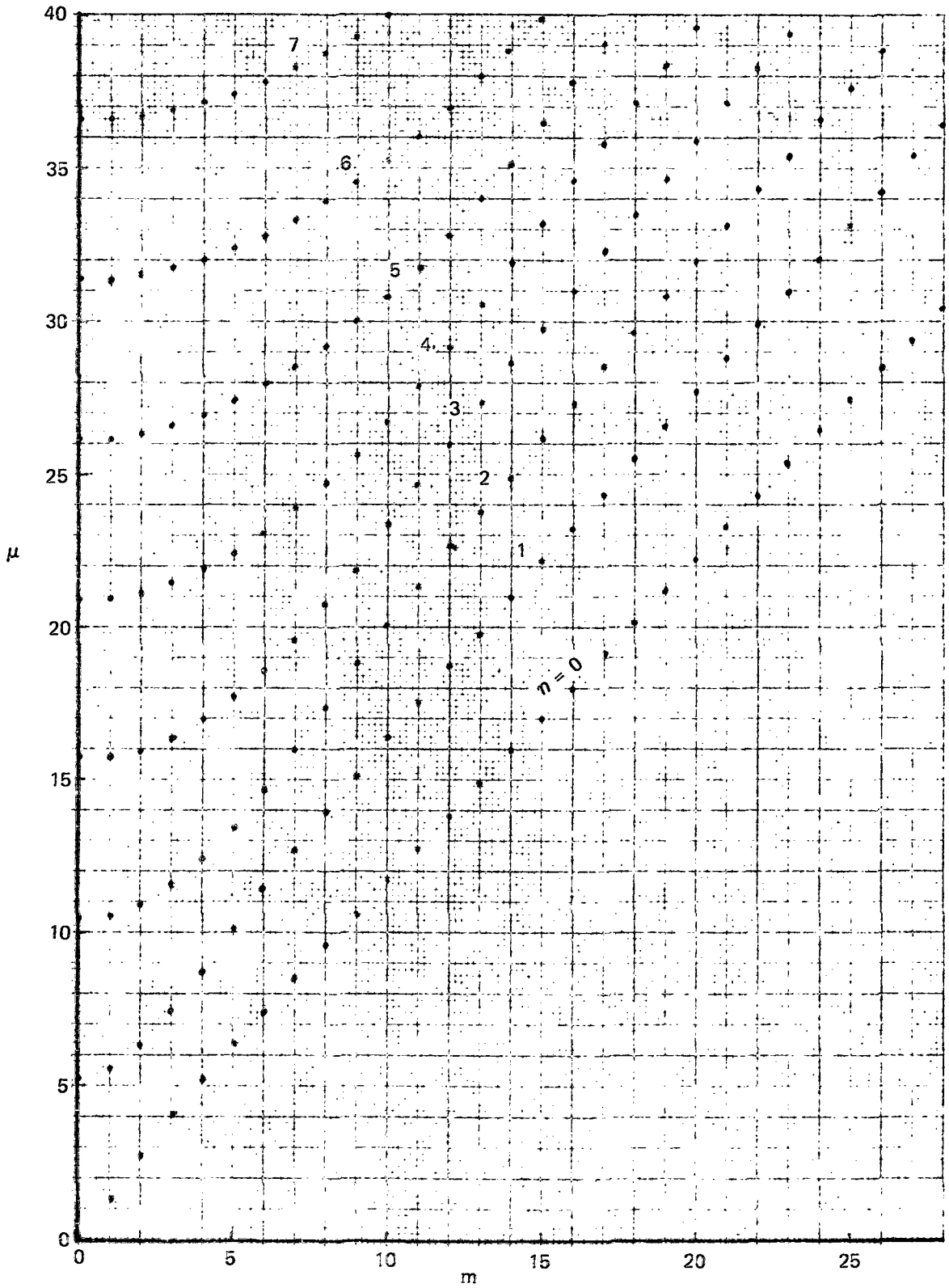

FIGURE 21. — ZEROS OF $\Delta_m(\mu)$, $\mu = \mu_{mn}$, $n = 0, 1, 2, \ldots$
NON-DIMENSIONAL INNER DUCT RADIUS $\eta = .4$

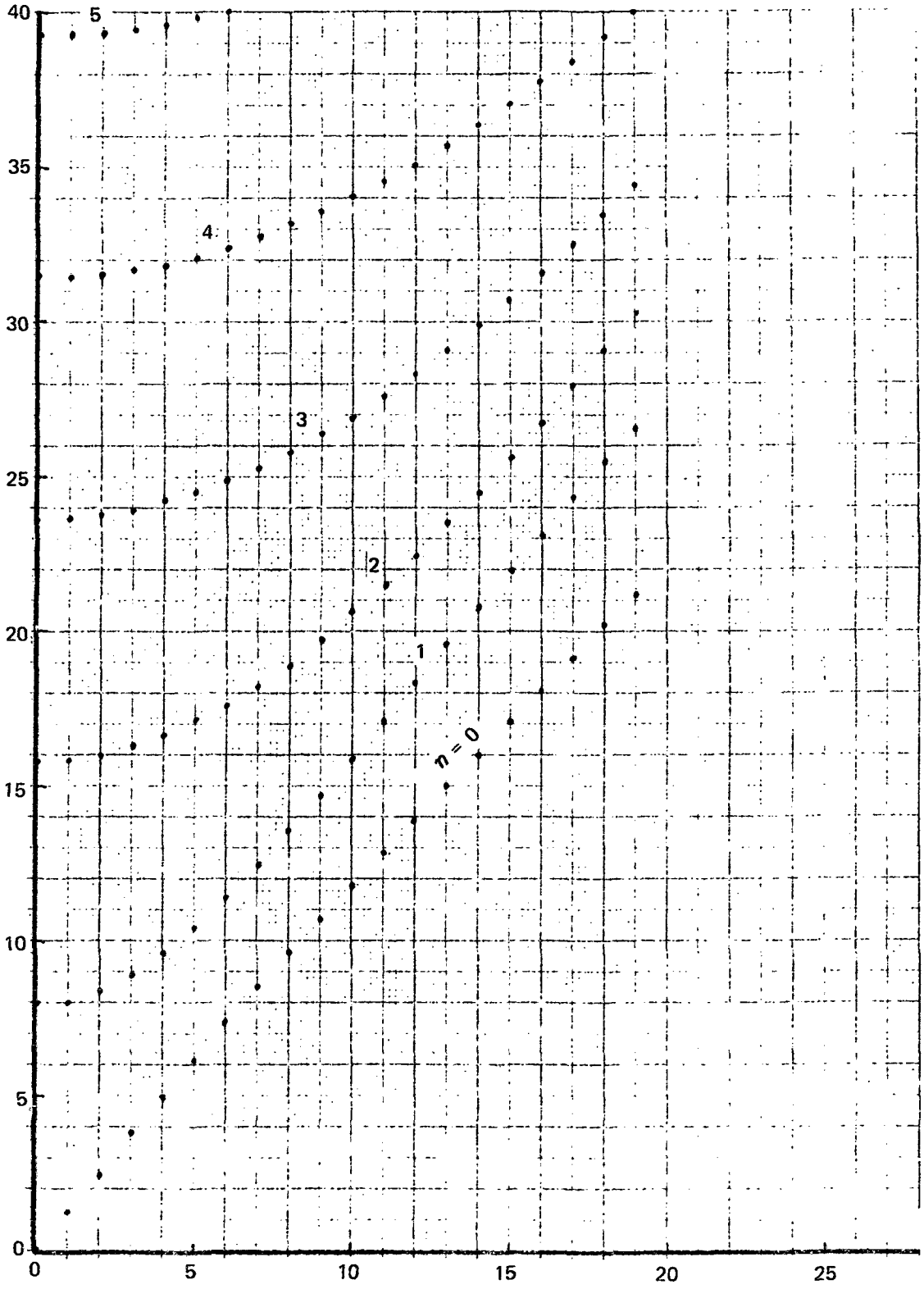

FIGURE 22. – ZEROS OF $\Delta_m(\mu)$, $\mu = \mu_{mn}$, $n = 0, 1, 2, \ldots$
NON-DIMENSIONAL INNER DUCT RADIUS $\eta = .6$

REFERENCES

1. Gutin, L.: On the Sound Field of a Rotating Propeller. Physik. Z. Sowjetunion, vol. 9, 1936, p. 57. Also, NACA TN 1194 (Trans.), Oct. 1948.

2. Van de Vooren, A. I.; and Zandbergen, P. J.: Noise Field of a Rotating Propeller in Forward Flight. AIAA J., vol. 1, no. 7, 1963.

3. Slutsky, S.; Mariano, S.; Baronti, P.; and Esses, H.: Analysis of Turbofan Sound Generation and Propagation. Technical report 234, Gen. App. Sci. Lab, Inc., 1961. Also, Slutsky, S.: Discrete Noise Generation and Propagation by a Fan Engine. Presented at the AFOSR-UTIAS Symposium on Aerodynamic Noise, Toronto, 1968.

4. Kemp, N. H.; and Sears, W. R.: Aerodynamic Interference Between Moving Blade Rows. J. Aeron. Sci., vol. 20, no. 9, 1953, p. 585.

5. Kemp, N. H.; and Sears, W. R.: The Unsteady Forces Due to Viscous Wakes in Turbomachines. J. Aeron. Sci., vol. 22, no. 7, 1955.

6. Tyler, J. M.; and Sofrin, T. G.: Axial Flow Compressor Noise Studies. SAE Trans., vol. 70, 1962, p. 309.

7. Hetherington, R.: Compressor Noise Generated by Fluctuating Lift Resulting From Rotor-Stator Interactions. AIAA J., vol. 1, 1963, p. 473.

8. Griffith, J. W. R.: The Spectrum of Compressor Noise of a Jet Engine. J. Sound Vib., vol. 2, 1964, p. 127.

9. Hulse, B.; Pearson, C.; Abbona, M.; and Andersson, A.: Some Effects of Blade Characteristics on Compressor Noise Levels. FAA-ADS-82, 1966.

10. Lighthill, M. J.: On Sound Generated Aerodynamically, Vol. I--General Theory. Proc. Roy. Soc., Series A, vol. 211, 1952.

11. Curle, N.: The Influence of Solid Boundaries Upon Aerodynamic Sound. Proc. Roy. Soc., Series A, vol. 231, 1955, p. 505.

12. Lowson, M. V.: The Sound Field of Singularities in Motion. Proc. Roy. Soc., Series A, vol. 286, 1965.

13. Lowson, M. V.: Theoretical Studies of Compressor Noise. NASA CR-1287, 1969.

14. Ffowcs Williams, J. E.; and Hawkings, D. L.: Theory Relating to the Noise of Rotating Machinery. J. Sound Vib., vol. 10, no. 1, 1969, p. 10.

15. Wright, S. E.: Sound Radiation From a Lifting Rotor Generated by Asymmetric Loading. J. Sound Vib., vol. 9, 1969, p. 223.

16. Morse, P. M.; and Ingard, K. U.: Theoretical Acoustics. McGraw-Hill, 1968.

17. Lowson, M. V.: Rotor Noise Radiation in Non-Uniform Flow. Presented at the Symposium on Aerodynamic Noise, Loughborough Univ. of Tech., England, 1970.

18. Pfenninger, W.: Note About Modulated Rotor Tone Noise of Subsonic Fans and Compressor Induced by Atmospheric Turbulence, Its Possible Reduction Through IGV's, and Design Consequences for Subsonic Fans. Technical document D6-25147, The Boeing Company, 1971.

19. Hanson, D. B.: The Spectrum of Turbomachine Rotor Noise Caused by Inlet Guide Vane Wakes and Atmospheric Turbulence. Document HSER 6191, Hamilton-Standard, 1973.

20. Hanson, D. B.: Unified Analysis of Fan Stator Noise. J. Acoust. Soc. Am., vol. 54, no. 6, 1974, p. 1571.

21. Lordi, J. A.: Report on a Study of Noise Generation by a Rotating Blade Row in an Infinite Annulus. Interim scientific report AI-2836-A-1, U.S. Air Force Office of Scientific Research, May 1971.

22. Drischler, J.: Analytic Studies of Sound Pressures Inside the Duct of Ducted Propellers. NASA TN D-6345, 1971.

23. Schaut, L. A.: Analytical Fan Tone Program. Technical document D6-25356TN, The Boeing Company, 1971.

24. Zorumski, W.: Acoustic Theory of Axisymmetric Multisectioned Ducts. NASA TR R-419, 1974.

25. Lansing, D.: Exact Solution for Radiation of Sound From a Semi-Infinite Circular Duct With Application to Fan and Compressor Noise. Presented at symposium held at Ames Research Center, Moffett Field, Calif., NASA SP-228, 1969, p. 323.

26. Clark, T. L.: Theory of Sound Generation by Ducted Turbomachinery, Vol. I--Acoustic Propagators. Technical document D6-40610, The Boeing Company, 1974.

27. Lansing, D.; and Zorumski, W. E.: Effects of Wall Admittance Changes on Duct Transmission and Radiation of Sound. J. Sound Vib., vol. 27, no. 1, 1971, p. 85.

28. Feynman, R. P.: Theory of Fundamental Processes. W. A. Benjamin, Inc., pub., 1962.

29. Morse, P. M.; and Feshbach, H.: Methods of Theoretical Physics. McGraw-Hill, 1953.

30. Abramowitz, M.; and Stegun, I. A.: Handbood of Mathematical Functions. AMS-55, Nat. Bur. Std., 1964.

31. Atassi, H.; and Goldstein, M.: Unsteady Lift Forces on Highly Cambered Airfoils Moving Through a Gust. Preprint 74-88, AIAA 12th Aerospace Sciences Meeting, 1974.

32. Sears, W. R.: Some Aspects of Nonstationary Airfoil Theory and Its Practical Applications. J. Aeron. Sci., vol. 8, no. 2, 1941, p. 104.

33. Kemp, N. H.: On the Lift and Circulation of Airfoils in Some Unsteady-Flow Problems. J. Aeron. Sci., vol. 19, no. 10, 1952, p. 713.

34. Horlock, J. H.: Fluctuation Lift Forces on Airfoils Moving Through Transverse and Chordwise Gusts. Trans. ASME, J. of Basic Eng., Series D, vol. 90, no. 4, 1968, p. 494.

35. Naumann, H.; and Yeh, H.: Lift and Pressure Fluctuations of a Cambered Airfoil Under Periodic Gusts and Applications in Turbomachinery. J. Eng. for Power, Jan. 1973, p. 1.

36. Filotas, L. T.: Theory of Airfoil Response in a Gusty Atmosphere, Vol. 1--Aerodynamic Transfer Function. UTIAS report 139, 1969; and Response of an Infinite Wing to an Oblique Sinusoidal Gust. 1969 Basic Aerodynamic Noise Research. NASA SP-207, 1969, p. 231.

37. Silverstein, A.; Katzoff, S.; and Bullivant, W. K.: Downwash and Wake Behind Plain and Flapped Airfoils. NACA report 651, 1939.

38. Glauert, H.: The Elements of Airfoil and Airscrew Theory. Second ed., Cambridge Univ. Press, England, 1948.

39. Lowson, M. W.; and Ollerhead, J. B.: A Theoretical Study of Helicopter Rotor Noise. J. Sound Vib., vol. 9, 1969, p. 197.

40. Barry, B.; and Moore, C. J.: Subsonic Fan Noise. J. Sound Vib., vol. 17, no. 2, 1971, p. 207.

41. Anon.: Subroutine BF4F. Vol. I of Computer Programming Manual, sec. C3.3, NASA-Langley Research Center, Aug. 1, 1968.

42. Anon.: Subroutine MTLUP. Vol. I of Computer Programming Manual, sec. E1.5, NASA-Langley Research Center, Sept. 12, 1969.

43. Anon.: Subroutine BSSLS. Vol. I of Computer Programming Manual, sec. C3.2, NASA-Langley Research Center, Aug. 1, 1968.

44. Levine, H.; and Schwinger, J.: On the Radiation of Sound From an Unflanged Circular Pipe. Phys. Rev., vol. 73, no. 4, 1948, p. 383.

45. Kaji, S.; and Okasaki, T.: Generation of Sound by Rotor-Stator Interaction. J. Sound Vib., vol. 13, no. 3, 1970, p. 281.

46. Mani, R.: Compressibility Effects in the Kemp-Sears Problem. Presented at the International Symposium on the Fluid Mechanics and Design of Turbomachinery, Pennsylvania State Univ., 1970.

47. Jarratt, P.; and Nudds, D.: The Use of Rational Functions in the Iterative Solution of Equations on a Digital Computer. The Computer Journal, vol. 8, no. 1, April 1965.

48. Anon.: Bessel Functions, Part II. Vol. X of Mathematical Tables, British Assoc. for Advance. Sci., Cambridge Univ. Press, 1952, p. xvii.

49. Olver, F. W. J.: Error Analysis of Miller's Recurrence Algorithm. Math. Computation, vol. 18, 1964, pp. 65-70.

50. Goldstein, M.; and Thaler, R. M.: Recurrence Techniques for the Calculation of Bessel Functions. MTAC, vol. 13, 1959, pp. 102-103.

51. Abramowitz, M.; and Stegun, I. A.: Generation of Bessel Functions on High Speed Computers. MTAC, vol. ii, 1957, pp. 255-257.

52. Anon.: Bessel Functions, Part I. Vol. X of Mathematical Tables, British Assoc. for Advance. Sci., Cambridge Univ. Press, 1958, pp. 202-212.

53. Goldstein, M.; and Abramson, H.: Subroutine NYU BES4. Control Data 6000 Series Users Group, VIM C3.

54. Anon.: Subroutine ALGAMF. Vol. I of Computer Programming Manual, sec. C3.5, NASA-Langley Research Center, August 1, 1968.

55. Anon.: Subroutine SICI, System/360, Scientific Subroutine Package (360A-CM-03X), Version II. Programmer.s Manual, H20-0205-3.